PNAS RESEARCH ARTICLE | PLANT BIOLOGY

Activation of ROPGEFs by a malectin-like receptor kinase is involved in tip growth regulation in *Physcomitrium patens*

Ruohan Lyu[a,1], Jingtong Ruan[a,1], Ying Chen[a,1], Haoyu Tian[a], and Peishan Yi[a,b,2]

Edited by Eugenia (Jenny) Russinova, Ghent University, Gent, Belgium; received June 8, 2026; accepted October 14, 2026

Rho-type GTPases of plants (ROPs) play essential roles in polarized cell growth, cell division, and organogenesis. Their activation depends on two types of guanine nucleotide exchange factors (GEFs): the plant-specific PRONE-domain-containing ROPGEFs and DOCK-type SPKGEFs. While ROPGEFs have been proposed to be autoinhibited in pollen and activated by receptor-like kinases (RLKs), the underlying mechanisms remain incompletely understood. Using the moss *Physcomitrium patens*, we show that moss ROPGEF4 and ROPGEF6 exhibit low intrinsic GEF activity and are not autoinhibited by non-PRONE regions, whereas the catalytic domain of SPK1 and SPK6 is highly active. Through a candidate screen, we identified MLRK1, a malectin-like receptor kinase, as a ROPGEF-interacting protein. MLRK1 directly phosphorylates ROPGEF4 and ROPGEF6 and stimulates their GEF activities in vitro. These effects are attenuated by substituting key phosphosites (Ser231 in ROPGEF4 and Ser524/Thr526 in ROPGEF6) with nonphosphorylatable residues. Structural modeling, pull-down assays, and functional analyses indicate that phosphorylation enhances ROPGEF-ROP interactions and promotes the membrane localization of ROPGEF4/6. Furthermore, ROPGEFs are not essential for polarized cell growth on their own but act redundantly with SPK2. At the apical membrane, ROPGEFs appear to activate ROPs, reduce their diffusion, promote actin filament assembly and vesicle secretion, and ultimately facilitate cell expansion and growth. Collectively, our findings provide functional evidence that RLK-ROPGEF-ROP signaling module has emerged in early land plants and is involved in cell growth regulation.

moss | tip growth | ROP GTPase | ROPGEF | receptor-like kinase

Significance

Rho-type GTPases (ROPs) are central regulators of polarized cell growth in plants, yet the mechanisms by which receptor-like kinases (RLKs) activate ROP guanine nucleotide exchange factors (ROPGEFs) have remained unclear. Using moss *Physcomitrium patens*, Lyu et al. demonstrate that a malectin-like-type RLK directly phosphorylates and activates ROPGEFs and this phosphorylation is involved in tip growth regulation. These findings expand current understanding of the RLK-ROPGEF-ROP signaling and provide functional evidence that this module has emerged in early land plants.

Rho-type small GTPases in plants (ROPs) are molecular switches that regulate diverse cellular and developmental processes, including cell expansion, cell division, cell wall integrity, and organogenesis (1–4). Their activity is tightly regulated by the opposing actions of guanine nucleotide exchange factors (GEFs), which catalyze the exchange of GDP for GTP and activate ROPs, and GTPase-activating proteins (GAPs), which enhance ROPs' GTPase activity, thus leading to their inactivation. Once in the active, GTP-bound state, ROPs interact with various effectors to modulate cytoskeletal organization, calcium gradients, exocytosis, endocytosis, and other cellular events (5–7). Given their central role in ROP signaling, ROP-related GEFs have become a major focus of plant biology research aimed at understanding their function and regulation (8).

Plants possess two distinct families of ROP-related GEFs: ROPGEFs contain a central, plant-specific PRONE (PLANT-SPECIFIC ROP NUCLEOTIDE EXCHANGE) domain (9, 10); SPIKE1-type GEFs (SPKGEFs) belong to the DOCK (DEDICATOR OF CYTOKINESIS) family (11, 12), which is conserved in animals (13). SPKGEFs comprise three DOCK homology regions (DHRs) and a long armadillo repeat (ARM) domain. Within this family, DHR2 serves as the catalytic domain. DHR1 and DHR3 adopt a C2 domain-like conformation, which facilitates membrane association (14). Accordingly, SPKGEFs localize to membranous organelles in a manner dependent on microtubules and endomembrane trafficking (15, 16). Notably, the DHR2 domain of *Arabidopsis* SPIKE1 exhibits GEF activity comparable to that of the full-length protein, suggesting that SPKGEF's activity may not be regulated by intramolecular interactions (12).

Unlike SPKGEFs, ROPGEFs lack well-recognized regulatory domains (9, 10). Their GEF activity depends on dimerization of the PRONE domain (17). Several ROPGEFs are autoinhibited by their carboxyl terminus, and the relief of this inhibition involves phosphorylation (10, 18). Consistently, receptor-like kinases (RLKs), including members of POLLEN-SPECIFIC RECEPTOR-LIKE KINASEs (PRKs) (18–23) and the *Catharanthus roseus* RECEPTOR-LIKE KINASE 1-LIKE (CrRLK1L) family (24–28), have been shown to genetically and physically interact with ROPGEFs. Several putative phosphorylation sites in ROPGEFs have been functionally characterized (18, 20, 29, 30). Nevertheless, direct evidence for ROPGEF phosphorylation by PRKs and CrRLK1Ls remains limited, with only a few cases reported—specifically, *Arabidopsis* AtPRK2 and

Author affiliations: [a]Key Laboratory of Bio-Resource and Eco-Environment of Ministry of Education, Laboratory for Ex Situ Conservation and Resource Utilization of Mountain Plants, College of Life Sciences, Sichuan University, Chengdu 610065, Sichuan, People's Republic of China; and [b]Chengdu Botanical Garden, Chengdu 610083, Sichuan, People's Republic of China

Author contributions: P.Y. designed research; R.L., J.R., Y.C., H.T., and P.Y. performed research; R.L., J.R., and P.Y. analyzed data; and R.L., J.R., and P.Y. wrote the paper.

The authors declare no competing interest.

This article is a PNAS Direct Submission.

Copyright © 2026 the Author(s). Published by PNAS. This article is distributed under Creative Commons Attribution-NonCommercial-NoDerivatives License 4.0 (CC BY-NC-ND).

[1]R.L., J.R., and Y.C. contributed equally to this work.

[2]To whom correspondence may be addressed. Email: yipeishan@scu.edu.cn.

This article contains supporting information online at https://www.pnas.org/lookup/suppl/doi:10.1073/pnas.2620413123/-/DCSupplemental.

Published November 17, 2026.

Downloaded from https://www.pnas.org by SICHUAN UNIVERSITY on November 17, 2026 from IP address 211.83.126.26.

AtPRK3, and *Pyrus bretschneideri* CrRLK1L13 (18, 20, 27). Moreover, studies in *Arabidopsis* have shown that PRK function may not require kinase activity (22, 23). Some ROPGEFs, such as *Arabidopsis* AtROPGEF10 and *Marchantia* MpROPGEF, are not autoinhibited (31, 32). These findings suggest that the autoinhibition-release model may not apply broadly to RLK-ROPGEF modules.

ROP signaling is highly conserved across land plants (33). As in flowering plants, bryophyte ROPs play essential roles in cell growth, division orientation, and organogenesis (34–37). Recently, two subtypes of ROP-related, namely ROPGAPs and RENGAPs, have been shown to redundantly regulate ROP activity (38, 39); loss of ROPGEF function impairs cell growth in the moss *Physcomitrium patens* (*P. patens*) and gemma development in the liverwort *Marchantia polymorpha* (*M. polymorpha*) (32, 40). Furthermore, *Marchantia* MpFER/MpTHE1, a CrRLK1L member, and its downstream factor MpMRI are critical for rhizoid growth and cell wall integrity (41–43), suggesting a potential role of RLKs in regulating ROP signaling (3). In this study, we show that moss ROPGEF4 and ROPGEF6 function as intrinsically low-activity GEFs that are not autoinhibited. Their full activation in vitro depends on phosphorylation of the PRONE domain by a CrRLK1L member kinase MLRK1. This phosphorylation is required for robust membrane localization and function in vivo. Furthermore, ROPGEFs cooperate with the SPK-type GEF SPK2 to promote cell expansion, a process involving the fine-tuning of membrane-localized ROP mobility and downstream cellular processes. Together, our findings provide evidence that an RLK biochemically activates ROP signaling via ROPGEF phosphorylation, and indicate that the RLK-ROPGEF-ROP signaling module has emerged early during land plant evolution.

Results

Moss ROPGEF4 and ROPGEF6 Tend to Preferentially Interact with the Active form of ROP4. ROPGEFs were initially identified as interactors of dominant-negative ROP variants in *Arabidopsis* (9, 10). However, individual family members exhibit differential binding preferences toward distinct forms of ROPs (10). For instance, AtROPGEF8 and AtROPGEF14 preferentially bind GDP-bound AtROP1, whereas AtROPGEF1 interacts strongly with GTP-bound AtROP1, and *Marchantia* MpROPGEF selectively binds nucleotide-free MpROP (10, 32). The moss *P. patens* genome encodes six ROPGEFs (44), which cluster into two subclades: one comprising ROPGEF3 and ROPGEF4, and the other containing ROPGEF1, ROPGEF2, ROPGEF5, and ROPGEF6 (*SI Appendix*, Fig. S1). Given that ROPGEF4 and ROPGEF6 are most highly expressed in tip-growing protonemata (45) and moss ROPs are functionally redundant (34, 37), we investigated the binding ability of ROPGEF4 and ROPGEF6 with various forms of ROP4 using yeast two-hybrid assays. As shown in Fig. 1*A*, both ROPGEF4 and ROPGEF6 interacted with wild-type and constitutively active ROP4 (ROP4CA^{G15V}), but not with dominant-negative ROP4 (ROP4DN^{T20N}) (46, 47). Pull-down experiments using purified bacterial proteins revealed a preferential binding to the active form of ROP4 (Fig. 1 *B*–*E*). Consistent with earlier reports (10), AtROPGEF1 interacted with all tested forms of AtROP1 (*SI Appendix*, Fig. S2). Interestingly, AtROPGEF1 also showed preferential binding to wild-type and active PpROP4 (*SI Appendix*, Fig. S2). This implies that the binding preference may result from structural differences in moss ROPs rather than in ROPGEFs themselves.

To map the regions mediating ROP interaction, we generated truncated versions of ROPGEF4 and ROPGEF6. Surprisingly, the PRONE domain alone failed to interact with any form of ROP4 in yeast two-hybrid assays (Fig. 1*A*). Removing either the N- or C-terminal regions individually did not impair binding. Further truncation analyses revealed that the relatively conserved N-terminal and C-terminal proximal regions flanking the PRONE domain (Fig. 1*A* and *SI Appendix*, Fig. S3), hereafter referred to as NP and CP, respectively, both contribute to ROPGEF–ROP4 interaction, with the CP domain playing a critical role in ROPGEF4 interaction. Neither NP nor CP domain alone interacted with ROP4 (Fig. 1*A*). In vitro pull-down assays corroborated the requirement of both flanking regions for robust ROPGEF4–ROP4 interaction (Fig. 1 *B* and *C*). Due to technical limitations, we were unable to express the full-length ROPGEF6 protein and therefore used the PRONE domain in combination with the NP and CP domains for analyses. Although binding affinities detected by yeast two-hybrid and pull-down assays slightly differed for PRONE6, PRONE4, and the N-PRONE4 truncations, all variants showed a clear binding preference toward active ROP4 in pull-down analyses (Fig. 1 *D* and *E*). Given that the endogenous GTP concentration in yeast is two- to fourfold higher than that of GDP (48), the interaction of ROPGEF4 and ROPGEF6 variants with wild-type ROP4 in yeast two-hybrid assays may also reflect the presence of GTP-bound ROP4. Collectively, our results suggest that moss ROPGEF4 and ROPGEF6 tend to preferentially interact with the active form of ROP4, and that regulatory regions flanking the PRONE domain may facilitate ROPGEF-ROP interaction.

Moss ROPGEF4 and ROPGEF6 Are Intrinsically Low-activity GEFs that Are Not Autoinhibited. We next assessed the GEF activity of ROPGEF4 and ROPGEF6 toward ROP4 using an endpoint GTPase assay as previously described (39). Surprisingly, none of the tested ROPGEFs, including the full-length protein, the PRONE domain alone, or the PRONE domain combined with NP and CP regions, enhanced ROP4-mediated GTP hydrolysis (Fig. 2 *A* and *B*). By contrast, the PRONE domain of *Arabidopsis* AtROPGEF1 (AtGEF1(PR)) exhibited robust GEF activity when incubated with AtROP1 and AtROPGAP1 in vitro (Fig. 2*C*). Notably, AtGEF1(PR) also stimulated GTP hydrolysis in combination with PpROP4 and PpROPGAP1, whereas the PRONE domains of PpROPGEF4 or PpROPGEF6 showed only minimal activity toward AtROP1. We further tested the GEF activity of the DHR2 domain from moss SPK1 and SPK6. In line with earlier reports of *Arabidopsis* AtSPK1 (9, 12), both proteins were highly active (Fig. 2*D*). Our sequence analyses identified conserved tandem Ser/Thr-Pro motifs in the CP domain of most ROPGEFs (*SI Appendix*, Fig. S4*A*). Given that the activity of some ROPGEFs appears to be activated through phosphorylation of the autoinhibitory C terminus (10, 18, 49), we introduced phosphomimic or deletion mutations in ROPGEF4 C-terminus and tested the GEF activity of these mutants. However, no enhancement in GEF activity was detected (*SI Appendix*, Fig. S4*B*). Together, these results indicate that moss ROPGEFs are low-activity GEFs, and the non-PRONE regions contribute minimally to modulating GEF activity.

MALECTIN-LIKE RECEPTOR KINASE 1 Interacts with Moss ROPGEFs. The low activity of moss ROPGEFs suggests the involvement of an activation mechanism. Since RLKs are potential activators of ROPGEFs (2–4), we performed a candidate screen to identify RLKs that interact with ROPGEF4 and ROPGEF6 using yeast two-hybrid assays. We first systematically analyzed all putative RLKs in *P. patens* and identified 239 members that contain at least one transmembrane domain (*SI Appendix*, Fig. S5). Based on phylogenetic relationships with RLKs from *Arabidopsis* (50), the moss RLKs are classified into 15 major groups, excluding the RECEPTOR-LIKE CYTOPLASMIC KINASE (RLCK) subfamily (*SI Appendix*, Fig. S5). We then selected 22 candidate RLKs

Downloaded from https://www.pnas.org by SICHUAN UNIVERSITY on November 17, 2026 from IP address 211.83.126.26.

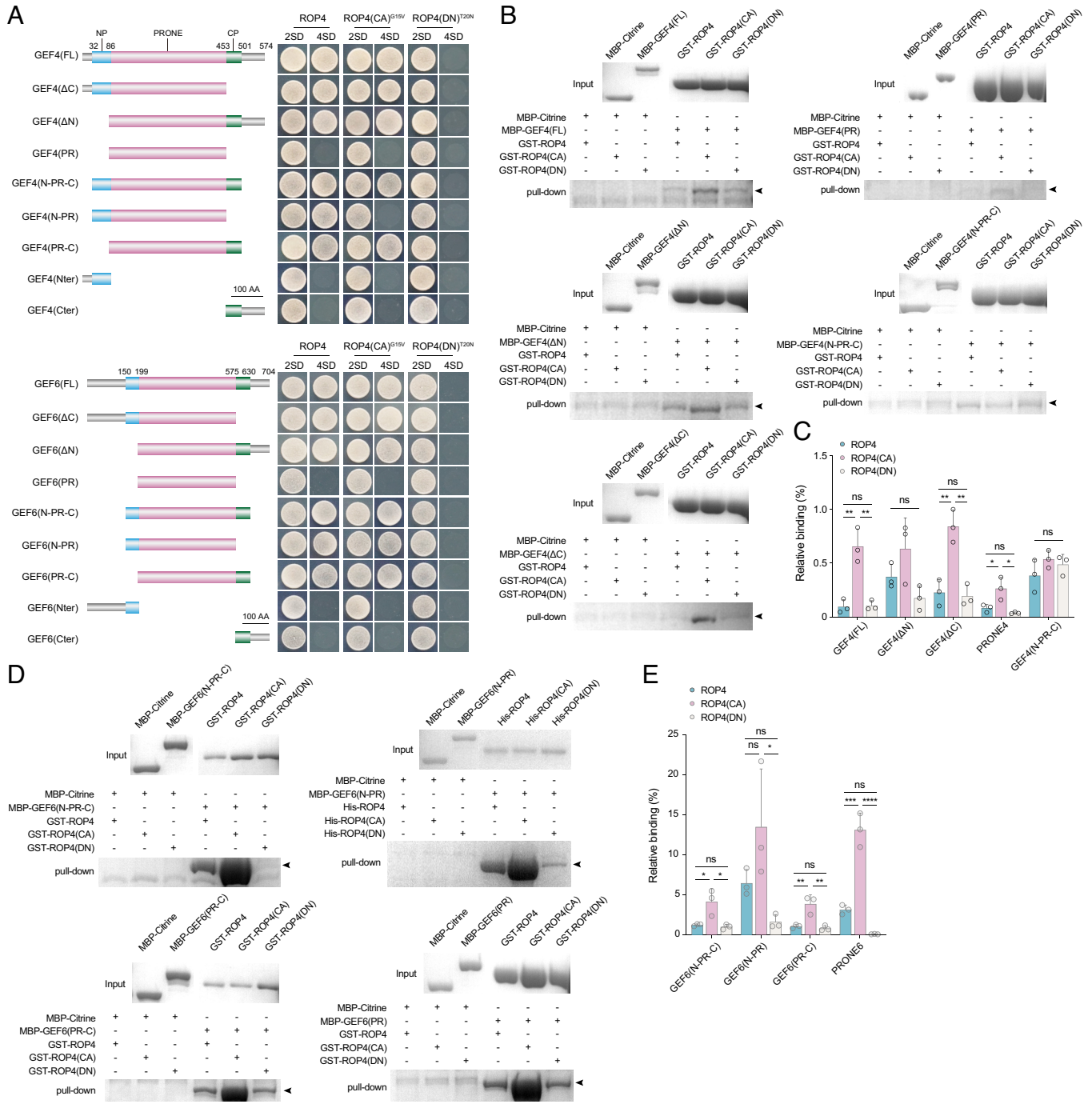


Fig. 1. Moss ROPGEF4 and ROPGEF6 preferentially interact with active ROP4. (*A*) Yeast two-hybrid analysis of interactions between truncated ROPGEF4/6 variants and three forms of ROP4. CA, constitutively active form; DN, dominant-negative form; NP, N-terminal proximal region; CP, C-terminal proximal region; FL, full-length; PR, PRONE domain; N-PR-C, PRONE domain with N- and C-terminal proximal regions; N-PR, PRONE domain with N-terminal proximal region; PR-C, PRONE domain with C-terminal proximal region; Nter, N-terminal portion; Cter, C-terminal portion. (*B*) Pull-down analysis of interactions of truncated ROPGEF4 variants with three forms of ROP4. SDS-PAGE gels are shown. Arrows indicate ROPGEF4 bands pulled down by the three forms of ROP4. (*C*) Quantification of relative amounts of ROPGEF4 pulled down by ROP4. (*D*) Pull-down analysis of interactions between truncated ROPGEF6 variants and three forms of ROP4. (*E*) Quantification of relative amounts of ROPGEF6 pulled down by ROP4. Data in (*C* and *E*) are mean ± SD (n = 3 per group). One-way ANOVA with Tukey's post hoc test was used for comparison in (*C* and *E*). ns, not significant; **P* < 0.05; ***P* < 0.01; ****P* < 0.001.

representing diverse subclades that showed high transcript levels in tip-growing protonema cells (*SI Appendix*, Fig. S6*A*). Among these candidates, the cytoplasmic domain (CD) of a malectin-like receptor kinase interacted with both ROPGEF4 and ROPGEF6 (*SI Appendix*, Fig. S6*B*). This gene, hereafter referred to as MALECTIN-LIKE RECEPTOR KINASE 1 (MLRK1), belongs to the CrRLK1L family, which comprises five members (MLRK1–MLRK5) in *P. patens* and includes *Arabidopsis* BUPS1/2 and FERONIA (*SI Appendix*, Fig. S5). MLRK1, MLRK2, and MLRK3 share over 95% sequence similarity in their kinase domains and form a distinct subclade, whereas MLRK4 and MLRK5 constitute a separate subgroup (*SI Appendix*, Figs. S5 and S7). Accordingly, MLRK2 and MLRK3 also interacted with ROPGEF4 and ROPGEF6, whereas MLRK4 and MLRK5 did not (Fig. 3*A* and *SI Appendix*, Fig. S6). Truncation experiments demonstrated the requirement of NP and CP domains of ROPGEF6 and a critical role of the ROPGEF4 CP domain for

Downloaded from https://www.pnas.org by SICHUAN UNIVERSITY on November 17, 2026 from IP address 211.83.126.26.

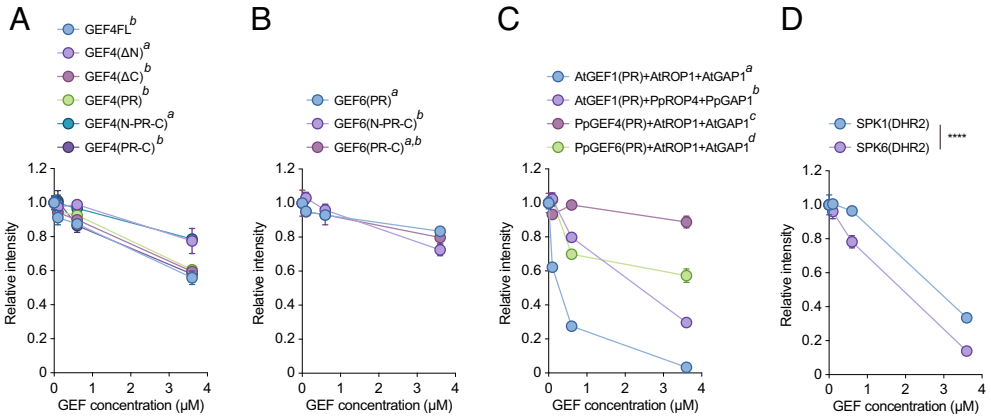


Fig. 2. ROPGEF4 and ROPGEF6 exhibit low GEF activity in vitro. (*A*) GEF activity of full-length and truncated PpROPGEF4 variants toward PpROP4. FL, full-length; PR, PRONE domain; N-PR-C, PRONE domain with N- and C-terminal proximal regions; PR-C, PRONE domain with C-terminal proximal region. (*B*) GEF activity of truncated PpROPGEF6 toward PpROP4. (*C*) GEF activity of PRONE domain from *Arabidopsis* ROPGEF1 (AtGEF1) and *P. patens* ROPGEF4(PpGEF4) and ROPGEF6(PpGEF6), tested with AtROP1, AtROPGAP1(AtGAP1), PpROP4, and PpROPGAP1(PpGAP1). (*D*) GEF activity of the DHR2 domain of *P. patens* SPK1 and SPK6 toward PpROP4. Data are mean ± SD (n = 3 per reaction). At the highest GEF concentration tested, one-way ANOVA with Tukey's post-hoc test was used for comparison in (*A–C*), and an unpaired two-tailed Student's test was used for (*D*). ****$P < 0.0001$.

interaction (*SI Appendix*, Fig. S8*A*). Given that PRONE domain in combination with NP and CP domains (N-PR-C) is sufficient for interactions with ROP4 and MLRK1 (Fig. 1*A* and *SI Appendix*, Fig. S8*A*), we recombinantly expressed and purified ROPGEF4(N-PR-C) and ROPGEF6(N-PR-C) to further test their interactions with MLRK1 using in vitro pull-down assays. As expected, both proteins showed strong binding with MLRK1(CD) (Fig. 3 *B–D*). We then generated truncated variants for MLRK1(CD) to examine the contribution of N-terminal and C-terminal cytoplasmic regions (cytoN and cytoC) for interaction. Interestingly, the cytoC domain of MLRK1 was found to be necessary and sufficient for robust interaction with ROPGEFs (Fig. 3 *B–D* and *SI Appendix*, Fig. S8*B*). Together, these findings demonstrate that a subset of CrRLK1L family members physically interact with ROPGEF4 and ROPGEF6 in *P. patens* and the C-terminal cytoplasmic region plays a critical role in this interaction.

MLRK1 Activates ROPGEF4 and ROPGEF6 Through Direct Phosphorylation In Vitro. We next examined whether MLRK1 is a functional kinase and could directly phosphorylate ROPGEF4 and ROPGEF6 in vitro. The purified CD domain of MLRK1 underwent strong autophosphorylation, consistent with the autophosphorylation-dependent activation reported for its *Arabidopsis* homolog FERONIA (51) (Fig. 4*A*). An activity-defective MLRK1 carrying the K551R mutation also exhibited marked phosphorylation; however, this is likely attributable to nonspecific phosphorylation derived from bacterial contaminants, as substantial phosphorylation signals were observed even in the absence of ATP (Fig. 4*A*). Indeed, in vitro kinase assays revealed rapid ATP consumption by MLRK1 but a minor change of ATP level by MLRK1(K551R) (*SI Appendix*, Fig. S9*A*). We next performed comparative mass spectrometry analyses and identified five phosphorylation sites within the activation segment of MLRK1, among which Ser669 and Ser687 were specifically phosphorylated in the wild-type protein (*SI Appendix*, Fig. S9*B*). Phospho-defective mutations at Ser669 or Ser687 markedly reduced autophosphorylation levels, whereas substitutions at other sites had subtle effects (*SI Appendix*, Fig. S9*C*). These results demonstrate that MLRK1 is a functional kinase activated via autophosphorylation at Ser669 and Ser687. Notably, Ser687 but not Ser669 is required for autoactivation of *Arabidopsis* FERONIA (51), suggesting divergence in the activation mechanisms of CrRLK1L members between bryophytes and angiosperms.

We next assessed whether ROPGEF4 and ROPGEF6 serve as phosphorylation substrates for MLRK1. As shown in Fig. 4*B*, full-length ROPGEF4, ROPGEF4(N-PR-C), and ROPGEF6(N-PR-C) were all robustly phosphorylated by MLRK1(CD). This phosphorylation was markedly reduced when the kinase-defective MLRK1(K551R) was used (Fig. 4 *C* and *D*). To examine the functional consequence, phosphorylated ROPGEF4 and ROPGEF6 were repurified by column filtration and subjected to GEF assays. Preincubation with wild-type MLRK1(CD), but not the kinase-defective version, significantly enhanced GEF activity of both ROPGEF4 and ROPGEF6 (Fig. 4 *E* and *F*).

Comparative mass spectrometry analyses of phosphorylated versus nonphosphorylated ROPGEF4 and ROPGEF6 identified multiple phosphosites (*SI Appendix*, Fig. S10*A*). Based on structural simulations derived from AtPRONE8–AtROP4 complex (17), several of these sites are predicted to impact ROPGEF-ROP interactions. Specifically, Ser231 of ROPGEF4 lies within the WW loop of the PRONE domain (*SI Appendix*, Fig. S10*B*), a region that contacts the P-loop and switch II of ROP4 and is essential for GEF activity (17). In ROPGEF6, Ser524 and Thr526 of ROPGEF6 are located in the loop region between α11 and α12, which directly interacts with ROP4 (*SI Appendix*, Fig. S10*C*). Replacing Ser231 of ROPGEF4 and Ser524/Thr526 of ROPGEF6 with a nonphosphorylatable alanine (S231A and S524A/T526A, respectively) markedly reduced phosphorylation of both ROPGEFs (Fig. 4 *G* and *H* and *SI Appendix*, Fig. S10*D*). Accordingly, in vitro kinase assays showed that MLRK1-dependent ATP consumption in reactions containing ROPGEF4(S231A), ROPGEF6(S524A), and ROPGEF6(T526A) was compromised (*SI Appendix*, Fig. S10*E*). However, the double mutant ROPGEF6(S524A/T526A) exhibited unexpectedly high ATP consumption in the absence of MLRK1, which prevented us from assessing its effect on MLRK1-catalyzed phosphorylation (*SI Appendix*, Fig. S10*E*). Nevertheless, these data collectively identify Ser231 of ROPGEF4 and Ser524/Thr526 of ROPGEF6 as key MLRK1 phosphosites. Notably, MLRK1(CD) failed to activate the GEF activity of ROPGEF4(S231A) and ROPGEF6(S524A), whereas it still activated ROPGEF6(T526A), indicating that Ser231 and Ser524 are critical for phosphorylation-dependent activation in vitro (Fig. 4*I*). Interestingly, deletion of MLRK1 cytoC domain, which is critical for interaction with both ROPGEFs (Fig. 3 *B–D* and *SI Appendix*, Fig. S8*B*), differentially affected their activation. ROPGEF4 activation was lost in the absence of cytoC, whereas ROPGEF6 activity remained largely unaffected (Fig. 4*I*). Together, these findings demonstrate that ROPGEF4 and ROPGEF6 are activated by MLRK1 through direct phosphorylation, but the molecular mechanisms differ between these two GEFs.

Phosphorylation of ROPGEF4 and ROPGEF6 Enhances Their Interactions with ROP4. To investigate how phosphorylation modulates ROPGEF function, we first predicted the structures of ROP4 and three variants of the PRONE domain—wild-type,

Downloaded from https://www.pnas.org by SICHUAN UNIVERSITY on November 17, 2026 from IP address 211.83.126.26.

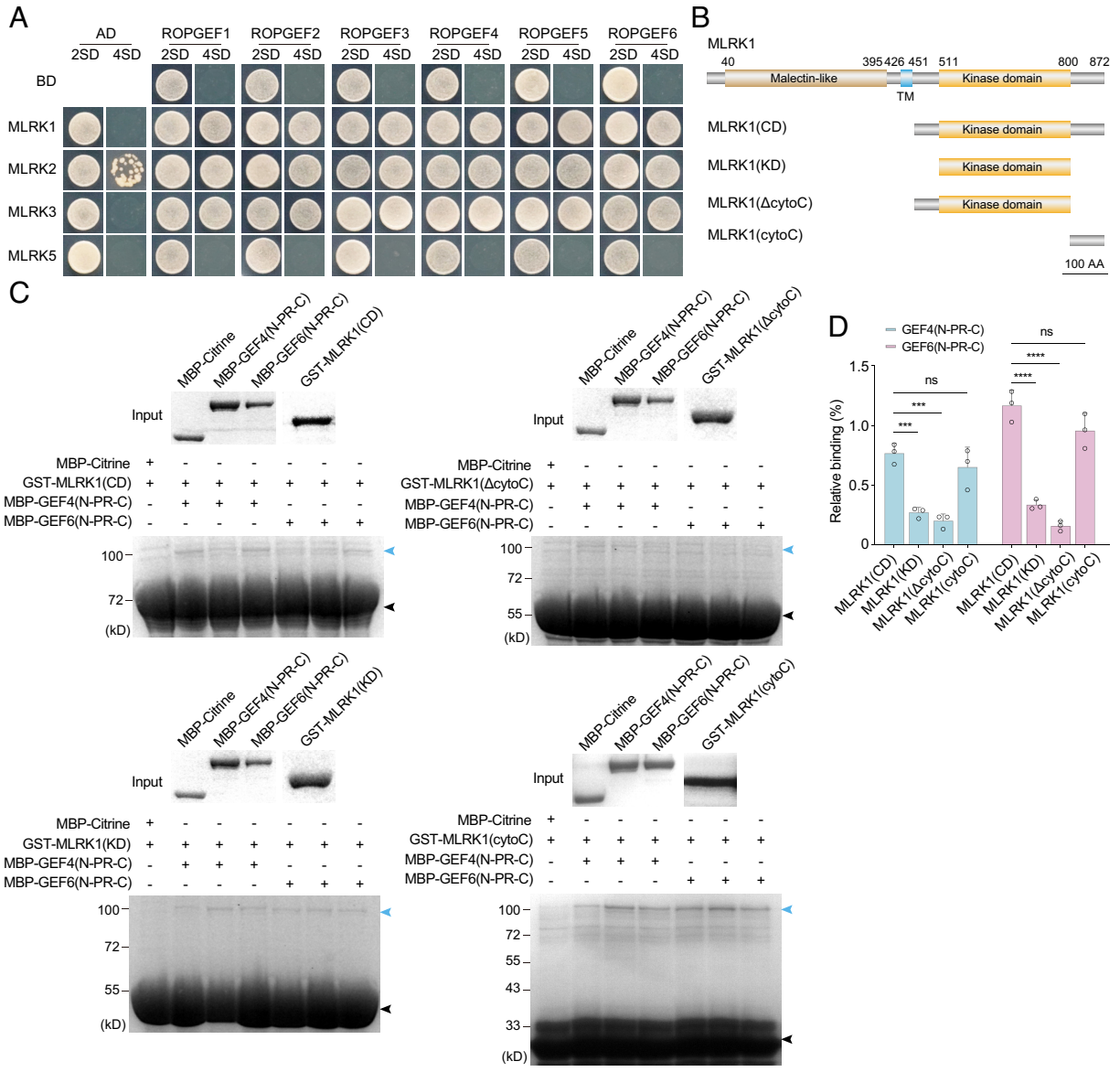


Fig. 3. ROPGEF4 and ROPGEF6 interact with MLRK1. (*A*) Yeast two-hybrid analysis of interactions between ROPGEFs and MLRKs. (*B*) Schematic of MLRK1 protein structure and its truncated variants. CD, cytoplasmic domain; KD, kinase domain; cytoC, C-terminal region of the cytoplasmic domain. (*C*) Pull-down analysis of interactions between truncated MLRK1 variants with ROPGEF4(N-PR-C) and ROPGEF6(N-PR-C). SDS-PAGE gels are shown. Arrows indicate ROPGEF bands (blue) pulled down by MLRK1 (black). MBP-Citrine served as a negative control. (*D*) Quantification of relative amounts of ROPGEF4 and ROPGEF6 pulled down by MLRK1. Data are mean ± SD (n = 3 per reaction). One-way ANOVA with Dunnett's post-hoc test was used to compare each variant against the wild-type MLRK1(CD). ns, not significant; ***$P < 0.001$; ****$P < 0.0001$.

phosphorylated, and phospho-defective—using Alphafold3 (52). We then modeled the PRONE–ROP4 complex in the presence of GTP or GDP through molecular docking. As shown in *SI Appendix*, Fig. S11*A*, phosphorylation of PRONE4 at Ser231 (pS231) did not substantially alter the overall conformation of the PRONE4–ROP4–GTP complex. However, it induced a clear shift of the WW loop along with the interacting α3 helix in ROP4-GDP, leading to marked changes in the contacts between the switch II of ROP4 and PRONE4 (*SI Appendix*, Fig. S11 *B* and *C*). In contrast, the nonphosphorylatable S231A mutation caused an opposite shift of the WW loop, which had little effect on the overall complex conformation but significantly reduced the size of nucleotide-binding pocket (*SI Appendix*, Fig. S11 *A*–*C*). In both pS231 and S231A variants, Glu121 of ROP4 formed an additional interaction with GDP (*SI Appendix*, Fig. S11*B*).

For PRONE6, phosphorylation at Ser524 (pS524) resulted in a subtle reorientation of the switch II of ROP4 in the GDP-bound state, whereas the phospho-defective S524A mutation influenced switch II orientation in the GTP-bound state (*SI Appendix*, Fig. S12*B*). These conformational changes appear to arise from altered intermolecular contacts with ROP4 (*SI Appendix*, Fig. S12*C*). Notably, pS524 engaged more polar or positively-charged residues, potentially stabilizing PRONE–ROP4 interaction. In the pS524–ROP4–GDP complex, GDP was deeply buried within the binding pocket (*SI Appendix*, Fig. S12*A*). In both pS524 and S524A variants, GTP and GDP formed additional contacts with Lys119 of ROP4 (*SI Appendix*, Fig. S12*D*). By contrast, phosphorylation or phospho-defective mutation at Thr526 had minimal impact on interactions with ROP4 (*SI Appendix*, Fig. S13), consistent with its dispensability for GEF activity. Together, these modeling results suggest that phosphorylation may modulate the interaction between the PRONE domain and the switch II region of ROP4, thereby influencing nucleotide binding and exchange.

Downloaded from https://www.pnas.org by SICHUAN UNIVERSITY on November 17, 2026 from IP address 211.83.126.26.

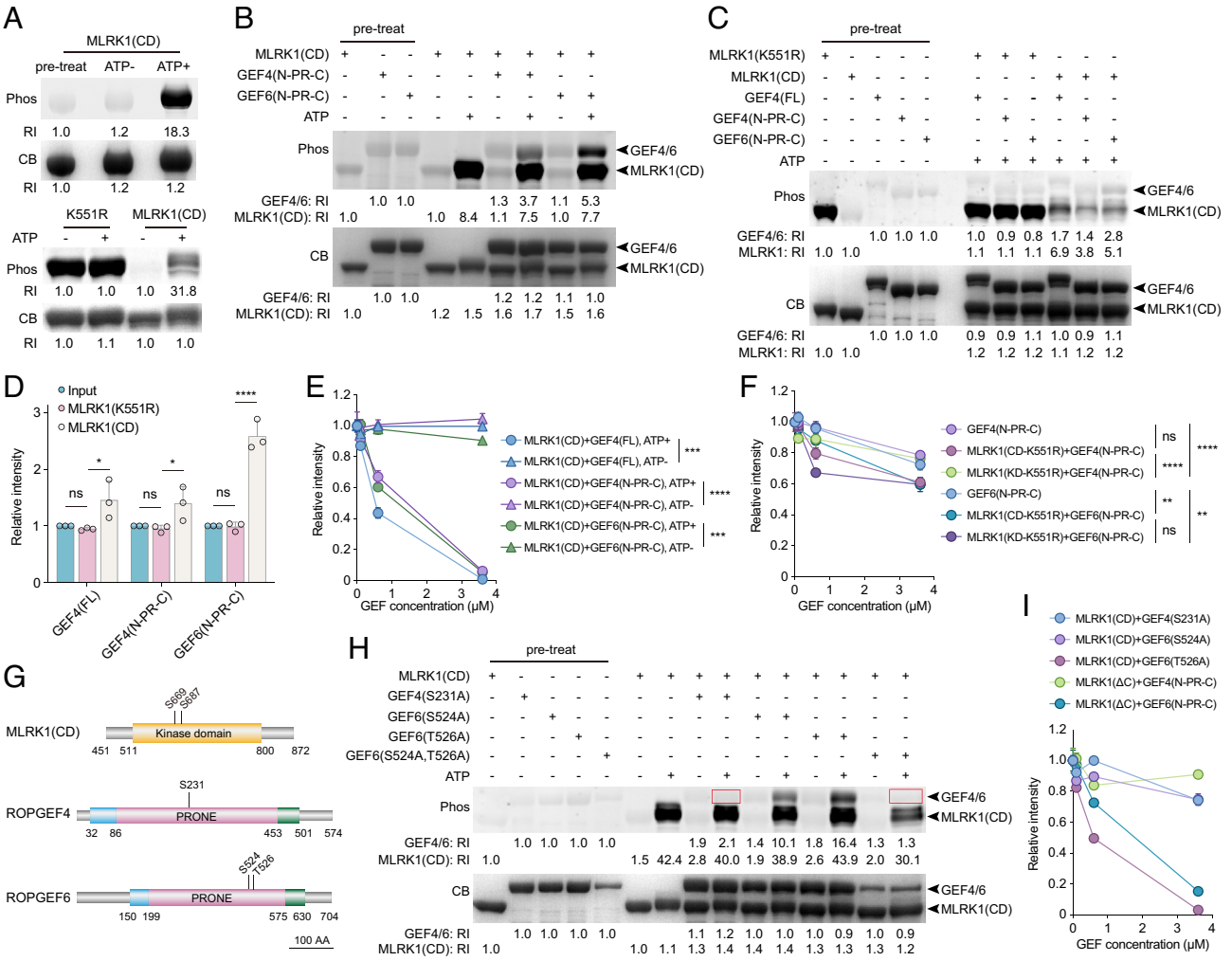


Fig. 4. MLRK1 phosphorylates and activates ROPGEF4 and ROPGEF6 in vitro. (*A*) Autophosphorylation of the MLRK1 cytoplasmic domain (CD) in vitro. The same SDS-PAGE gel was stained with a phosphoprotein stain and Coomassie blue. The high phosphorylation level of the kinase-defective MLRK1(K551R) likely results from nonspecific bacterial phosphorylation in the absence of ATP. RI, relative intensity normalized to pretreated samples; CB, Coomassie Blue stain; Phos, phosphoprotein stain. (*B*) Phosphorylation of ROPGEF4 and ROPGEF6 by MLRK1(CD). (*C*) Comparison of ROPGEF4 and ROPGEF6 phosphorylation by MLRK1(CD) vs. MLRK1(K551R). Despite high levels of MLRK1(K551R) autophosphorylation, the phosphorylation levels of ROPGEF4 and ROPGEF6 are lower with MLRK1(K551R) than with MLRK1(CD). (*D*) Quantification of ROPGEF4 and ROPGEF6 phosphorylation in untreated (input) samples and samples treated with MLRK1(CD) or MLRK1(K551R). (*E*) GEF activity of ROPGEF4 and ROPGEF6 treated with MLRK1(CD) toward ROP4 in the presence or absence of ATP. (*F*) GEF activity of ROPGEF4 and ROPGEF6 treated with or without MLRK1(K551R) toward ROP4. (*G*) Schematic of MLRK1(CD), ROPGEF4, and ROPGEF6 domain organization, with key phosphorylation residues indicated. (*H*) Phosphorylation of ROPGEF4 and ROPGEF6 mutants by MLRK1(CD). Phosphorylated bands of ROPGEF4(S231A) and ROPGEF6(S524A, T526A) are indicated with red boxes. (*I*) GEF activity of mutant ROPGEF4 and ROPGEF6 treated with MLRK1(CD) and wild-type proteins treated with MLRK1(ΔcytoC) toward ROP4. Data are mean ± SD in (*E*, *F*, and *I*) (n = 3 per reaction). At the highest GEF concentration tested, unpaired *t* test with Welch's correction was used for comparison in (*E*) and one-way ANOVA with Tukey's post-hoc test was used in (*F*). ns, not significant; $^{**}P < 0.01$; $^{***}P < 0.001$; $^{****}P < 0.0001$.

To gain more insight into the functional consequence of phosphorylation, we expressed phosphomimic versions, of which the Ser231 of ROPGEF4 and Ser524 of ROPGEF6 were substituted by a glutamate residue (S231E and S524E, respectively), and examined their binding ability with ROP4 through pull-down analyses. In line with structural modeling results, both phosphomimic ROPGEFs showed higher binding ability with all forms of ROP4 than wild-type proteins, with a ~3.5-fold increase toward ROP4CA (Figs. 1 *C* and *E* and 5 *A* and *B*). When these proteins were cotransformed with ROP4CA or ROP4DN into yeasts, no viable clones could be obtained, suggesting that ROPGEF–ROP4 complexes may disrupt endogenous signaling in yeasts due to their overactivation or dominant-negative effects.

Phosphorylation Sites Are Required for Robust Membrane Localization and In Vivo Function of ROPGEF4 and ROPGEF6. We next generated *ropgef4(S231E)* and *ropgef6(S524E)* mutants through CRISPR/Cas9-assisted genome editing (53). As shown in Fig. 5 *C* and *D*, both mutants exhibited significantly increased cell length and width, indicating that phosphorylation promotes tip growth. We then assessed whether phosphorylation influences the localization of ROPGEF4 and ROPGEF6. To this end, we generated knock-in lines expressing N-terminally or C-terminally tagged fluorescent fusion proteins. Unexpectedly, C-terminal tagging of both proteins in the wild-type background led to slightly shorter and severely wider cells (*SI Appendix*, Fig. S14 *A* and *B*). In contrast, N-terminal tagging had little effect on cell morphology. Altered cell morphology was also observed for ROPGEF4 when different fluorescent proteins were used for C-terminally tagging (*SI Appendix*, Fig. S14 *C* and *D*). Quantitative analyses indicate that both transcript and protein levels were increased in C-terminal tagging lines, possibly due to the use of an exogenous *nos* terminator (*Materials and Methods*) (*SI Appendix*, Fig. S14 *E*–*G*). Interestingly, in-frame deletion of the fluorescent protein-coding

Downloaded from https://www.pnas.org by SICHUAN UNIVERSITY on November 17, 2026 from IP address 211.83.126.26.

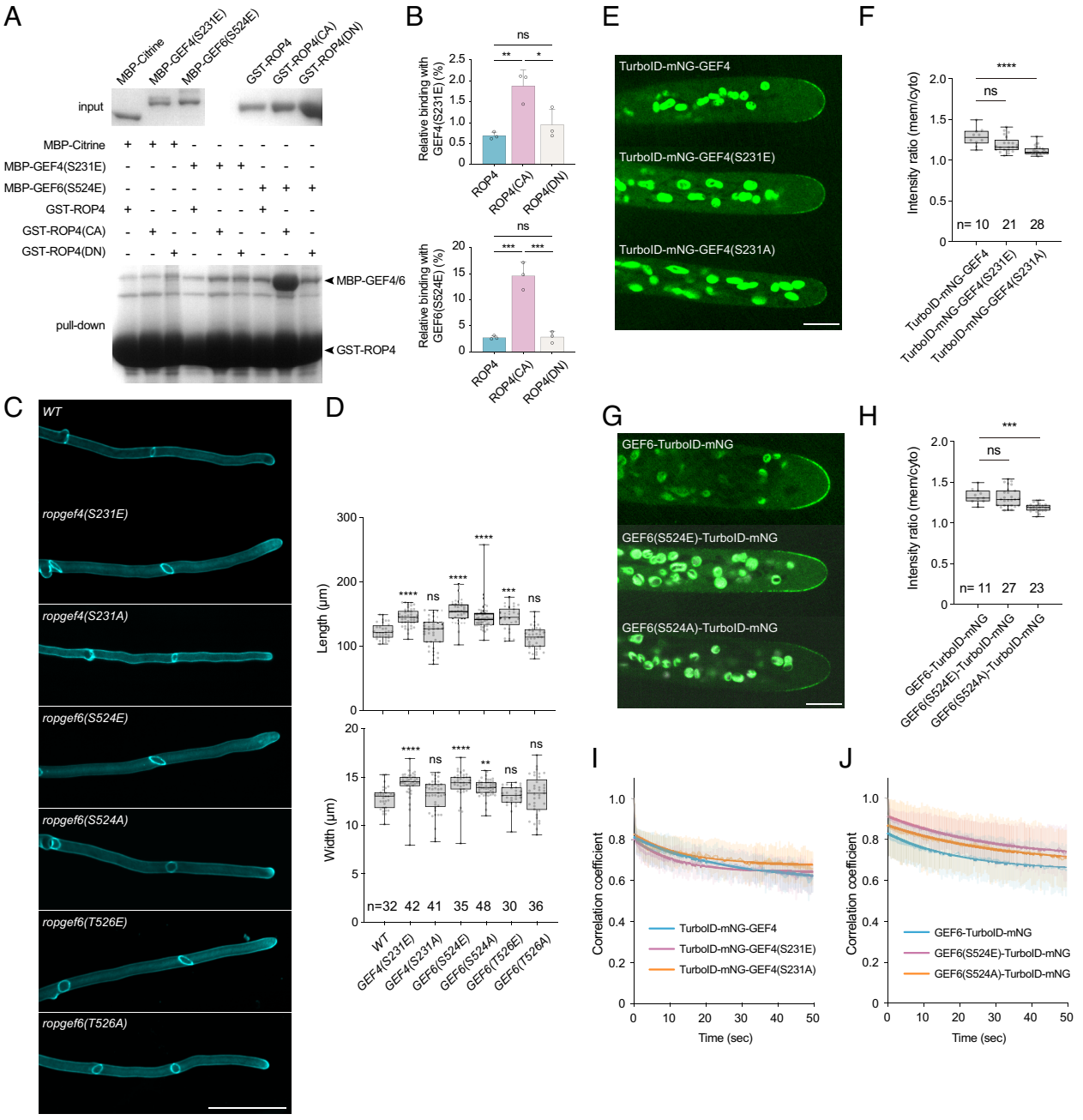


Fig. 5. Phosphorylation of ROPGEF4 and ROPGEF6 enhances their binding with ROP4 and promotes their membrane localization. (*A*) Pull-down assays of phosphomimic ROPGEF4/6 mutants with three forms of ROP4. ROPGEF4(N-PR-C) carrying S231E and ROPGEF6(N-PR-C) carrying S524E were used. CA, constitutively active form; DN, dominant-negative form. (*B*) Quantification of relative amounts of ROPGEF4/6 mutants pulled down by ROP4 (n = 3 per group). ROPGEF4(S231E) and ROPGEF6(S524E) show a ~3.5-fold increase in ROP4(CA) binding compared to wild-type ROPGEFs in (Fig. 1 *C* and *E*). (*C*) Protonema cell morphology of wild-type (WT) and *ropgef4* and *ropgef6* knock-in mutants. (Scale bar, 100 μm.) (*D*) Quantification of cell length and width. (*E*) Localization of endogenously mNG-fused wild-type and mutant ROPGEF4. (Scale bar, 10 μm.) (*F*) Quantification of the ROPGEF4 fluorescence intensity ratio at the apical membrane vs. in the cytosol. (*G*) Localization of endogenously mNG-fused wild-type and mutant ROPGEF6. (Scale bar, 10 μm.) (*H*) Quantification of the ROPGEF6 fluorescence intensity ratio at the apical membrane versus in the cytosol. (*I*) Dynamics of wild-type and mutant ROPGEF4 measured by correlation coefficient analysis, fitted with a one-phase association curve. n = 12 (wild-type), 10 (S231E), 9 (S231A). (*J*) Dynamics of wild-type and mutant ROPGEF6, fitted with a one-phase association curve. n = 13 (wild-type), 9 (S524E), 9 (S524A). Data are shown as mean ± SD in (*B*, *I*, and *J*) and box plots with median and range (min to max) in (*D*, *F*, and *H*). Sample sizes in (*D*, *F*, and *H*) are indicated below the bars. Comparisons were performed using one-way ANOVA with Tukey's post-hoc test in (*B*), Kruskal–Wallis with Dunn's post hoc test in (*D* and *F*), and Welch's ANOVA with Dunnett's T3 post hoc test in (*H*). ns, not significant; **P* < 0.05; ***P* < 0.01; ****P* < 0.001; *****P* < 0.0001.

regions via CRISPR/Cas9-mediated genome editing partially suppressed the cell morphology phenotypes (*SI Appendix*, Fig. S14 *C* and *D*), suggesting that the tag itself also contributed to the observed phenotypes. Indeed, when tagged with glutathione S-transferase (GST) at the C-terminus, both ROPGEF4 and ROPGEF6 exhibited enhanced GEF activity in vitro (Fig. 2 *A* and *B* and *SI Appendix*, Fig. S14*H*). These data suggest that the expression level and activity of ROPGEF4 and ROPGEF6 are both increased in C-terminal tagging lines.

We next introduced S-to-E and S-to-A mutations into the fluorescent protein knock-in lines via CRISPR/Cas9-mediated genome editing and compared the localization patterns. As shown in Fig. 5 *E–H*, the S-to-E mutation had subtle effects on the localization of ROPGEF4 and ROPGEF6. By contrast, the S-to-A

Downloaded from https://www.pnas.org by SICHUAN UNIVERSITY on November 17, 2026 from IP address 211.83.126.26.

substitution severely reduced, but did not completely block, membrane localization. As C-terminal tagging increased the expression and activity of ROPGEF6 and N-terminal knock-in generated no detectable fluorescence (*SI Appendix*, Fig. S14), we additionally overexpressed the N-terminally tagged ROPGEF6 to examine how Ser524 influences its localization. Consistently, the wild-type and S524E proteins both exhibited a prominent membrane localization, whereas the S524A variant was mostly cytoplasmic (*SI Appendix*, Fig. S15*A*). The localization of ROPGEF6(S524A) did not result from misexpression as western blotting of two independent lines confirmed the correct expression of full-length proteins (*SI Appendix*, Fig. S15*B*).

Since overexpression of ROPGEF4 and ROPGEF6 caused shorter and wider cells possibly due to the hyperactivation of ROP signaling (*SI Appendix*, Fig. S15 *A, C and D)*, we asked whether phosphomimic and phospho-defective mutations could render ROPGEFs hyperactive or inactive in vivo. Indeed, overexpression of ROPGEF4(S231E) significantly increased the cell width and decreased the cell length, a phenotype mimicking ROP hyperactivation, whereas ROPGEF4-(S231A) did not affect cellular morphology (*SI Appendix*, Fig. S15 *C* and *D*). Consistently, *ropgef4(S231E)* knock-in plants produced longer and wider protonema cells, while *ropgef4(S231A)* knock-in lines showed no morphological changes (Fig. 5 *C* and *D*). Intriguingly, overexpression of ROPGEF6(S524E) and ROPGEF6(S524A) both caused severe growth defects comparable to wild-type protein overexpression (*SI Appendix*, Fig. S15 *A* and *D*). We hypothesized that ROPGEF6(S524A) may induce dominant-negative effects on ROP signaling. However, *ropgef6(S524A)* knock-in plants showed increased cell growth and cell width as *ropgef6(S524E)* (Fig. 5 *C* and *D*), suggesting that ROPGEF6(S524A) is not dominant-negative but remains active in vivo. In line with this notion, membrane-localized ROPGEF6(S524E) and ROPGEF6(S524A) both exhibited reduced dynamics as shown by time-lapse imaging and correlation coefficient analyses (Fig. 5*J*). In contrast, S231E and S231A oppositely changed the dynamics of ROPGEF4 (Fig. 5*I*). The similar phenotypes of ROPGEF6(S524E) and ROPGEF6(S524A) knock-in mutants and overexpression lines raised the possibility that ROPGEF6(S524A) retains residual activity and/or promotes an alternative activation route, for example, via Thr526 phosphorylation. To test this, we generated *ropgef6(T526E)* and *ropgef6(T526A)* knock-in mutants, as well as ROPGEF6(S524/T526A) overexpression plants. Indeed, *ropgef6(T526E)* but not *ropgef6(T526A)* plants developed elongated cells, albeit to a lesser extent than *ropgef6(S524E)* (Fig. 5 *C* and *D*), whereas overexpression of ROPGEF6(S524/T526A) had no effect on cell morphology (*SI Appendix*, Fig. S15 *C* and *D*). Collectively, these findings indicate that Ser231 of ROPGEF4 and S524/Thr526 of ROPGEF6 are critical phosphosites required for their functions in vivo.

ROPGEFs Control Cell Expansion by Regulating the Dynamics of ROPs, Actin Filaments, and Vesicles Together with SPK2. To further investigate how ROPGEFs regulate cell growth, we generated knockout mutants for all six ROPGEFs using CRISPR/Cas9 genome editing (53). This yielded frameshift single mutants for *ropgef4* and *ropgef6*, *ropgef4,6* double mutants, and *ropgef1,2,3,4,5,6* sextuple mutants (hereafter *ropgef-KO*) (*SI Appendix*, Fig. S16*A*). Unexpectedly, none of these mutants exhibited discernible developmental defects, despite a slight reduction in cell width in the *ropgef-KO* line (Fig. 6 *A* and *B*). As overexpression of ROPGEF4 and ROPGEF6 leads to strong growth defects (*SI Appendix*, Fig. S15), we used the β-estradiol-based XVE system to induce their expression and examine the effects on cell growth. Time-lapse imaging following transient β-estradiol treatment revealed a gradual increase in membrane-localized ROPGEF4 and ROPGEF6, which correlated tightly with enhanced lateral membrane expansion and reduced apical elongation (Fig. 6 *C* and *D*). These results suggest that ROPGEFs are targeted to the membrane and undergo lateral diffusion, leading to cell expansion and depolarized growth.

As cell growth was not markedly affected in *ropgef-KO* plants, we speculate that SPKGEFs may play redundant roles with ROPGEFs. Indeed, CRISPR/Cas9-generated *spk2* knockout mutant exhibited severe growth defects, leading to shorter and wider cells (Fig. 6 *A* and *B* and *SI Appendix*, Fig. S16*B*). These phenotypes were further enhanced in the *ropgef-KO,spk2* septuple mutant. Some tip cells occasionally formed two apices, implying a deficiency in tip specification (Fig. 6*A*). Constitutive expression of ROPGEF4 largely rescued the observed phenotypes, demonstrating functional redundancy between ROPGEFs and SPK2.

Because C-terminal tagging increases the expression and activity of ROPGEF4 and ROPGEF6 (*SI Appendix*, Fig. S14), we used C-terminal tagging lines of ROPGEF4 (*gef4-cKI*) as gain-of-function variants, alongside the loss-of-function *ropgef-KO* mutants, to dissect how ROPGEFs regulate ROP signaling. Compared to wild-type plants, endogenous ROP4 and ROPGAP1 fused with an mNG tag in *gef4-cKI* lines exhibited significantly stronger enrichment at the apical membrane (Fig. 7 *A–F*). Interestingly, enhanced ROP4 membrane localization was also observed in *ropgef-KO* and *ropgef-KO,spk2* mutants, and to a lesser extent, in the *spk2* single mutant (Fig. 7 *A–C*). ROPGAP1 localization remained largely unchanged in the *ropgef-KO* mutant. However, it was markedly reduced in *spk2* and *ropgef-KO,spk2* plants and its bilateral enrichment at the apex was almost completely lost (Fig. 7 *D–F*). Given that ROPGAP1 preferentially interacts with the active form of ROP4 (39), these findings suggest that compromised ROP activation triggers feedback signaling that reinforces ROP membrane targeting, although the level of active ROPs could not be proportionally upregulated. We next assessed ROP4 motility using fluorescence recovery after photobleaching (FRAP). Consistent with *Arabidopsis* studies showing that activation reduces ROP motility (55, 56), ROP4 motility was severely decreased in *gef4-cKI* gain-of-function plants (*SI Appendix*, Fig. S17). By contrast, *ropgef-KO*, *spk2,* and *ropgef-KO,spk2* mutants exhibited a slight increase in motility within the first 20 s after photobleaching. However, recovery rates eventually declined at later time points, with the *ropgef-KO,spk2* mutant showing the strongest reduction (*SI Appendix*, Fig. S17*B*). These observations imply that, although activation restricts ROP motility, this process remains essential for establishing a fully polarized membrane domain, a phenomenon consistent with the requirement for activation-inactivation cycling of ROPs in microdomain formation, as shown in heterologous expression assays (55). Altogether, our data indicate that ROPGEFs and SPK2 coordinate the polar organization of ROPs at the apical membrane likely by promoting their local activation and modulating their diffusivity.

We next investigated cellular events downstream of ROP signaling by examining the dynamics of actin filaments and secretory vesicles, labeled by Lifeact-mCherry and SCAMP4-mNG, respectively. Time-lapse imaging and correlation analysis of fluorescence signals at the apical regions revealed an increase in actin filament dynamics in *ropgef-KO* mutants, as evidenced by a rapid decline in the correlation coefficient (Fig. 7 *G* and *H*). Conversely, actin dynamics were markedly suppressed in *gef4-cKI* gain-of-function lines, with the correlation curve shifting from exponential decay to a near-linear relationship. The dynamics of SCAMP4-labeled vesicles were not markedly affected in *ropgef-KO* mutants; however, it was significantly enhanced in *gef4-cKI* gain-of-function lines, as shown by both correlation coefficient analyses and FRAP assays (Fig. 7 *I–L*). Together, these results suggest that ROPGEFs

Downloaded from https://www.pnas.org by SICHUAN UNIVERSITY on November 17, 2026 from IP address 211.83.126.26.

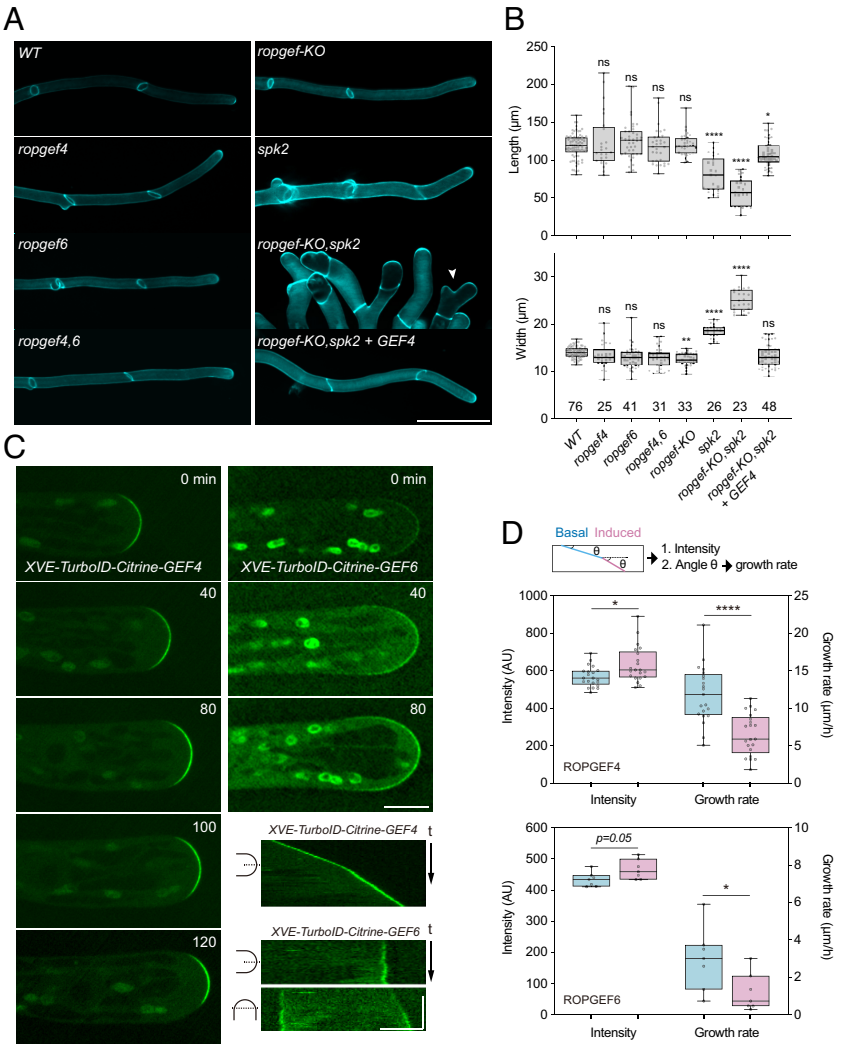


Fig. 6. ROPGEFs control cell expansion and growth redundantly with SPK2. (*A*) Cell morphology of *ropgef* and *spk2* mutants and rescue lines. The *ropgef-KO,spk2* septuple mutant occasionally forms two tips (arrowhead). In the rescue line, ROPGEF4 fused with an N-terminal TurboID-Citrine tag is expressed under the EF1α promoter (54). (Scale bar, 100 μm.) (*B*) Quantification of cell length and width. Sample sizes are indicated below the bars. (*C*) Time-lapse images of tip cells transiently expressing ROPGEF4 or ROPGEF6. (Scale bar in cell images, 10 μm; Kymograph scale: horizontal, 5 μm; vertical, 1 h.) (*D*) Quantification of fluorescence intensity and growth rate derived from kymographs in (*C*). Basal and induced regions are defined by the absence or presence of abrupt ROPGEF recruitment. n = 21 (ROPGEF4), 7 (ROPGEF6). Data in (*B*) and (*D*) are presented as box plots showing the median and range (min to max). For (*B*), comparisons were performed using Kruskal–Wallis with Dunn's post hoc test. For (*D*), unpaired two-tailed Student's *t* test was used, except for the ROPGEF4 intensity analysis, which was evaluated using Mann-Whitney U test. ns, not significant; $*P < 0.05$; $**P < 0.01$; $****P < 0.0001$.

promote the assembly of actin filaments, which may in turn facilitate vesicle delivery during polarized cell growth.

Discussion

In this study, we report that moss ROPGEFs are phosphorylated and activated by the CrRLK1L family member MLRK1 in vitro, thus providing evidence that an RLK-ROPGEF module is involved in ROP signaling activation in early land plants. Since moss ROPGEFs preferentially bind active ROPs and are not essential for cell growth, we propose that they are activated by membrane signals to reinforce the assembly of a polar ROP domain, whereas SPKGEFs play a central role in initiating the domain (Fig. 7*M*).

It should be noted that ROPGEF-activating mechanisms in moss differ from those in flowering plants in several aspects. First, moss ROPGEFs exhibit low basal GEF activity and are not auto-inhibited by non-PRONE regions. Second, phosphorylation sites appear to species- and gene-specific. The S231 site is specific in *P. patens* ROPGEF3-ROPGEF5 and is not conserved in other land plants (*SI Appendix*, Fig. S10 *B* and *C*). The S524 site is present only in certain members, such as moss ROPGEF1 and ROPGEF6, and *Arabidopsis* ROPGEF2-4 and ROPGEF10-13. These observations suggest that distinct ROPGEFs may depend on different phosphorylation sites for activation. Third, phosphorylation-dependent activation of ROPGEFs in flowering plants may involve additional factors. While several PRKs and CrRLK1Ls have been reported to phosphorylate ROPGEFs (18, 20, 27), direct activation of ROPGEFs by RLKs has not been widely demonstrated in flowering plants. Instead, emerging evidence points to a critical role of cytoplasmic kinases, particularly members of the PROTEIN KINASE A, G, and C (AGC) family and RLCKs, in activating ROPGEFs (57–59). Given the expansion of ROPGEFs in flowering plants (9, 10), it is plausible that distinct regulatory mechanisms have evolved to activate individual members, as exemplified by studies on ROPGEF1 (20, 57, 59, 60), ROPGEF8 (29), ROPGEF4 and ROPGEF10 (58), and ROPGEF12 (18). Beyond RLKs, other kinases also regulate ROPGEFs across diverse processes, including cotton fiber growth (61), symbiosis (62), and seed germination (60). These findings underscore the functional versatility of ROPGEFs and the intricate nature of their phosphorylation-dependent regulation.

ROPGEFs have drawn considerable attention since their discovery (9, 10). However, to what extent ROPGEFs contribute to ROP activation needs more careful assessment. Mounting evidence suggests that ROPGEFs may play a limited role than previously assumed. For instance, knockout of all moss ROPGEFs results in only subtle defects in cell morphology (Fig. 6 *A* and *B*), whereas loss of ROPs causes severe growth abnormalities (34, 37). Similarly, in *Marchantia*, loss of the single ROPGEF impairs gemma development but does not affect other aspects of vegetative development, including rhizoid growth (32). In contrast, ROPs are essential for tip growth, diffuse growth, and organogenesis (36). In *Arabidopsis*, loss of four ROPs (ROP1;3;5;9) completely blocks pollen germination (63), whereas loss of ROPGEFs

Downloaded from https://www.pnas.org by SICHUAN UNIVERSITY on November 17, 2026 from IP address 211.83.126.26.

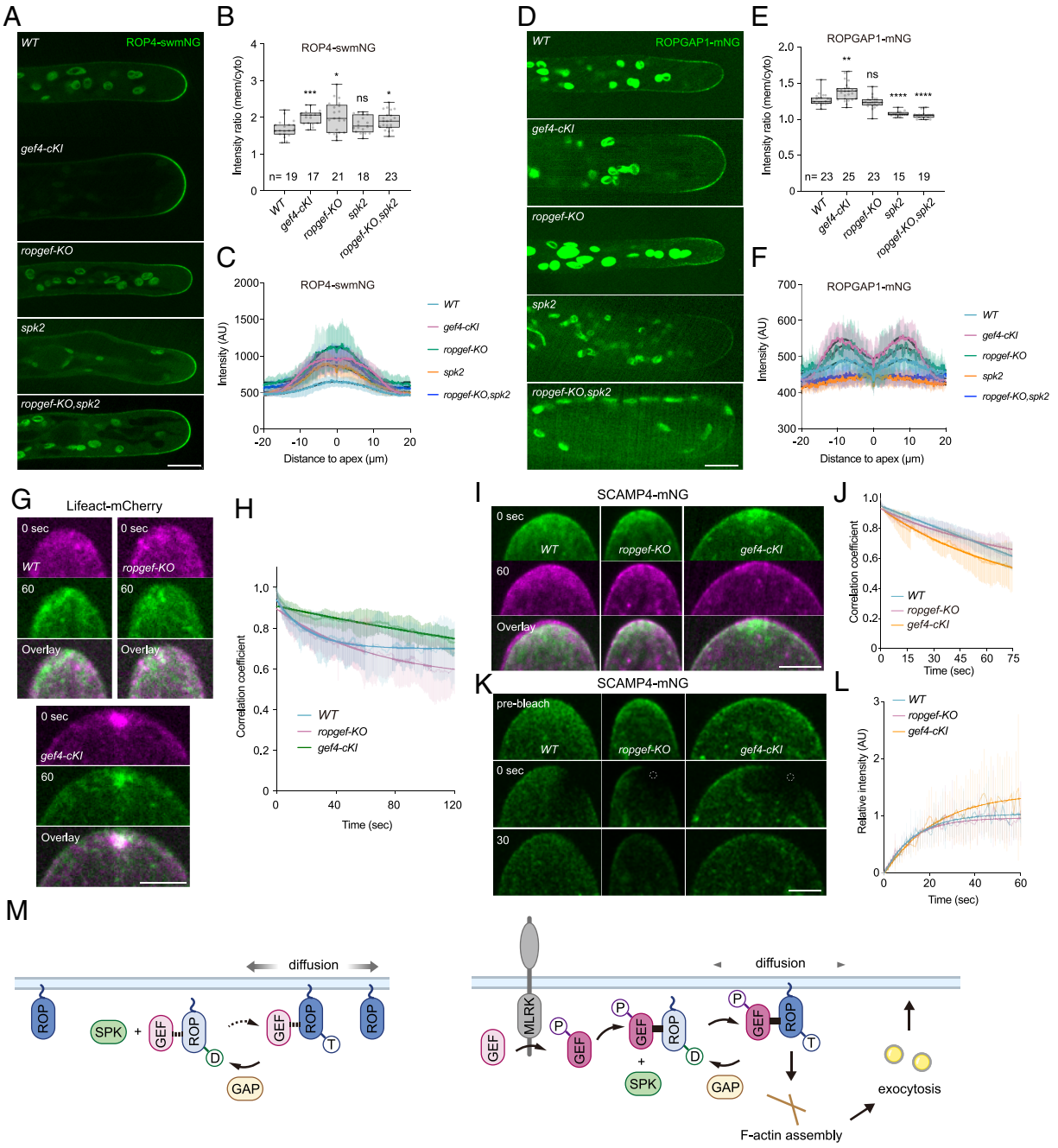


Fig. 7. ROPGEFs regulate the dynamics of ROP4, actin filaments, and secretory vesicles. (*A*) Localization of ROP4 in wild-type (WT), *gef4-cKI*, and mutant lines. Endogenous ROP4 is fused with a sandwiched mNG tag (swmNG) between Gly134 and Ala135 at its genomic locus (37). (Scale bar, 10 μm.) (*B*) Quantification of ROP4 membrane/cytosolic fluorescence intensity ratio. (*C*) Distribution of ROP4 fluorescence intensity along the apical membrane. Data are fitted by a sum of two Gaussians with baseline curve. n = 12 (wild-type), 17 (*gef4-cKI*), 21 (*ropgef-KO*), 16 (*spk2*), and 22 (*ropgef-KO,spk2*). (*D*) Localization of ROPGAP1 in WT, *gef4-cKI*, and mutant lines. Endogenous ROPGAP1 is C-terminally fused with mNG. (Scale bar, 10 μm.) (*E*) Quantification of ROPGAP1 membrane/cytosolic fluorescence intensity ratio. (*F*) Distribution of ROPGAP1 intensity along the apical membrane. Data are fitted by a sum of two Gaussians with baseline curve. n = 20 (wild-type), 24 (*gef4-cKI*), 15 (*ropgef-KO*), 14 (*spk2*), and 12 (*ropgef-KO,spk2*). (*G*) Time-lapse images of actin filaments labeled with Lifeact-mCherry. (Scale bar, 5 μm.) (*H*) Actin dynamics quantified by correlation coefficient analysis. n = 10 (wild-type), n = 13 (*ropgef-KO*), 13 (*gef4-cKI*). (*I*) Time-lapse images of vesicles labeled with SCAMP4-mNG. (Scale bar, 5 μm.) (*J*) SCAMP4 dynamics quantified by correlation coefficient analysis. n = 12 (wild-type), 11 (*ropgef-KO*), 8 (*gef4-cKI*). (*K*) FRAP assays of SCAMP4 dynamics. Bleached region indicated by dashed circle. (Scale bar, 5 μm.) (*L*) Quantification of SCAMP4 fluorescence recovery. n = 9 (wild-type), 9 (*ropgef-KO*), 11 (*gef4-cKI*). (*M*) Proposed model for ROPGEF function in ROP signaling. Under basal conditions, ROPGEFs bind ROPs weakly and have low GEF activity; ROPs possess high diffusion ability, possibly due to GAP-stimulated conversion to GDP-bound form. Upon MLRK-mediated phosphorylation, ROPGEFs bind ROPs more strongly and efficiently exchange GDP for GTP. This reduces ROP diffusion and activates ROP signaling, which subsequently drives actin filament assembly and exocytosis. SPKGEFs act redundantly with ROPGEFs and may serve as primary initiators of nucleotide exchange. ROPGEFs preferentially interact with ROP-GTP and facilitate subsequent rounds of exchange following GAP-stimulated GTP hydrolysis. Data are presented as box plots showing the median and range (min to max) in (*B* and *E*) and shown as mean ± SD in (*C*, *F*, *H*, *J*, and *L*). Sample sizes in (*B* and *E*) are indicated below the bars. Data are fitted by a one-phase association curve in (*H*, *J*, and *L*). Comparisons were performed using Welch's ANOVA with Dunnett's T3 test in (*B* and *E*).

expressed in mature pollen tubes does not result in comparable phenotypes (20, 29, 64). In contrast, SPKGEFs play a profound role in development, as evidenced by severe defects upon their loss in moss (Fig. 6 *A* and *B*), *Marchantia*, and *Arabidopsis* (11, 38). Given that SPKGEFs exhibit intrinsically high GEF activity and SPK2 is critical for ROP4 activation in vivo (Figs. 2*D* and 7 *D*

Downloaded from https://www.pnas.org by SICHUAN UNIVERSITY on November 17, 2026 from IP address 211.83.126.26.

and *E*) (12), we propose that SPKGEFs mediate default ROP activation, whereas ROPGEFs fine-tune and reinforce ROP activity. The regulatable nature of ROPGEFs makes ROP signaling tunable in response to various cues, such as during pollen tube guidance (21). Since ROPGEFs and SPKGEFs emerged earlier than ROPs (33, 65), ROPs may have evolved to be differentially activated by these two classes of GEFs from the outset. Similar diversification has been reported for ROP-related GAPs in ROP inactivation (33, 38, 39, 66, 67). ROPGEFs and SPK2 are structurally different yet functionally redundant as has been observed for the two subtypes of ROP-related GAPs. It will be worthwhile to investigate how SPKGEFs and ROPGEFs collaborate in activating ROPs and integrate upstream signaling in the future.

Materials and Methods

. Moss plants used in this study were derived from the Gransden ecotype of *Physcomitrium patens* and cultured under standard conditions as previously reported (39). To identify receptor-like kinases (RLKs), protein sequences were retrieved from the genomes of *P. patens* (v6.1) and *Arabidopsis* (Araport11) and aligned using Clustal Omega implemented in Jalview (68); phylogenetic analysis was then performed using FASTTREE (69). Sequence analysis and cross-referencing with previous reports (50, 70) identified 239 putative RLKs in *P. patens*, excluding receptor-like cytoplasmic kinases that lack a transmembrane domain. Based on transcriptomic data from ref. 45, 22 candidates that showed relatively high expression in protonemata and represented diverse RLK classes were selected for interaction analysis. A full description of the materials and methods in detail is available in *SI Appendix*.

Data, Materials, and Software Availability. All study data are included in the article and/or *SI Appendix*.

ACKNOWLEDGMENTS. We are grateful to Dr. Yongliang Zhang (China Agricultural University), Dr. Zhiwen Zhu (Soochow University), and Dr. Gohta Goshima (Nagoya University) for generously sharing the TurboID, lambda protein phosphatase, and pMY337/pPGX8 plasmids, respectively. GEF assays were performed using a luminescence plate reader provided by Dr. Yang Zhang (Sichuan University). Molecular docking was conducted with assistance from Dr. Yan Yu (Sichuan University). Confocal imaging was performed with technical support from Linzhu Li and Junyang Shi at the Core Facilities, College of Life Sciences, Sichuan University. This work was supported by grants from Organization Department of the Communist Party of China Central Committee (Grant No. SQ2024QB02593) and National Natural Science Foundation of China (Grant No. 32270776) to P.Y.

1. H. Tian, R. Lyu, P. Yi, Crosstalk between Rho of plants GTPase signalling and plant hormones. *J. Exp. Bot.* **75**, 3778–3796 (2024).
2. S. Muller, Update: On selected ROP cell polarity mechanisms in plant cell morphogenesis. *Plant Physiol.* **193**, 26–41 (2023).
3. H. Ou, P. Yi, ROP GTPase-dependent polarity establishment during tip growth in plants. *New Phytol.* **236**, 49–57 (2022).
4. E. Li *et al.*, Signaling network controlling ROP-mediated tip growth in *Arabidopsis* and beyond. *Plant Commun.* **4**, 100451 (2023).
5. G. Feiguelman, Y. Fu, S. Yalovsky, ROP GTPases structure-function and signaling pathways. *Plant Physiol.* **176**, 57–79 (2018).
6. S. Yalovsky, D. Bloch, N. Sorek, B. Kost, Regulation of membrane trafficking, cytoskeleton dynamics, and cell polarity by ROP/RAC GTPases. *Plant Physiol.* **147**, 1527–1543 (2008).
7. C. Craddock, I. Lavagi, Z. Yang, New insights into Rho signaling from plant ROP/Rac GTPases. *Trends Cell Biol.* **22**, 492–501 (2012).
8. P. Denninger, Rho of plants signalling and the activating ROP guanine nucleotide exchange factors: Specificity in cellular signal transduction in plants. *J. Exp. Bot.* **75**, 3685–3699 (2024).
9. A. Berken, C. Thomas, A. Wittinghofer, A new family of RhoGEFs activates the Rop molecular switch in plants. *Nature* **436**, 1176–1180 (2005).
10. Y. Gu, S. Li, E. M. Lord, Z. Yang, Members of a novel class of *Arabidopsis* Rho guanine nucleotide exchange factors control Rho GTPase-dependent polar growth. *Plant Cell* **18**, 366–381 (2006).
11. J. L. Qiu, R. Jilk, M. D. Marks, D. B. Szymanski, The *Arabidopsis* SPIKE1 gene is required for normal cell shape control and tissue development. *Plant Cell* **14**, 101–118 (2002).
12. D. Basu, J. Le, T. Zakharova, E. L. Mallery, D. B. Szymanski, A SPIKE1 signaling complex controls actin-dependent cell morphogenesis through the heteromeric WAVE and ARP2/3 complexes. *Proc. Natl. Acad. Sci. U.S.A.* **105**, 4044–4049 (2008).
13. M. Laurin, J. F. Cote, Insights into the biological functions of Dock family guanine nucleotide exchange factors. *Genes Dev.* **28**, 533–547 (2014).
14. E. L. Mallery *et al.*, Tandem C2 domains mediate dynamic organelle targeting of a DOCK family guanine nucleotide exchange factor. *J. Cell Sci.* **135**, jcs259825 (2022).
15. M. Yanagisawa, J. M. Alonso, D. B. Szymanski, Microtubule-dependent confinement of a cell signaling and actin polymerization control module regulates polarized cell growth. *Curr. Biol.* **28**, 2459–2466 (2018).
16. C. Zhang, S. O. Kotchoni, A. L. Samuels, D. B. Szymanski, SPIKE1 signals originate from and assemble specialized domains of the endoplasmic reticulum. *Curr. Biol.* **20**, 2144–2149 (2010).
17. C. Thomas, I. Fricke, A. Scrima, A. Berken, A. Wittinghofer, Structural evidence for a common intermediate in small G protein-GEF reactions. *Mol. Cell* **25**, 141–149 (2007).
18. Y. Zhang, S. McCormick, A distinct mechanism regulating a pollen-specific guanine nucleotide exchange factor for the small GTPase Rop in *Arabidopsis thaliana*. *Proc. Natl. Acad. Sci. U.S.A.* **104**, 18830–18835 (2007).
19. P. Kaothien *et al.*, Kinase partner protein interacts with the LePRK1 and LePRK2 receptor kinases and plays a role in polarized pollen tube growth. *Plant J.* **42**, 492–503 (2005).
20. F. Chang, Y. Gu, H. Ma, Z. Yang, AtPRK2 promotes ROP1 activation via RopGEFs in the control of polarized pollen tube growth. *Mol. Plant* **6**, 1187–1201 (2013).
21. H. Takeuchi, T. Higashiyama, Tip-localized receptors control pollen tube growth and LURE sensing in *Arabidopsis*. *Nature* **531**, 245–248 (2016).
22. Y. Yu *et al.*, *Arabidopsis* PRK6 interacts specifically with AtRopGEF8/12 and induces depolarized growth of pollen tubes when overexpressed. *Sci. China Life Sci.* **61**, 100–112 (2018).
23. X. Y. Zhao *et al.*, The juxtamembrane and carboxy-terminal domains of *Arabidopsis* PRK2 are critical for ROP-induced growth in pollen tubes. *J. Exp. Bot.* **64**, 5599–5610 (2013).
24. Q. Duan, D. Kita, C. Li, A. Y. Cheung, H. M. Wu, FERONIA receptor-like kinase regulates RHO GTPase signaling of root hair development. *Proc. Natl. Acad. Sci. U.S.A.* **107**, 17821–17826 (2010).
25. L. Zhu *et al.*, The *Arabidopsis* CrRLK1L protein kinases BUPS1 and BUPS2 are required for normal growth of pollen tubes in the pistil. *Plant J.* **95**, 474–486 (2018).
26. X. Zhou *et al.*, Membrane receptor-mediated mechano-transduction maintains cell integrity during pollen tube growth within the pistil. *Dev. Cell* **56**, 1030–1042 (2021).
27. X. Kou *et al.*, PbrROP1/2-elicited imbalance of cellulose deposition is mediated by a CrRLK1L-ROPGEF module in the pollen tube of *Pyrus*. *Hortic. Res.* **9**, uhab034 (2022).
28. W. Lin *et al.*, *Arabidopsis* pavement cell morphogenesis requires FERONIA binding to pectin for activation of ROP GTPase signaling. *Curr. Biol.* **32**, 497–507 (2022).
29. A. M. Bouatta, F. Anzenberger, L. Riederauer, A. Lepper, P. Denninger, Polarized subcellular activation of Rho proteins by specific ROPGEFs drives pollen germination in *Arabidopsis thaliana*. *PLoS Biol.* **23**, e3003139 (2025).
30. T. Zhao *et al.*, An AGC kinase cascade regulates ROP signaling for the correct timing of pollen germination. *New Phytologist*, 10.1111/nph.71665 (2026).
31. G. Q. Huang *et al.*, *Arabidopsis* RopGEF4 and RopGEF10 are important for FERONIA-mediated developmental but not environmental regulation of root hair growth. *New Phytol.* **200**, 1089–1101 (2013).
32. T. Hiwatashi *et al.*, The RopGEF KARAPPO is essential for the initiation of vegetative reproduction in *Marchantia polymorpha*. *Curr. Biol.* **29**, 3525–3531 (2019).
33. H. Mulvey, L. Dolan, Rho of plant signaling was established early in streptophyte evolution. *Curr. Biol.* **33**, 5515–5525 (2023).
34. P. Yi, G. Goshima, Rho of plants GTPases and cytoskeletal elements control nuclear positioning and asymmetric cell division during *Physcomitrella patens* branching. *Curr. Biol.* **30**, 2860–2868 (2020).
35. A. Le Bail *et al.*, Essential developmental processes in *Physcomitrium patens* require distinct levels of total activity provided by functionally redundant PpROP GTPases. *New Phytol.* **248**, 2865–2890 (2025).
36. H. Mulvey, L. Dolan, Rho GTPase of plants regulates polarized cell growth and cell division orientation during morphogenesis. *Curr. Biol.* **33**, 2897–2911 (2023).
37. X. Cheng, B. W. Mwaura, S. R. Chang Stauffer, M. Bezanilla, A fully functional ROP fluorescent fusion protein reveals roles for this GTPase in subcellular and tissue-level patterning. *Plant Cell* **32**, 3436–3451 (2020).
38. Y. Sakai *et al.*, Regulation of ROP GTPase cycling between active and inactive states is essential for vegetative organogenesis in *Marchantia polymorpha*. *Development* **151**, dev202928 (2024).
39. J. Ruan, L. Lai, H. Ou, P. Yi, Two subtypes of GTPase-activating proteins coordinate tip growth and cell size regulation in *Physcomitrium patens*. *Nat. Commun.* **14**, 7084 (2023).
40. C. Bascom Jr. *et al.*, Systematic survey of the function of ROP regulators and effectors during tip growth in the moss *Physcomitrella patens*. *J. Exp. Bot.* **70**, 447–457 (2019).
41. M. A. Mecchia *et al.*, The single *Marchantia polymorpha* FERONIA homolog reveals an ancestral role in regulating cellular expansion and integrity. *Development* **149**, dev200580 (2022).
42. S. Honkanen *et al.*, The mechanism forming the cell surface of tip-growing rooting cells is conserved among land plants. *Curr. Biol.* **26**, 3238–3244 (2016).
43. J. Westermann *et al.*, An evolutionarily conserved receptor-like kinases signaling module controls cell wall integrity during tip growth. *Curr. Biol.* **29**, 3899–3908 (2019).
44. D. M. Eklund, E. M. Svensson, B. Kost, *Physcomitrella patens:* A model to investigate the role of RAC/ROP GTPase signalling in tip growth. *J. Exp. Bot.* **61**, 1917–1937 (2010).
45. C. Ortiz-Ramirez *et al.*, A transcriptome atlas of *Physcomitrella patens* provides insights into the evolution and development of land plants. *Mol. Plant* **9**, 205–220 (2016).
46. B. Kost *et al.*, Rac homologues and compartmentalized phosphatidylinositol 4,5-bisphosphate act in a common pathway to regulate polar pollen tube growth. *J. Cell Biol.* **145**, 317–330 (1999).
47. H. Li, Y. Lin, R. M. Heath, M. X. Zhu, Z. Yang, Control of pollen tube tip growth by a Rop GTPase-dependent pathway that leads to tip-localized calcium influx. *Plant Cell* **11**, 1731–1742 (1999).
48. P. O. Ljungdahl, B. Daignan-Fornier, Regulation of amino acid, nucleotide, and phosphate metabolism in *Saccharomyces cerevisiae*. *Genetics* **190**, 885–929 (2012).
49. M. Chen *et al.*, RopGEF7 regulates PLETHORA-dependent maintenance of the root stem cell niche in *Arabidopsis*. *Plant Cell* **23**, 2880–2894 (2011).
50. S. H. Shiu, A. B. Bleecker, Receptor-like kinases from *Arabidopsis* form a monophyletic gene family related to animal receptor kinases. *Proc. Natl. Acad. Sci. U.S.A.* **98**, 10763–10768 (2001).
51. Y. Kong *et al.*, Structural and biochemical basis of *Arabidopsis* FERONIA receptor kinase-mediated early signaling initiation. *Plant Commun.* **4**, 100559 (2023).

Downloaded from https://www.pnas.org by SICHUAN UNIVERSITY on November 17, 2026 from IP address 211.83.126.26.

52. J. Abramson *et al.*, Accurate structure prediction of biomolecular interactions with AlphaFold 3. *Nature* **630**, 493–500 (2024).
53. P. Yi, G. Goshima, Transient cotransformation of CRISPR/Cas9 and oligonucleotide templates enables efficient editing of target loci in *Physcomitrella patens*. *Plant Biotechnol. J.* **18**, 599–601 (2020).
54. Y. Zhang *et al.*, TurboID-based proximity labeling reveals that UBR7 is a regulator of N NLR immune receptor-mediated immunity. *Nat. Commun.* **10**, 3252 (2019).
55. H. Sternberg *et al.*, Formation of self-organizing functionally distinct Rho of plants domains involves a reduced mobile population. *Plant Physiol.* **187**, 2485–2508 (2021).
56. Y. Nagashima *et al.*, A Rho-based reaction-diffusion system governs cell wall patterning in metaxylem vessels. *Sci. Rep.* **8**, 11542 (2018).
57. E. Li *et al.*, AGC1.5 kinase phosphorylates RopGEFs to control pollen tube growth. *Mol. Plant* **11**, 1198–1209 (2018).
58. E. Li *et al.*, A positive feedback circuit for ROP-mediated polar growth. *Mol. Plant* **14**, 395–410 (2021).
59. X. Zhang *et al.*, RLCKs phosphorylate RopGEFs to control auxin-dependent *Arabidopsis* development. *Nat. Plants* **11**, 2130–2144 (2025).
60. Z. Li *et al.*, Abscisic acid-induced degradation of *Arabidopsis* guanine nucleotide exchange factor requires calcium-dependent protein kinases. *Proc. Natl. Acad. Sci. U.S.A.* **115**, E4522–E4531 (2018).
61. Z. Shi *et al.*, A GhSnRK10-GhRopGEF5-GhROP10 signaling pathway regulates cotton fiber cell growth. *Plant Commun.* **6**, 101483 (2025).
62. M. Wang *et al.*, Phosphorylation of MtRopGEF2 by LYK3 mediates MtROP activity to regulate rhizobial infection in *Medicago truncatula*. *J. Integr. Plant Biol.* **63**, 1787–1800 (2021).
63. X. Xiang *et al.*, Rho of plant proteins are essential for pollen germination in *Arabidopsis*. *Plant Physiol.* **193**, 140–155 (2023).
64. X. Zhou *et al.*, SPA, a stigma-style-transmitting tract physical microenvironment assay for investigating mechano-signaling in pollen tubes. *Proc. Natl. Acad. Sci. U.S.A.* **120**, e2314325120 (2023).
65. M. Elias, The guanine nucleotide exchange factors Sec2 and PRONE: Candidate synapomorphies for the Opisthokonta and the Archaeplastida. *Mol. Biol. Evol.* **25**, 1526–1529 (2008).
66. G. Wu, H. Li, Z. Yang, *Arabidopsis* RopGAPs are a novel family of rho GTPase-activating proteins that require the Cdc42/Rac-interactive binding motif for rop-specific GTPase stimulation. *Plant Physiol.* **124**, 1625–1636 (2000).
67. J. U. Hwang, V. Vernoud, A. Szumlanski, E. Nielsen, Z. Yang, A tip-localized RhoGAP controls cell polarity by globally inhibiting Rho GTPase at the cell apex. *Curr. Biol.* **18**, 1907–1916 (2008).
68. A. M. Waterhouse, J. B. Procter, D. M. Martin, M. Clamp, G. J. Barton, Jalview version 2–A multiple sequence alignment editor and analysis workbench. *Bioinformatics* **25**, 1189–1191 (2009).
69. M. N. Price, P. S. Dehal, A. P. Arkin, FastTree 2–Approximately maximum-likelihood trees for large alignments. *PLoS ONE* **5**, e9490 (2010).
70. A. Dievart, C. Gottin, C. Perin, V. Ranwez, N. Chantret, Origin and diversity of plant receptor-like kinases. *Annu. Rev. Plant Biol.* **71**, 131–156 (2020).

Downloaded from https://www.pnas.org by SICHUAN UNIVERSITY on November 17, 2026 from IP address 211.83.126.26.

PNAS

Supporting Information for

Activation of ROPGEFs by a malectin-like receptor kinase is involved in tip growth regulation in *Physcomitrium patens*

Ruohan Lyu[1,3], Jingtong Ruan[1,3], Ying Chen[1,3], Haoyu Tian[1], Peishan Yi[1,2 *]

[1] Key Laboratory of Bio-Resource and Eco-Environment of Ministry of Education, Laboratory for Ex Situ Conservation and Resource Utilization of Mountain Plants, College of Life Sciences, Sichuan University, Chengdu 610065, Sichuan, P.R. China
[2] Chengdu Botanical Garden, Chengdu 610083, Sichuan, P.R. China
[3] These authors contributed equally to this work

[*] Corresponding author: yipeishan@scu.edu.cn

This PDF file includes:

Supporting text (Detailed Materials and Methods)
Figures S1 to S17
Tables S1 to S3
SI References

Supporting Text

Materials and Methods

Moss plants and culture conditions

All moss plants used in this study were derived from the Gransden ecotype of *Physcomitrium patens*. Plants were cultured on standard solid BCDAT medium at 24 °C under continuous light and were propagated via homogenization to maintain vegetative growth at the protonemal stage. Imaging samples were prepared by inoculating a small piece of protonemal tissue into 35 mm glass-bottom imaging dishes containing solid BCD medium. Imaging was performed after 5–7 days of culture.

Sequence analyses

DNA and protein sequences were retrieved from Phytozome and Uniprot databases. To identify receptor-like kinases (RLKs), kinases that encode >200 amino acids and were predicted to contain one to three transmembrane domains by TMHMM2.0 were isolated from the genomes of *P. patens* (v6.1) and *Arabidopsis* (Araport11). Protein sequences containing an intact kinase domain were aligned using Clustal Omega implemented in Jalview (1). Phylogenetic tree was constructed using FASTTREE (2). Through cross-referencing with previous reports (3, 4), 239 RLK candidates in *P. patens* were identified and used to build a phylogenetic tree. Receptor-like cytoplasmic kinases (RLCKs) lacking a transmembrane domain in moss were excluded from this analysis. Based on transcriptomic data from (5), 22 candidate RLKs showing relatively high expression in protonemata and representing diverse RLK classes were selected for interaction analysis.

Structural prediction and molecular docking

Alphafold3 was used to generate structural models for ROP4(1-180, excluding the C-terminal tail) and the PRONE domains for ROPGEF4(86-451) and ROPGEF6(203-574). For each GEF, three variants were modeled: wild-type, a phosphorylated form, and a Ser-to-Ala non-phosphorylatable form. These predicted structures were used as inputs for protein-protein docking with HADDOCK3. Docking simulations were performed in the presence of GTP, GDP, or in the absence of nucleotide, using experimentally validated AtROP4-AtPRONE8 complex (PDB: 2NTY) as a reference (6). The docking protocol followed a standard three-stage procedure consisting of rigid-body docking, semi-flexible refinement, and water refinement. Dynamic molecular simulations using GROMACS

(AMBER99SB-ILDN force field, TIP3P water model) was performed to further assess the reliability of the predicted complexes.

Molecular biology

CRISPR targets for genome editing were manually selected and added to the single-guide RNA (sgRNA) expression vector (pPY156) via site-directed mutagenesis. Single-stranded oligonucleotide templates were synthesized at a concentration of 50 μM. Target and template sequences were provided in Figure S16. For fluorescent protein knock-in, targeting plasmids were constructed by inserting three fragments, comprising two 1-1.3 kb homology arms flanking the insertion site and an insert fragment, into the pPY22 vector using InFusion (Takara, cat. 638948). For N-terminal tagging, fluorescent protein coding sequence, with or without a TurboID tag, was placed immediately downstream of the start codon. For C-terminal tagging, the insert fragment contained fluorescent protein coding sequence (with or without a TurboID tag) followed by a *nos* terminator and a hygromycin B or geneticin resistance cassette, and was inserted upstream of the stop codon. For overexpression constructs, the coding sequence of target proteins was fused in-frame with a fluorescent protein and cloned into a pENTR vector via InFusion. This cassette was then transferred into the pPY138, pMY337, or pPGX8 vectors through LR recombination (Thermo, cat. 11791019). Plasmids for yeast two-hybrid assays and recombinant protein expression were constructed by inserting protein-coding sequences into the widely available pGADT7/pGBKT7, pET28a-His, pET28a-MBP, or pGEX-GST vectors via InFusion. Mutations or truncations were introduced via site-directed mutagenesis. Details for primers, plasmids, and moss strains are provided in Table S1-S3.

Moss transformation

Transformations were performed following a modified protocol. Briefly, fresh protonemata were harvested after seven days of culture and digested with 0.5% driselase to remove cell walls. Protoplasts were washed with 8% mannitol and resuspended in MMM buffer (9% mannitol, 0.1% MES pH5.6, 15 mM $MgCl_2$). For each transformation, 300 μl of protoplasts were mixed with 30 μg of DNA, combined with 300 μl of PEG6000 solution, and incubated at room temperature for 30 min. Subsequently, 1.5 ml of pre-chilled W5 buffer (2 mM MES pH5.7, 5 mM KCl, 125 mM $CaCl_2$, 154 mM NaCl) was added and gently mixed. Protoplasts were then collected, resuspended in PRMT medium, plated, and cultured under standard conditions. After five days of regeneration, protoplast-derived plants were subject to one or two rounds of drug selection. Surviving clones were isolated, and genome modifications

were validated by PCR and DNA sequencing. CRISPR-mediated genome editing was performed by co-transforming 10 µg of the sgRNA plasmid and an equal amount of the pAct-Cas9 plasmid. 10 µL of 50 µM oligonucleotide donor template was additionally supplemented in the transformation mixture for *ropgef* knockout, whereas no templates were used for *spk2* editing. For homology-directed insertion of fluorescent protein overexpression cassettes, 30 µg of targeting plasmids were linearized by restriction enzyme digestion prior to transformation. To generate fluorescent protein knock-in lines, 30 µg of targeting plasmids were co-transformed with sgRNA and Cas9 plasmids (10 µg each).

Confocal microscopy

Imaging was performed using an Olympus SpinSR spinning disk confocal microscope, controlled by cellSens Dimension software. The system's core components include an IX83P2ZF inverted microscope equipped with a range of objectives (10×/NA 0.40, 20×/NA 0.70, 40×/NA 0.95, 60×/NA 1.42, and 100×/NA 1.48), a Yokogawa CSU-W1 confocal scanner unit powered by 405-nm, 488-nm, and 561-nm diode lasers, and a Hamamatsu ORCA Flash 4.0 V3 sCMOS camera for detection. The laser power was set to 50% for all wavelengths. Exposure times were 500 ms for the 488-nm and 561-nm lasers and 100 ms for the 405-nm laser. Time-lapse images were acquired at intervals of two minutes for cell growth analysis and 500 ms for monitoring subcellular dynamics. Fluorescence recovery after photobleaching (FRAP) experiments were performed using the FV3000 scanning module. A circular region of interest was photobleached by applying a 5-second pulse from a 561-nm or 488-nm diode laser (10% power). Recovery of fluorescence was subsequently monitored and recorded through time-lapse imaging at 500ms intervals with the same laser attenuated to 2% power using FV31S-SW software. To image calcofluor-stained samples, plants were incubated in 100 µl of 10 µg/ml Calcofluor White (Sigma 18909-100ML-F) and kept in the dark for 15 min at room temperature. For inducible expression of ROPGEFs, samples were transiently treated with 100 µl of 1 µM β-estradiol for 5 min prior to imaging.

Image processing and analyses

All images were processed and analyzed using Fiji software (version 2.14.0). Fluorescence intensity distribution along the apical membrane was quantified by measuring signal intensity along a 1-pixel-wide line tracing approximately 20 µm of the apical membrane. To compare membrane and cytosolic signals, mean intensities were measured from three equivalently sized regions (~5 µm in length): one positioned at the apical membrane, one

in the adjacent cytosol, and one in a background area. The subcellular dynamics of ROPGEFs, actin filaments, and SCAMP4-labeled vesicles was measured from time-lapse images of the ~5-μm-long apex. Correlation coefficients were calculated using the Image CorrelationJ 1o plugin with default settings under the fixed slide model. For FRAP experiments, normalized fluorescence intensity at the bleached region in each frame was calculated as $I = (I_{bleach} - I_{background}) / (I_{non\text{-}bleach} - I_{background})$, where I_{bleach} is the intensity of the bleached region, $I_{non\text{-}bleach}$ is the intensity of a non-bleached reference region, and $I_{background}$ is the background intensity. Fluorescence recovery was subsequently calculated as $R_t = (I_t - I_1) / (I_0 - I_1)$, where I_0 is the pre-bleach intensity, I_1 is the intensity of the first post-bleach frame, and I_t is the intensity at each subsequent time point.

Yeast two-hybrid assay

Approximately 0.1 μg of plasmids encoding AD- or BD-fusion proteins were co-transformed along with 100 μg of carrier DNA into competent AH109 yeast cells. Transformants were initially selected on solid medium lacking tryptophan and leucine (2SD). Positive colonies were then propagated and spotted onto medium lacking tryptophan, leucine, histidine, and adenine (4SD) to assess protein–protein interactions. For each transformation, similar results were obtained with at least three independent clones.

Protein purification and pull-down assays

Recombinant proteins were expressed in *E. coli* BL21(DE3) cells and purified as follows. ROP4(2-180) and its CA/DN variants were purified with a 6xHis tag using TALON Metal Affinity Resin (Takara, cat. 635501) for GEF assay or with a GST tag using Pierce Glutathione Agarose (Thermo, cat. 16100) for pull-down analysis. MBP-tagged ROPGAP1(2-469), various ROPGEF4/6 constructs, and DHR2 domain of SPK1(1440-1887) and SPK6(1420-1887) were purified using Amylose Resin (New England Biolabs, cat. E9021V). The cytoplasmic domain of MLRK1 (residues 457-872) and its mutant variants containing a functional kinase domain were toxic to bacteria. The relevant proteins were co-expressed with lambda protein phosphatase. For *in vitro* phosphorylation assays, MLRK1(457-872) and its variants were purified as MBP fusions; for pull-down assays, they were purified as GST fusions. To assess ROPGEF-ROP4 interactions, pull-down assays were performed by incubating equal amounts (20 μg each) of MBP-ROPGEFs with on-bead GST-ROP4 at 4°C overnight. The beads were subsequently washed six times, and bound proteins were eluted by boiling and analyzed by SDS-PAGE. For ROPGEF-MLRK interactions, assays were conducted similarly using on-bead GST-MLRK1 and eluted

MBP-ROPGEFs. MBP-Citrine served as a negative control. Each experiment was repeated at least three times. Relative binding was quantified using Fiji by measuring band intensities, normalizing them to the input signal, and calculating protein amounts as percentages without background subtraction.

In vitro phosphorylation assay

MBP-MLRK1(457-872) or its variants and MBP-ROPGEFs were enriched by column filtration in Tris-HCl buffer (20 mM Tris-HCl, 150 mM NaCl). Then equal amounts (10 μg each) of MLRK1 and ROPGEFs were mixed in phosphorylation buffer (40 mM HEPES pH 7.5, 80 mM $MgCl_2$, 0.4 mM ATP, 40 mM DTT, 20 mM EGTA pH 8.0) and incubated at 37°C for 2 h. Reactions were terminated by boiling, and samples were resolved by SDS-PAGE. Phosphorylation was detected using Pro-Q Diamond Phosphoprotein Gel Stain (Invitrogen, cat. P33300) following the manufacturer's instructions. Total protein loading was visualized by subsequent staining with Coomassie Blue. Phosphorylation levels were quantified in Fiji by measuring the intensity of the phospho-band normalized to the untreated samples. Untreated purified proteins (without phosphorylation buffer) served as the pre-treatment control, whereas a parallel ATP-free reaction containing phosphorylation buffer served as the non-phosphorylation control. Identical treatments were performed for wild-type MLRK1(CD) and MLRK1(K551R).

Kinase assay

All kinase assays were performed using the Kinase-Glo Luminescent Kinase Assay Platform kit (Promega, cat. V6711) according to the manufacturer's instruction. Briefly, purified proteins were pre-cleaned by column filtration in Tris-HCl buffer (20 mM Tris-HCl, 150 mM NaCl) to remove potential contaminants. Then, kinase reactions (10 μl each) were conducted with the indicated amounts of kinase, substrate, and ATP in kinase buffer (40 mM HEPES pH 7.5, 20 mM $MgCl_2$, 1mM DTT) and incubated for 30 min at room temperature. After adding an equal volume of Kinase-Glo reagent and incubating for 10 min, luminescence was measured. For MLRK1 autophosphorylation, 10 μM ATP was used without exogenous substrates, and reactions contained 0~2.0 μM MLRK1(CD) or MLRK1(K551R). Luminescence from reactions lacking MLRK1 was used for normalization. For ROPGEF4/6 phosphorylation, MLRK1(CD) was first autophosphorylated and re-purified by column filtration. Subsequent kinase reactions contained 0.25 μM pre-phosphorylated MLRK1(CD) and, 1 μM ATP, and 0~0.5 μM ROPGEF4 or ROPGEF6.

Reactions without ROPGEF4/6 serves as the normalization reference. All assays were performed in three technical replicates.

GEF assay

GEF activity was detected using GTPase-Glo Assay Kit (Promega, cat. V7681) according to the manufacturer's instructions. Each reaction (16 µl) contained 10 µM GTP, 2 µM His-ROP4(2–180), 1 µM MBP-ROPGAP1, and varying concentrations of MBP-ROPGEFs or MBP-SPKs (0.1, 0.6, or 3.6 µM) in GEF buffer. Reactions were incubated at room temperature for 2 h, followed by the addition of an equal volume of reconstituted GTPase-Glo reagent and a further 30 min incubation. Subsequently, 32 µl of detection buffer was added, and the mixture was incubated for 10 min prior to luminescence recording. For assays involving phosphorylated proteins, phosphorylated samples were enriched through column filtration (Beyotime Biotechnology, cat. FUF051) using Tris-HCl buffer (20 mM Tris-HCl, 150 mM NaCl) and washed three times to remove residual ATP. ROPGEFs in the enriched fractions were analyzed with SDS-PAGE to determine the concentration and then used for GEF activity detection. MBP alone was included as a negative control, and its post-reaction fluorescence intensity was used as a reference for normalization. All assays were conducted with at least three technical replicates.

Phosphosite mapping

Liquid chromatography-tandem mass spectrometry (LC-MS/MS) was used to identify phosphosites in MLRK1, ROPGEF4, and ROPGEF6, with technical support from Shanghai OE Biotech Co., Ltd. Briefly, protein samples were separated by SDS-PAGE, digested with 0.02 µg/µL trypsin, and desalted using a C18 column. The resulting peptides were resuspended in Nano-HPLC Buffer A (0.1% formic acid in water), separated by Nano-HPLC (UltiMate3000 RSLCnano, Thermo Fisher Scientific), and detected using a Q-Exactive Plus mass spectrometer (Thermo Fisher Scientific). The detected peptides were mapped against the *Physcomitrium patens* proteome (UniProt ID: 3218) using Proteome Discoverer 2.5.

Statistical analysis

Graphical data are presented as mean ± standard deviations (SD) or box plots with median and range (min to max). Individual data points are shown in all graphs except for GEF assays, wherein the SD is too small to display data points. Sample sizes (n) were specified in figure panels, figure legends, or in the main text. Our statistical analyses followed a

structured workflow based on data distribution and group comparisons. All datasets were initially assessed for normality. For comparisons involving two groups, normally distributed data were analyzed using an unpaired, two-tailed Student's t-test, applied with Welch's correction when group variances were significantly different, or without it when variances were equal. Non-normally distributed data were analyzed using the Mann-Whitney U test. For comparisons involving three or more groups, normally distributed data were evaluated using one-way ANOVA, whereas non-normally distributed data were assessed using the Kruskal–Wallis test. Both overall tests were followed by appropriate post-hoc procedures. For ANOVA post-hoc, pairwise comparisons across all groups were performed using Tukey's test (equal variances) or Holm-Šídák test (unequal variances); comparisons against a single reference were performed using Dunnett's test (equal variances) or Dunnett's T3 test (unequal variances). For Kruskal–Wallis post-hoc, comparisons were conducted using Dunn's multiple comparisons test. A *p*-value of less than 0.05 was considered statistically significant.

Accession numbers

ROPGEF1, Pp6c2_2730/Pp3c2_4460; ROPGEF2, Pp6c10_5320/Pp3c10_9910; ROPGEF3, Pp6c1_10/Pp3c1_20; ROPGEF4, Pp6c2_15530/Pp3c2_28420; ROPGEF5, Pp6c14_12390/Pp3c14_22480; ROPGEF6, Pp6c1_19180/Pp3c1_36410; MLRK1, Pp6c9_5300/Pp3c9_10730; MLRK2, Pp6c9_5280/Pp3c9_10640; MLRK3, Pp6c9_5320/Pp3c9_10760; MLRK4, Pp6c20_9480/Pp3c20_17290; MLRK5, Pp6c20_9280/Pp3c20_16970; ROP4, Pp6c10_2660/Pp3c10_4950; ROPGAP1, Pp6c4_8830/Pp3c4_16800; SPK1, Pp6c15_4830/Pp3c15_8680; SPK2, Pp6c9_7500/Pp3c9_15160; SPK6, Pp6c10_8890/Pp3c10_16640; AtROPGEF1, AT4G38430; AtROP1, AT3G51300; AtROPGAP1, AT5G22400.

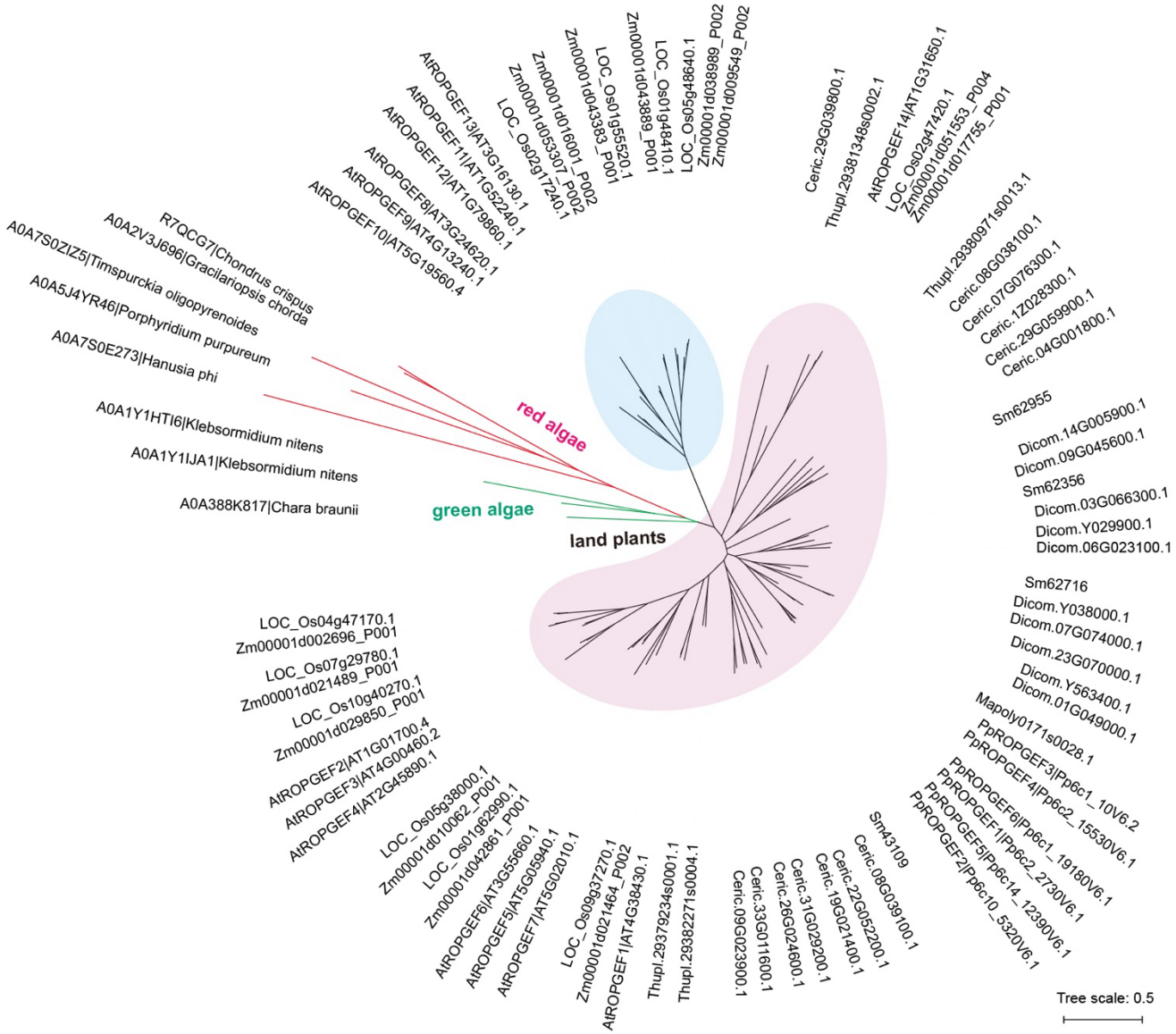


Figure S1. Phylogeny of ROPGEFs in representative plant lineages.

The phylogenetic tree was constructed using FASTTREE with aligned sequences of selected ROPGEFs in red algae (red branches), green algae (green branches), and land plants (black branches). Note that ROPGEFs in land plants form two distinct clades, with one present in all land plants and the other specifically found in angiosperms.

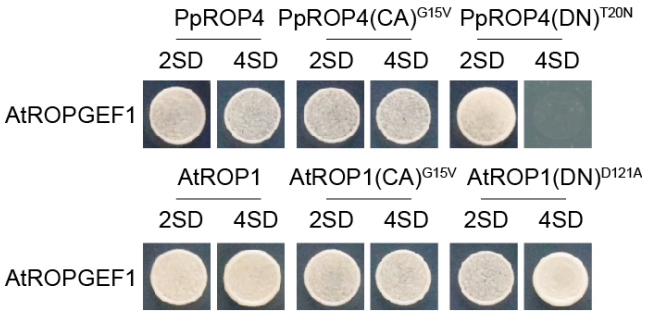


Figure S2. AtROPGEF1 interacts with AtROP1 and PpROP4.

AtROPGEF1 interacts with three forms of AtROP1 but preferentially binds nucleotide-free and constitutively active PpROP4 in yeast two-hybrid assays. CA, constitutively active form; DN, dominant-negative form.

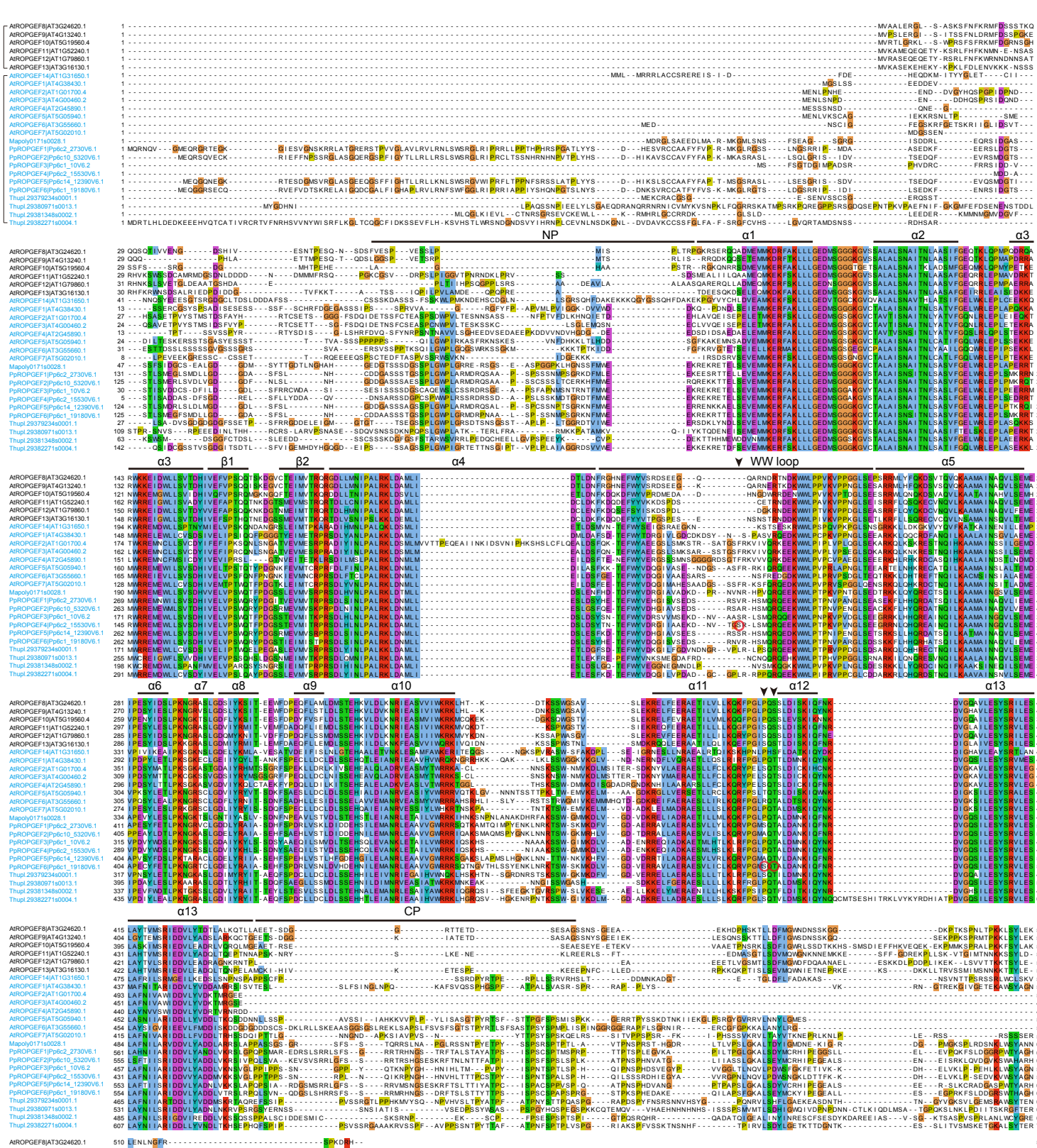


Figure S3. Sequence alignment of representative ROPGEFs in land plants.
ROPGEFs in *P. patens* (moss), *M. polymorpha* (liverwort), *Thuja plicata* (gymnosperm), and *Arabidopsis* (angiosperm) were aligned using Clustal Omega. Secondary structures are annotated based on the experimentally resolved AtPRONE8 structure (PDB: 2NTY) (6). The S231 residue in PpROPGEF4 and S524/T526 residues in PpROPGEF6, which are phosphorylated by MLRK1, are highlighted with arrowheads and circles. NP, N-terminal proximal region of PRONE domain; CP, C-terminal proximal region of PRONE domain.

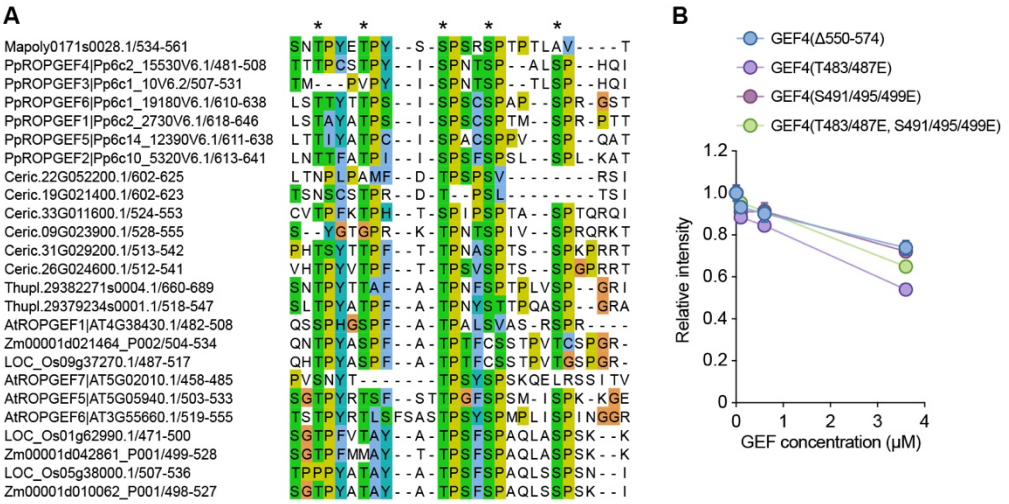
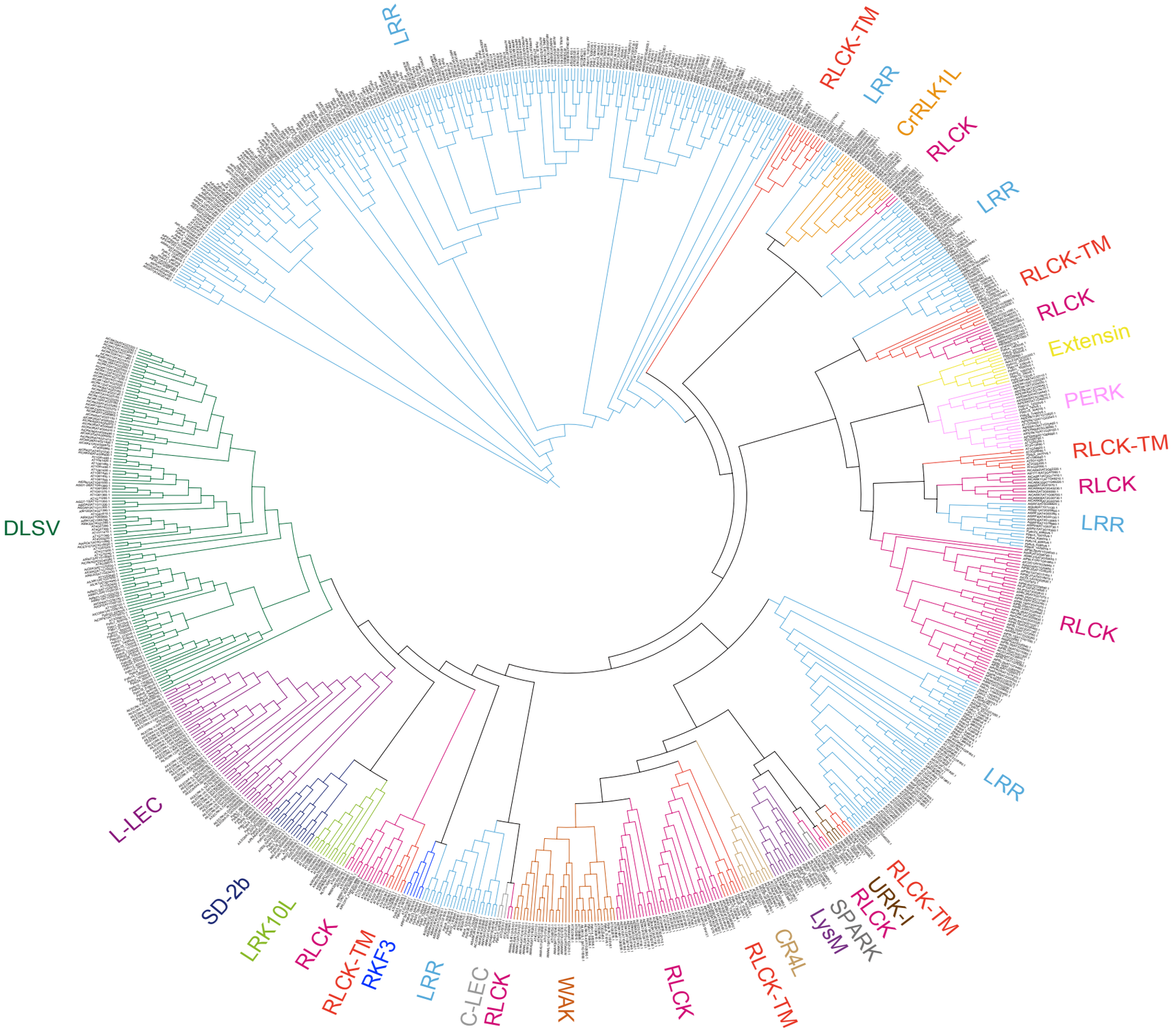


Figure S4. Deletion or phosphomimic mutations in ROPGEF4 C-terminus did not increase GEF activity.

(A) Sequence alignment of the relatively conserved region in ROPGEF C-terminus. Asterisks indicate putative phosphorylatable S/T-P motifs.

(B) GEF activity of deletion or phosphomimic variants of ROPGEF4 toward ROP4. Data are mean ± SD (n = 3 per group).



GROUP	LRR	RLCK	DLSV	L-LEC	WAK	RLCK-TM	PERK	CrRLK1L	CR4L
Arabidopsis	223	130	89	45	28	27	18	15	9
P. patens	138	ND	28	7	4	18	4	5	1
GROUP	LRK10L	URK-I	SD-2b	LysM	Extensin	RKF3	SPARK	C-LEC	
Arabidopsis	13	0	9	7	3	2	2	1	
P. patens	0	4	7	7	9	4	1	2	

Figure S5. Phylogeny of putative receptor-like kinases in *P. patens* and *Arabidopsis*.
The phylogenetic tree was constructed using FASTTREE. Subclades were categorized based on (3, 4). Receptor-like cytoplasmic kinases (RLCKs) that lack a transmembrane domain in *P. patens* are not included.

A

Number	Gene v6.1	Gene v3.3	Transcript v1.1	Type[a]
T1	Pp6c1_10080	Pp3c1_18260	Pp1s43_33V6.1	LRR
T2	Pp6c22_5320	Pp3c22_10000	Pp1s121_138V6.1	LRR
T3	Pp6c20_9480[b]	Pp3c20_17290	Pp1s44_215V6.1	CrRLK1L
T4	Pp6c9_5300[c]	Pp3c9_10730	Pp1s29_343V6.1	CrRLK1L
T5	Pp6c1_11720	Pp3c1_22560	Pp1s59_314V6.1	LRR
T6	Pp6c22_600	Pp3c22_1220	Pp1s162_151V6.1	LRR
T7	Pp6c26_5020	Pp3c26_8100	Pp1s217_54V6.1	LRR
T8	Pp6c7_11850	Pp3c7_22250	Pp1s2_206V6.1	RLCK-TM
T9	Pp6c3_10010	Pp3c3_19490	Pp1s204_22V6.1	LRR
T10	Pp6c8_1920	Pp3c8_3330	Pp1s35_219V6.1	LRR
T11	Pp6c15_8660	Pp3c15_17310	Pp1s359_8V6.1	LRR
T12	Pp6c2_13310	Pp3c2_23960	Pp1s135_48V6.1	LRR
T13	Pp6c2_9950	Pp3c2_17640	Pp1s281_115V6.1	LRR
T14	Pp6c25_2430	Pp3c27_4590	Pp1s54_23V6.1	DLSV
T15	Pp6c1_6190	Pp3c1_10810	Pp1s139_84V6.1	DLSV
T16	Pp6c2_16790	Pp3c2_30340	Pp1s22_36V6.1	DLSV
T17	Pp6c5_9540	Pp3c5_17880	Pp1s116_173V6.1	L-LEC
T18	Pp6c15_9400	Pp3c15_19160	Pp1s206_38V6.1	URK-I
T19	Pp6c11_3510	Pp3c11_6330	Pp1s364_10V6.1	LysM
T20	Pp6c1_10060	Pp3c1_18280	Pp1s43_35V6.1	Extensin
T21	Pp6c14_8820	Pp3c14_15710	Pp1s209_44V6.1	WAK
T22	Pp6c4_9910	Pp3c4_18780	Pp1s13_59V6.1	LRR

[a] categorized based on Shiu and Bleecker, 2001. PNAS, 98(19): 10763-10768.
[b] MLRK4 in this study.
[c] MLRK1 in this study.

B

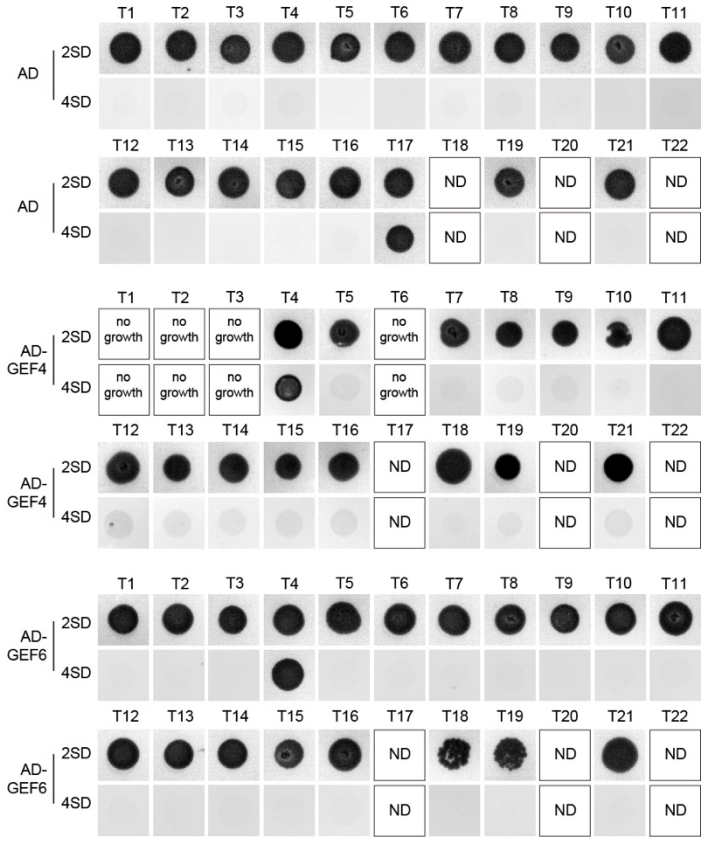
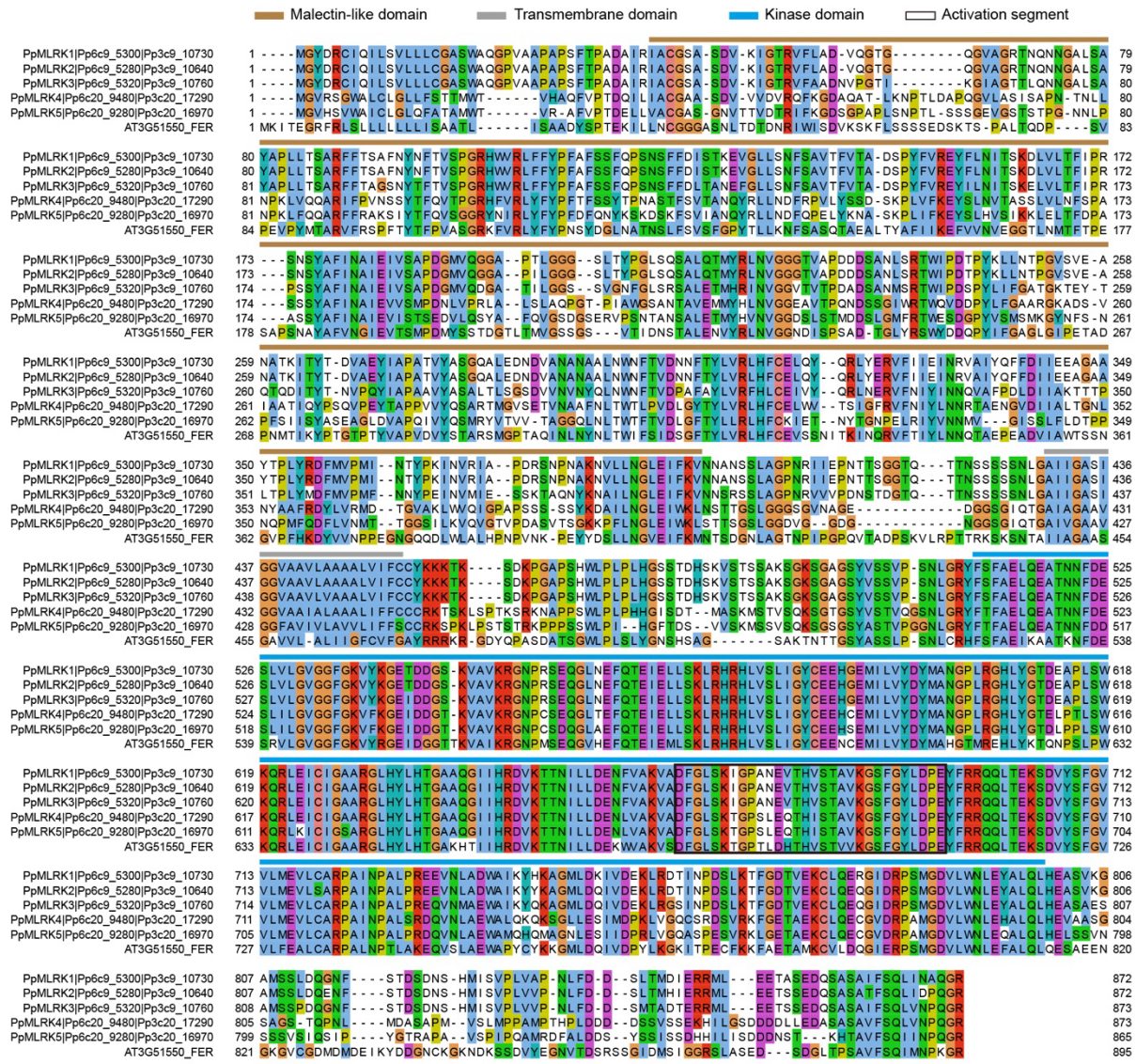


Figure S6. Candidate screen identifies MLRK1 as a ROPGEF-interacting protein.

(A) Selected RLKs that span distinct subclades and are highly expressed in protonemata.

(B) Yeast two-hybrid results for testing interactions between candidate RLKs and ROPGEF4/6. ND, not determined due to unsuccessful plasmid construction or yeast transformation.



Pairwise identity of the cytoplasmic domain

	PpMLRK1	PpMLRK2	PpMLRK3	PpMLRK4	PpMLRK5	AtFER
PpMLRK1		97.36	95.19	71.26	69.14	62.21
PpMLRK2			95.19	71.02	68.90	62.68
PpMLRK3				72.68	70.10	62.76
PpMLRK4					80.14	59.63
PpMLRK5						58.22
AtFER						

Figure S7. Sequence alignment of moss MLRKs and *Arabidopsis* FERONIA.

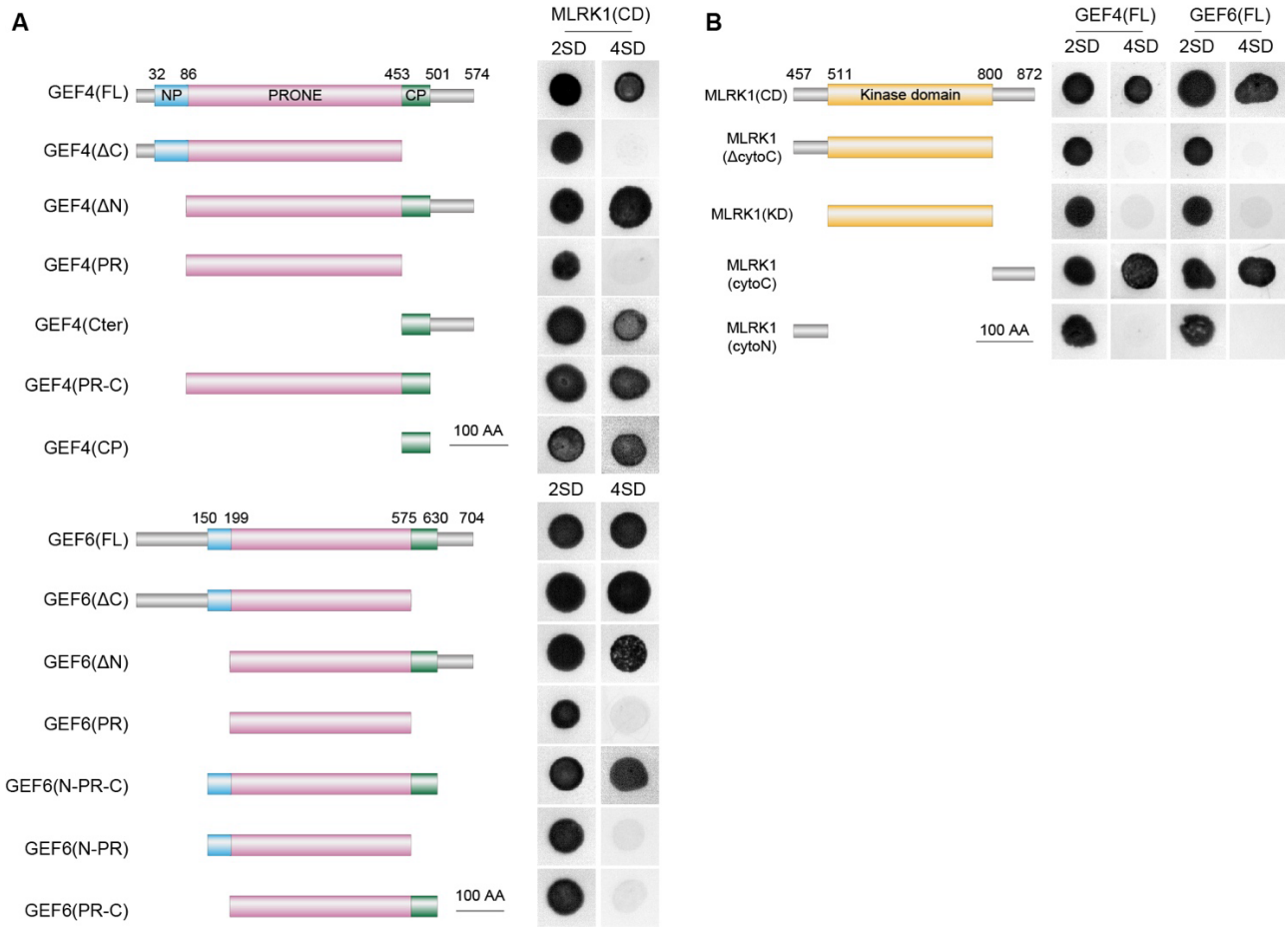
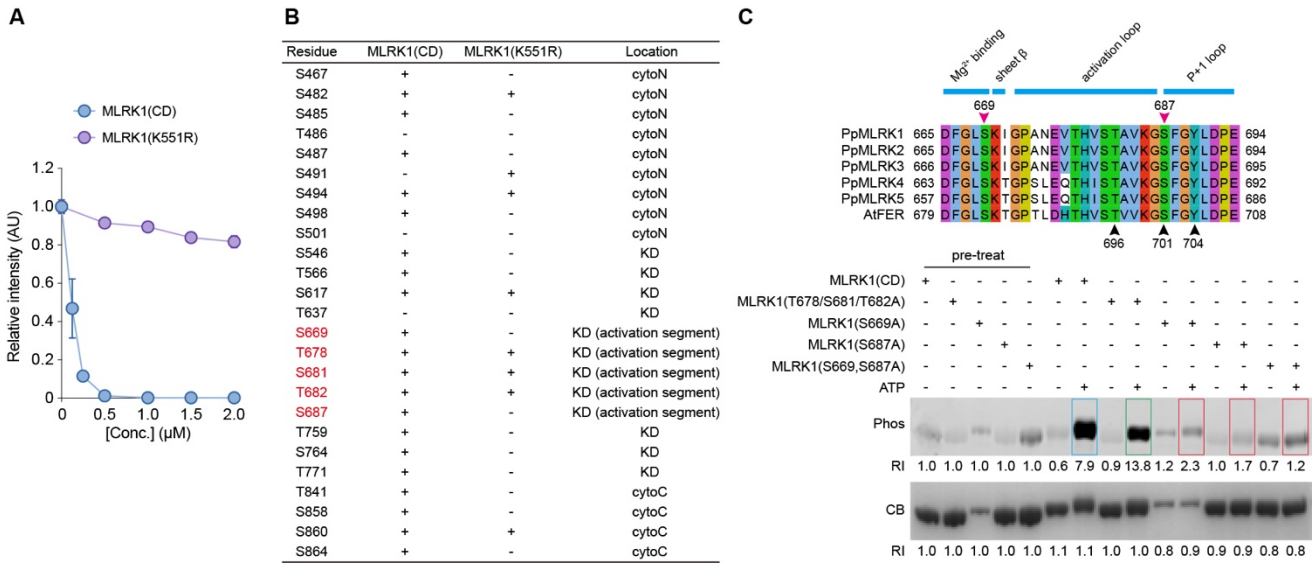


Figure S8. Truncation analyses identify functional domains involved in ROPGEF4-MLRK1 and ROPGEF6-MLRK1 interactions.

(A) Yeast two-hybrid assays reveal a critical role of the PRONE-flanking domains of ROPGEF4 and ROPGEF6 in interacting with MLRK1 cytoplasmic domain. FL, full-length; PR, PRONE domain; N-PR-C, PRONE domain with N- and C-terminal proximal regions; N-PR, PRONE domain with N-terminal proximal region; PR-C, PRONE domain with C-terminal proximal region.

(B) The C-terminal region of MLRK1 cytoplasmic domain is necessary and sufficient for robust interactions with ROPGEF4 and ROPGEF6 revealed by yeast two-hybrid assays. CD, cytoplasmic domain; KD, kinase domain; cytoN, N-terminal region of the cytoplasmic domain; cytoC, C-terminal region of the cytoplasmic domain.



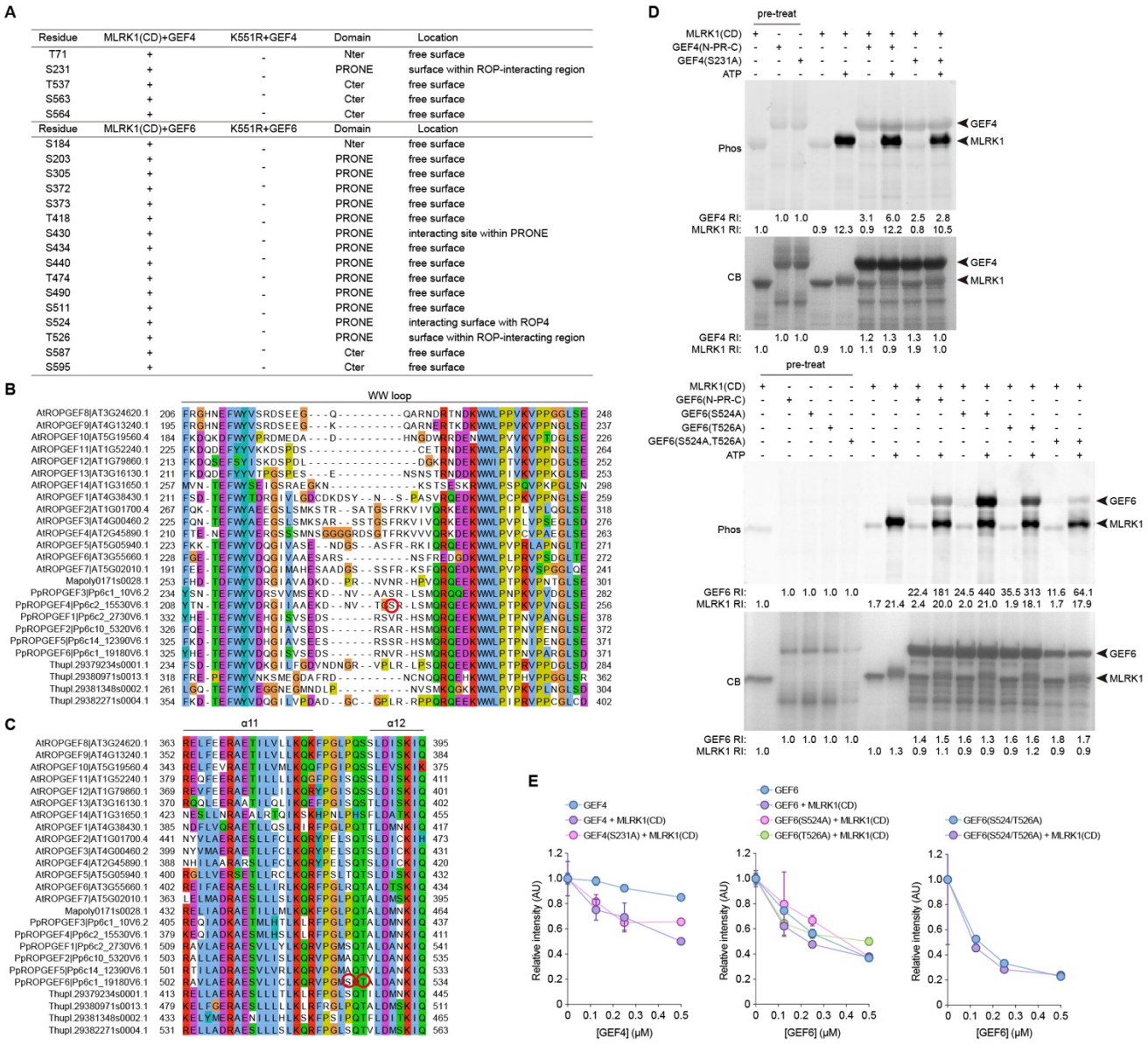
Residue	MLRK1(CD)	MLRK1(K551R)	Location
S467	+	-	cytoN
S482	+	+	cytoN
S485	+	-	cytoN
T486	-	-	cytoN
S487	+	-	cytoN
S491	-	+	cytoN
S494	+	+	cytoN
S498	+	-	cytoN
S501	-	-	cytoN
S546	+	-	KD
T566	+	-	KD
S617	+	+	KD
T637	-	-	KD
S669	+	-	KD (activation segment)
T678	+	+	KD (activation segment)
S681	+	+	KD (activation segment)
T682	+	+	KD (activation segment)
S687	+	-	KD (activation segment)
T759	+	-	KD
S764	+	-	KD
T771	+	-	KD
T841	+	-	cytoC
S858	+	-	cytoC
S860	+	+	cytoC
S864	+	-	cytoC

Figure S9. Characterization of MLRK1 autophosphorylation sites.

(A) *In vitro* kinase assays detecting MLRK1(CD) and MLRK1(K551R) autophosphorylation. Data are mean ± SD (n = 3 per group).

(B) Phosphosites identified through comparative mass spectrometry analyses. Candidate autophosphorylation sites in the activation segment are highlighted in red. CD, cytoplasmic domain; KD, kinase domain; cytoN, N-terminal region of the cytoplasmic domain; cytoC, C-terminal region of the cytoplasmic domain.

(C) Sequence alignment of MLRK activation segments and the identification of autophosphorylation sites via *in vitro* phosphorylation assays. Note that substitution of Ser669 and S687 (red arrowheads) with alanine markedly reduced MLRK1 autophosphorylation (red boxes), whereas MLRK1 carrying T678A, S681A, and T682A mutations (blue box) exhibited an autophosphorylation level comparable to wild-type MLRK1 (green box). Autophosphorylation sites for AtFER activation are indicated by black arrowheads.



Residue	MLRK1(CD)+GEF4	K551R+GEF4	Domain	Location
T71	+	-	Nter	free surface
S231	+	-	PRONE	surface within ROP-interacting region
T537	+	-	Cter	free surface
S563	+	-	Cter	free surface
S564	+	-	Cter	free surface
Residue	**MLRK1(CD)+GEF6**	**K551R+GEF6**	**Domain**	**Location**
S184	+	-	Nter	free surface
S203	+	-	PRONE	free surface
S305	+	-	PRONE	free surface
S372	+	-	PRONE	free surface
S373	+	-	PRONE	free surface
T418	+	-	PRONE	free surface
S430	+	-	PRONE	interacting site within PRONE
S434	+	-	PRONE	free surface
S440	+	-	PRONE	free surface
T474	+	-	PRONE	free surface
S490	+	-	PRONE	free surface
S511	+	-	PRONE	free surface
S524	+	-	PRONE	interacting surface with ROP4
T526	+	-	PRONE	surface within ROP-interacting region
S587	+	-	Cter	free surface
S595	+	-	Cter	free surface

Figure S10. Identification of phosphosites in ROPGEF4 and ROPGEF6.

(A) Candidate phosphosites identified through comparative mass spectrometry analyses. The putative location of each phosphosite was determined from AlphaFold3 predicted structures. Nter, N-terminal portion; Cter, C-terminal portion.

(B-C) Sequence alignment of representative ROPGEFs showing ROPGEF4(S231) and ROPGEF6(S524/T526) sites (red circles).

(D) Phosphorylation of wild-type ROPGEF4/6 and phospho-defective mutants by MLRK1(CD). RI, relative intensity normalized to pre-treated samples; CB, Coomassie Blue stain; Phos, phosphoprotein stain.

(E) In vitro kinase assays for wild-type ROPGEF4/6 and phospho-defective mutants. Data are mean ± SD (n = 3 per group).

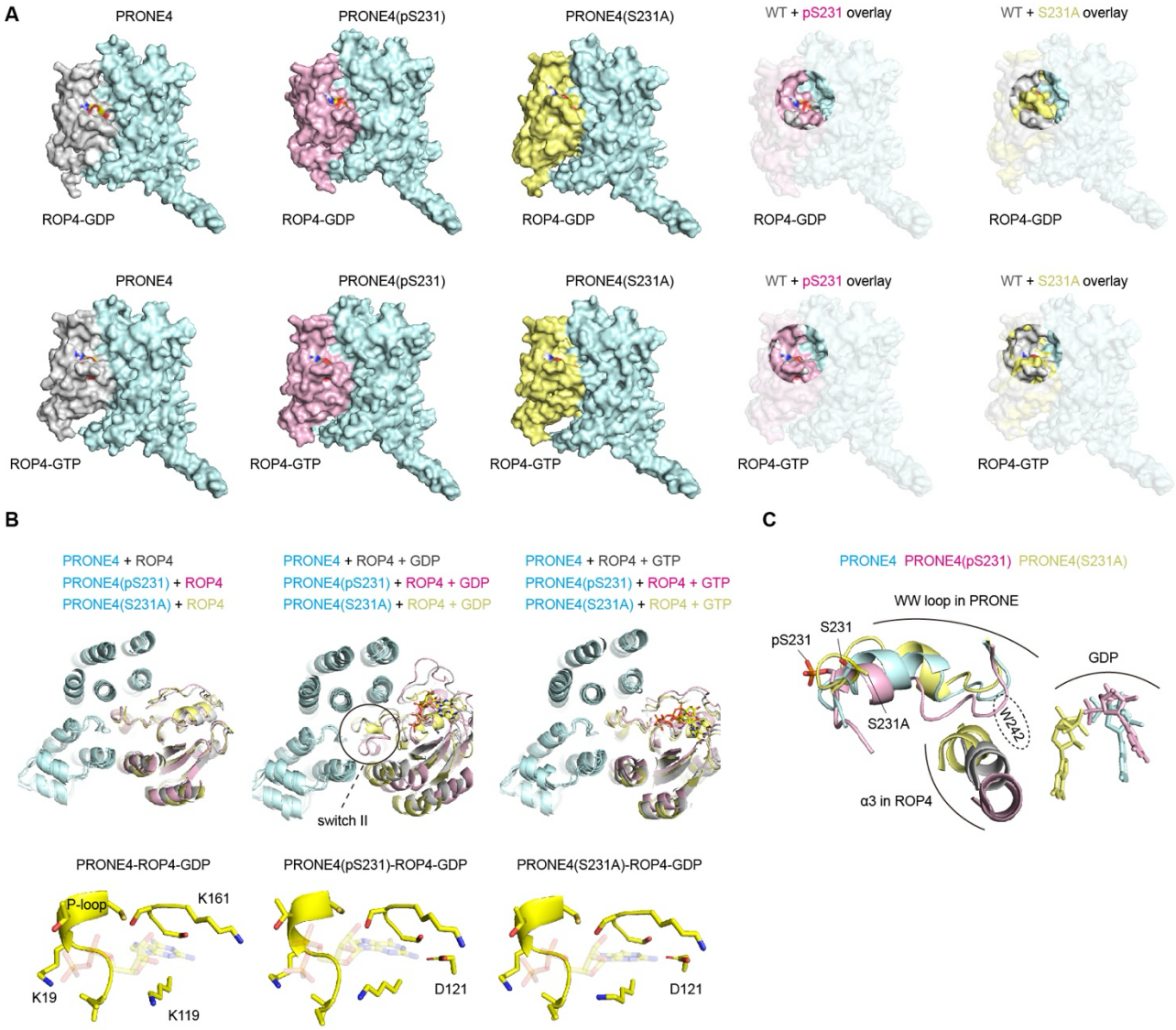


Figure S11. Predicted structures of wild-type, phosphorylated, and non-phosphorylatable ROPGEF4 variants in complex with ROP4.

(A) Surface view of ROPGEF4-ROP4 complexes in the presence of GDP or GTP. The nucleotide-binding pocket is highlighted on the right. pS231, phosphorylated Ser231; S231A, Ser-to-Ala mutant.

(B) Orientation of switch II and GDP-interacting residues of ROP4.

(C) Positioning of the WW loop of ROPGEF4 in relation to switch II, GDP, and α3 in ROP4.

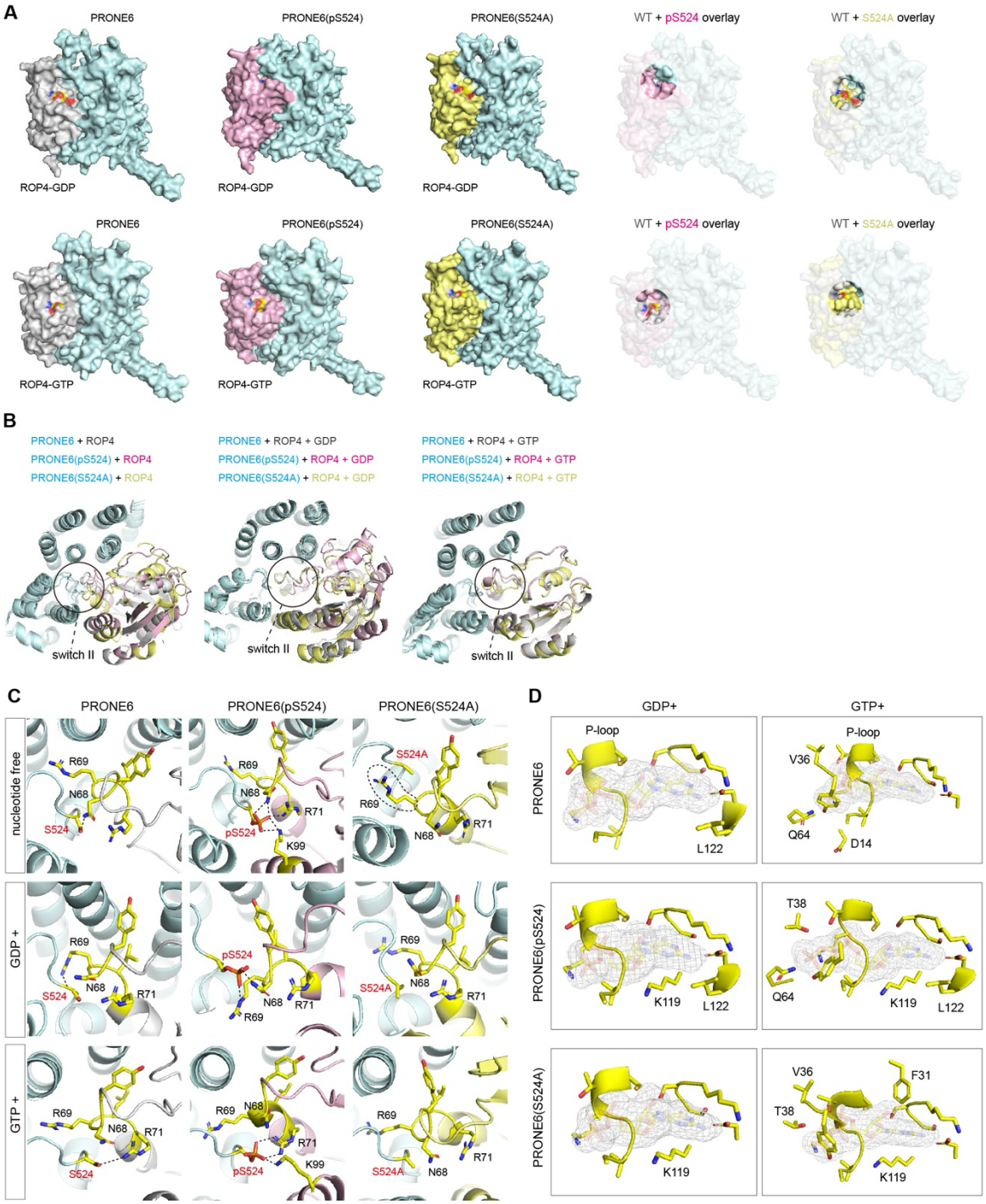


Figure S12. Predicted structures of ROPGEF6(S524) variants in complex with ROP4.

(A) Surface view of ROPGEF6(S524)-ROP4 complexes in the presence of GDP or GTP. The nucleotide-binding pocket is highlighted on the right. pS524, phosphorylated Ser524; S524A, Ser-to-Ala mutant.

(B) Orientation of the switch II region of ROP4.

(C) Interacting residues between ROPGEF6 and switch II of ROP4.

(D) Nucleotide-interacting residues in ROP4.

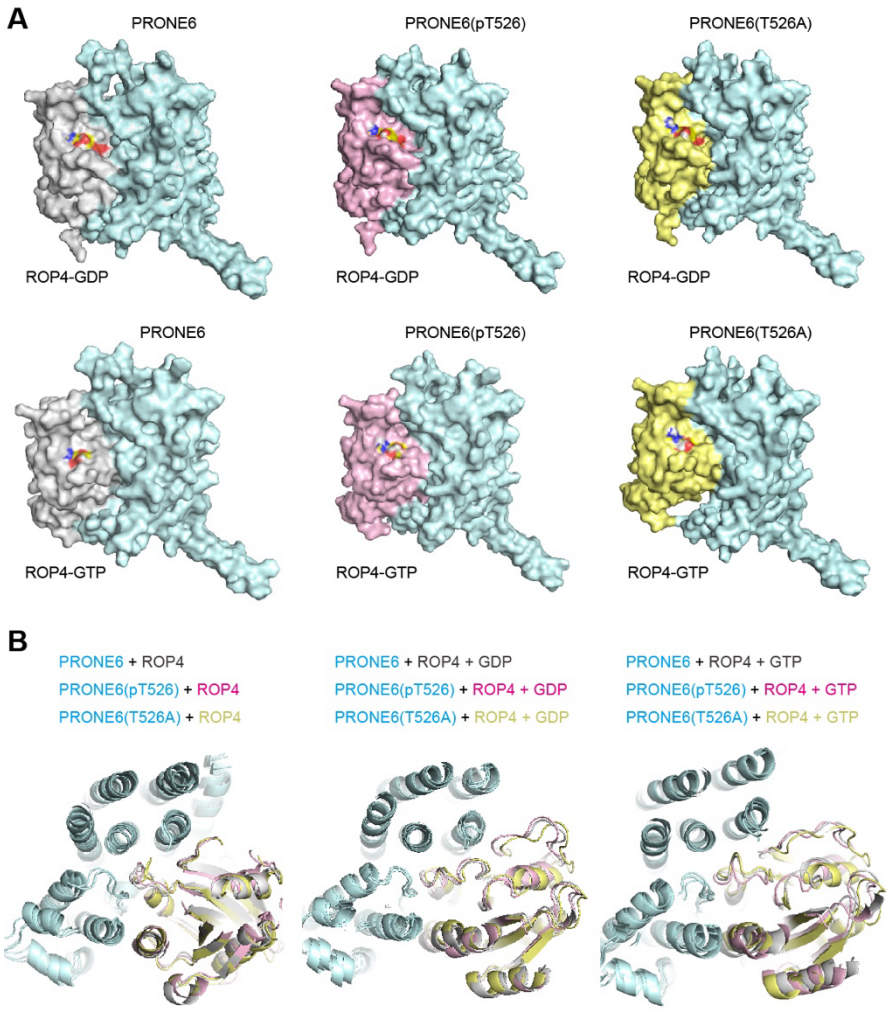


Figure S13. Predicted structures of ROPGEF6(T526) variants in complex with ROP4.

(A) Surface view of ROPGEF6(T526)-ROP4 complexes in the presence of GDP or GTP. pT526, phosphorylated Thr526; T526A, Thr-to-Ala mutant.

(B) Orientation of the switch II region of ROP4.

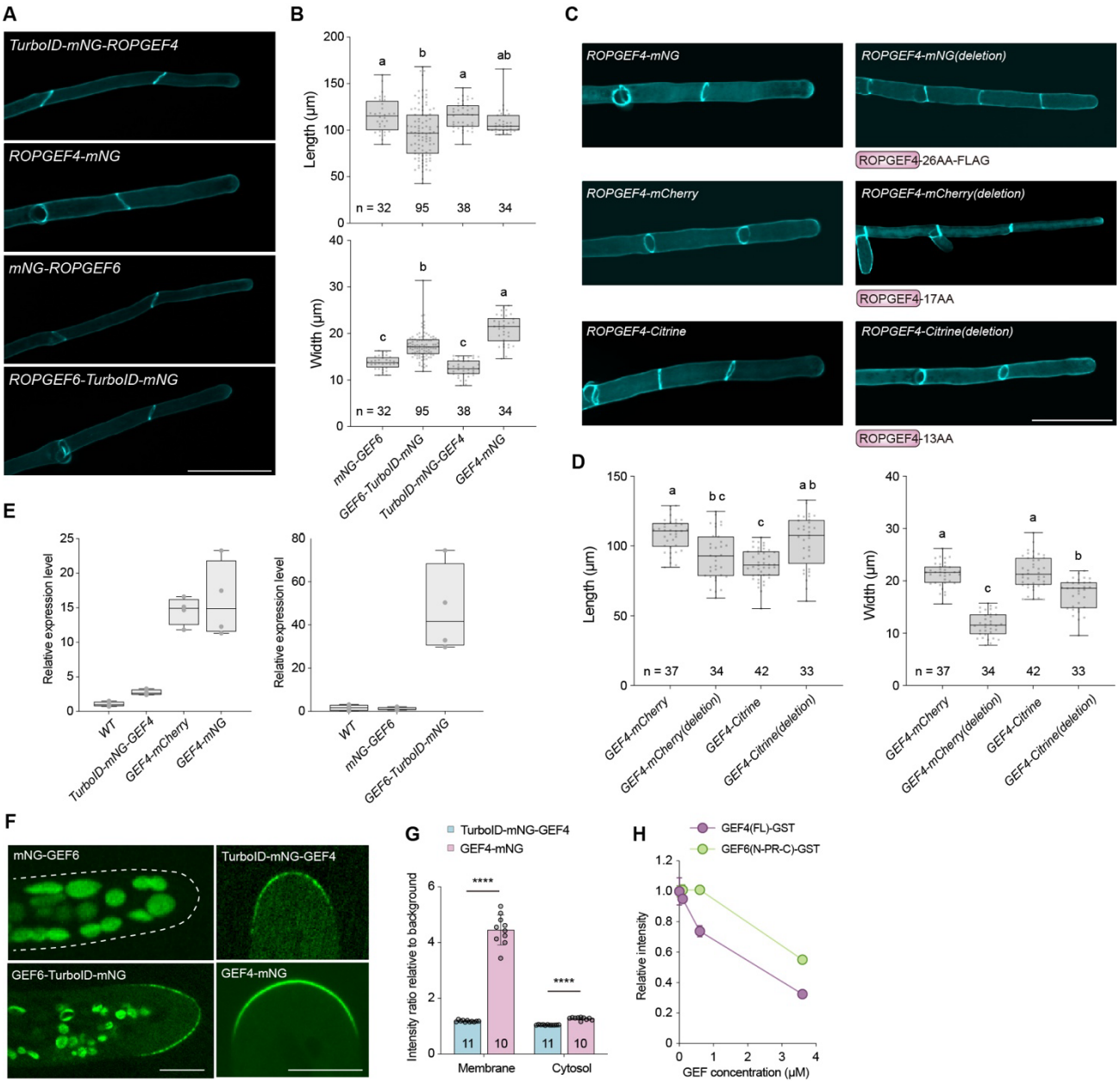


Figure S14. C-terminal tagging promotes the expression and activity of ROPGEF4 and ROPGEF6.

(A) Protonema cells of ROPGEF4 and ROPGEF6 knock-in lines. Scale bar: 100 μm.

(B) Quantification of cell length and cell width of ROPGEF4 and ROPGEF6 knock-in lines.

(C) Deletion of C-terminal tags via genome editing suppresses cell morphology defects in ROPGEF4 knock-in plants.

(D) Quantification of cell length and cell width of ROPGEF4 knock-in and genome-edited plants.

(E) Transcript levels of ROPGEF4 and ROPGEF6 are increased in knock-in plants carrying a C-terminal tag. Four technical repeats were performed for each group.

(F) Localization of ROPGEF4 and ROPGEF6 tagged with N-terminal and C-terminal fluorescent proteins. Note that N-terminally tagged ROPGEF6 is not detectable. Scale bars: 10 μm.

(G) Quantification of fluorescence intensity ratio of N-terminally and C-terminally tagged ROPGEF4 normalized to background signal.

(H) *In vitro* GEF activity of ROPGEF4 and ROPGEF6 fused with a C-terminal GST tag toward ROP4. Three technical repeats were performed for each group. FL, full-length; N-PR-C, PRONE domain with N- and C-terminal proximal regions.

Data are represented as mean ± SD in (G and H) and box plots displaying the median and range (min to max) in (B, D, and E). Sample sizes are indicated below the bars in (B, D, and G). Comparisons were performed using Kruskal–Wallis with Dunn's post-hoc test in (B), Welch's ANOVA with Dunnett's T3 test in (D), and Mann-Whitney U test in (G). ****, $p<0.0001$.

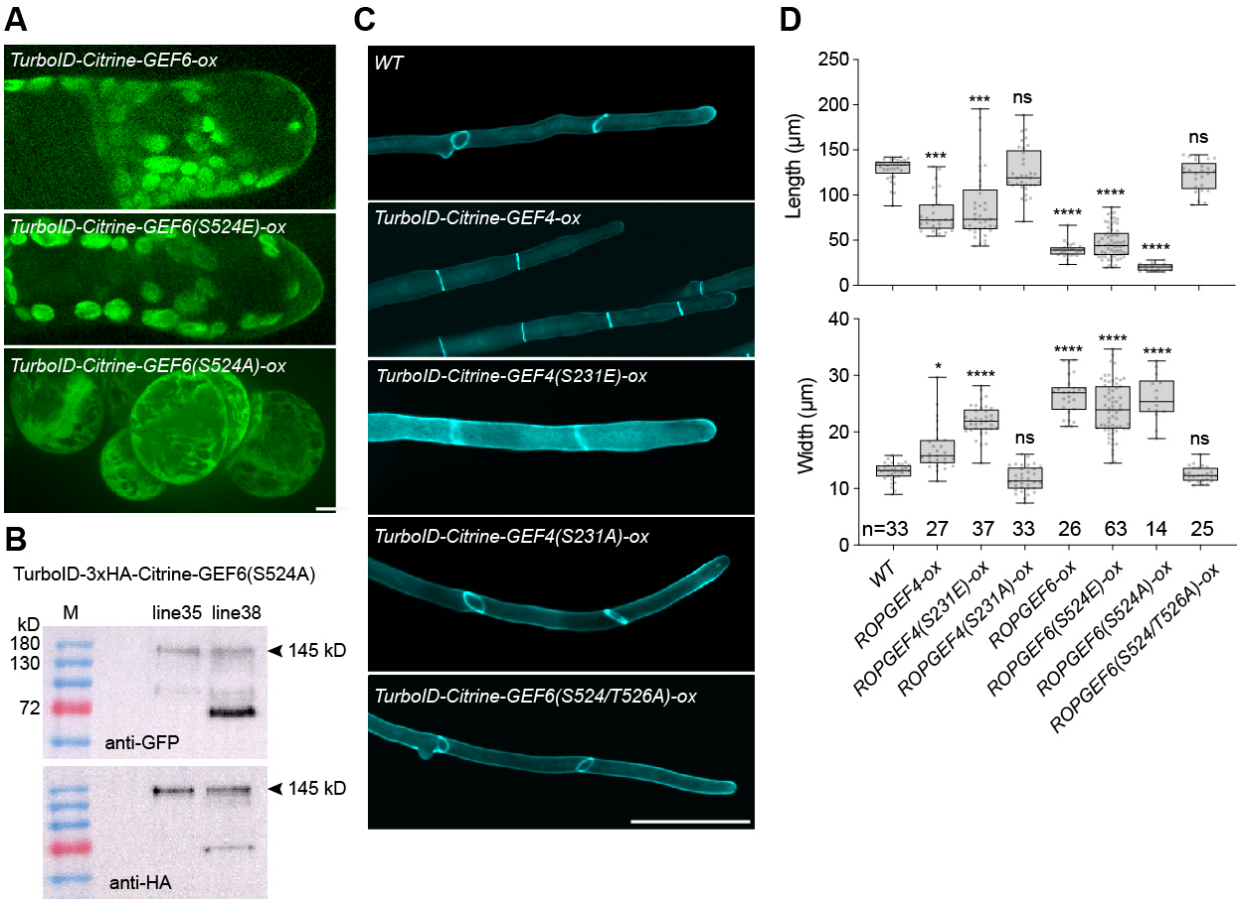


Figure S15. Overexpression of ROPGEF4 and ROPGEF6 alters cell morphology.

(A) Localization of wild-type, phosphomimic (S524E), and non-phosphorylatable (S524A) ROPGEF6 variants in overexpression lines. Scale bar: 10 μm.

(B) Western blotting confirms the correct expression of ROPGEF6(S524A).

(C) Cell morphology of wild-type (WT) and overexpression lines. Scale bar: 100 μm.

(D) Quantification of cell length and cell width. Sample sizes are shown below the bars. Kruskal–Wallis with Dunn's post-hoc test was used to compare each overexpression line against WT. ns, no significant difference; *, $p<0.05$; ***, $p<0.001$; ****, $p<0.0001$.

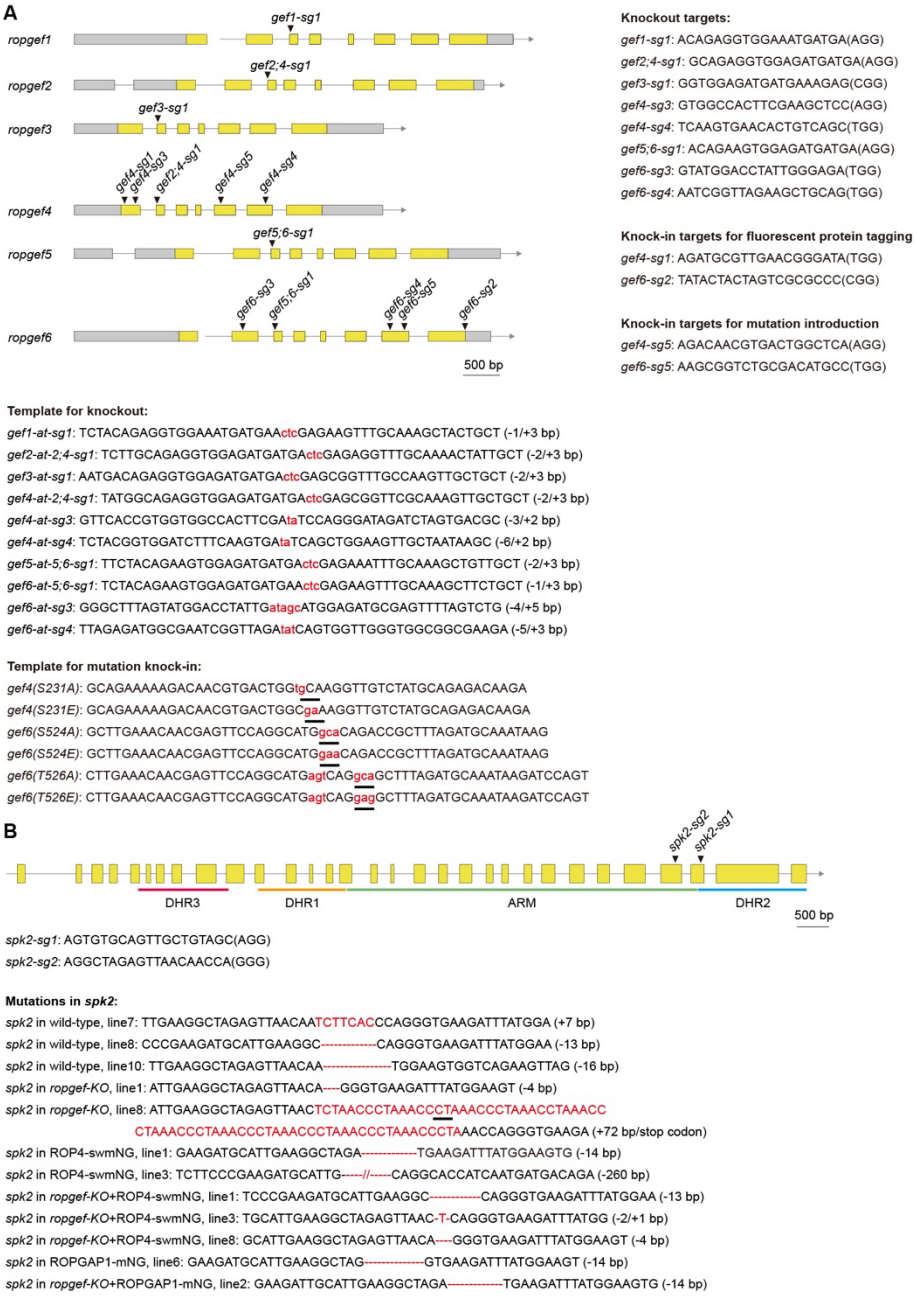


Figure S16. CRISPR targets, oligonucleotide templates, and mutant sequences of *ropgef* and *spk2*.

(A) Gene structures of *ropgef1-6*. Sequences of CRISPR targets and templates are shown. Protospacer-adjacent motif (PAM) downstream of each target is marked by the bracket. S-to-E or S-to-A mutations are underlined. Exons are represented by yellow boxes.

(B) Gene structure of *spk2*. CRISPR targets and mutations (red) generated by genome editing without a template are shown. Genomic regions encoding key protein domains are indicated. Note that two CRISPR targets were used for genome editing but only *spk2-sg2* was effective. A stop codon (underlined) was introduced in the *ropgef-KO,spk2* line8.

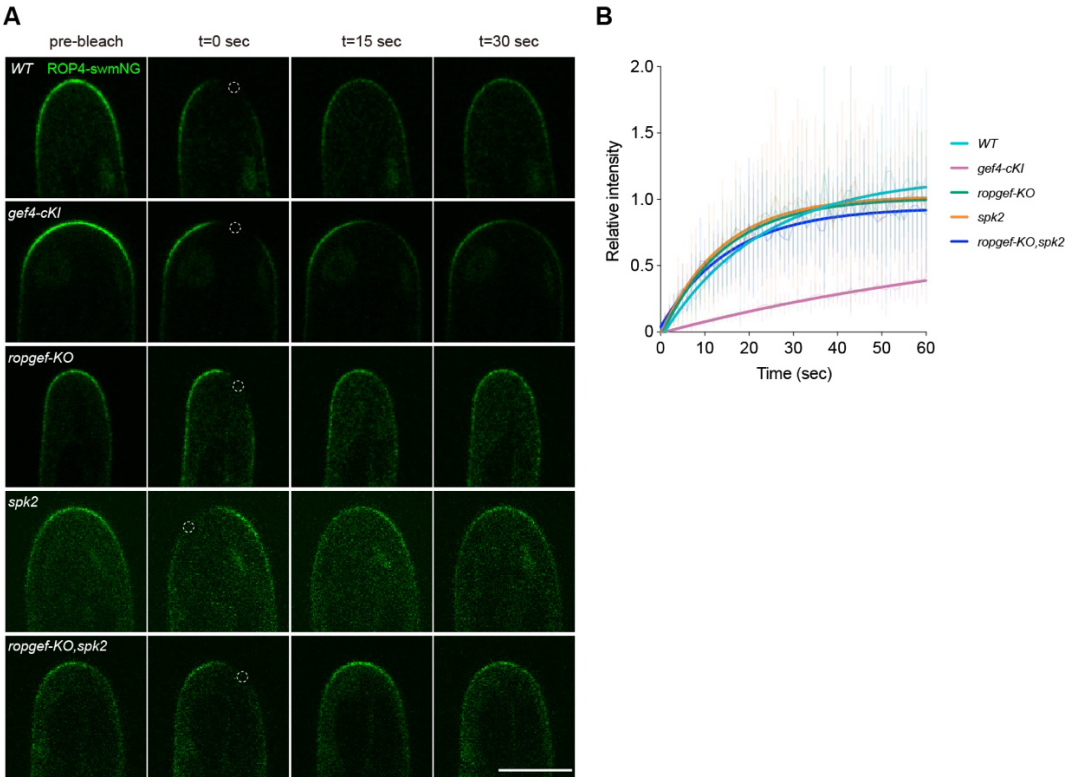


Figure S17. FRAP assays of ROP4 dynamics.

(A) Representative images of wild-type (WT) and mutant lines at pre-bleach and post-bleach time points. The bleached region is outlined by a dashed circle. Scale bar: 10 μm.

(B) Quantification of ROP4 fluorescence recovery. Data are fitted by a one-phase association curve. Sample sizes: n = 16 (WT), 9 (*gef4-cKI*), 15 (*ropgef-KO*), 16 (*spk2*), and 10 (*ropgef-KO,spk2*).

Table S1. Primers used in this study.

ID	Description	Sequence (5'-3')
oPY681	ROP4-P180-Rv	TGCGGCCGCAAGCTTTGGTTGGAGAACCACCTTG
oPY239	GGGGS-ROP4-Fw	GGAGGAGGAGGAAGCAGCACTTCACGGTTTATCAAGTGC
oPY309	ROP4-G15V-Rv	ACAGCGACGTCTCCAACAGTCACGCA
oPY310	ROP4-G15V-Fw	GGAGACGTCGCTGTCGGGAAGACGTG
oPY311	ROP4-T20N-Rv	AGCATACAGTTCTTCCCGACAGCTCC
oPY312	ROP4-T20N-Fw	GAAGAACTGTATGCTTATTTCATACAC
oPY371	ROPGAP1-nKI-3HR-Fw	GGATCAGGAAGTGGTACACAGGTTCTCCCGACCCAGA
oPY568	ROPGAP1-cKI-5HR-Rv	GCTTCCTCCTCCTCCCCAAGCTTCTACCCTTTG
oPY1986	GSGSG-ROPGEF1-Fw	GGATCAGGAAGTGGTATGCAGAGGAACCAGGTAGGGATG
oPY1987	ROPGEF1-GGGGS-Rv	GCTTCCTCCTCCTCCATCCCGCCCGGGGGGACTAT
oPY1988	GSGSG-ROPGEF2-Fw	GGATCAGGAAGTGGTATGGAACAAAGAAGCCAAGTCG
oPY1989	ROPGEF2-GGGGS-Rv	GCTTCCTCCTCCTCCATCCCGCCCAAGACTGTG
oPY1990	GSGSG-ROPGEF3-Fw	GGATCAGGAAGTGGTATGGCATCGGAGCGCAAC
oPY1991	ROPGEF3-GGGGS-Rv	GCTTCCTCCTCCTCCATCTCGACTTGGAGGGCTG
oPY780	ROPGEF4-GSGSG-Fw	GGATCAGGAAGTGGTATGGACGATGCAAGTACTATTAGC
oPY1992	GSGSG-ROPGEF5-Fw	GGATCAGGAAGTGGTATGGAACAAGGTCAGAACGAAGG
oPY1993	ROPGEF5-GGGGS-Rv	GCTTCCTCCTCCTCCATGCCGTCCAGGAGGACTATG
oPY407	ROPGEF6-nKI-3HR-Fw	GGATCAGGAAGTGGTGAACAAGGAGGCCGAAGCGAAT
oPY1048	ROPGEF6-GGGGS-Rv	GCTTCCTCCTCCTCCGTCTCGCCCCGGAGGACTGTGAAG
oPY1471	ROPGEF4(D32)GSGSG-Fw	GGATCAGGAAGTGGTGACAATTCGGCTAGGAGCTCC
oPY1472	ROPGEF4(P500)GGGGS-Rv	GCTTCCTCCTCCTCCCGGACTAAGAGCCGGAGAG
oPY1473	ROPGEF6(D150)GSGSG-Fw	GGATCAGGAAGTGGTGATGATGCCGCAAGCAGTTC
oPY1474	ROPGEF6(P629)GGGGS-Rv	GCTTCCTCCTCCTCCAGGACTCGGCGCAGGGCTA
oPY1881	ROPGEF4-S231A-Fw	AAGGTTGTCTATGCAGAGACAAG
oPY1882	ROPGEF4-S231A-Rv	TGCATAGACAACCTTGCGCCAGTCACGTTGTCTTTTTCTG
oPY1883	ROPGEF6-S524/T526-Fw	GCTTTAGATGCAAATAAGATCCAG
oPY1884	ROPGEF6-S524A-Rv	ATTTGCATCTAAAGCGGTCTGTGCCATGCCTGGAACTCGTTGTTTC
oPY1885	ROPGEF6-T526A-Rv	ATTTGCATCTAAAGCTGCCTGCGACATGCCTGGAACTCGTTGTTTC
oPY1886	ROPGEF6-S524A+T526A-Rv	ATTTGCATCTAAAGCTGCCTGAGCCATGCCTGGAACTCGTTGTTTC
oPY1984	ROPGEF4(S231E)-Rv	TGCATAGACAACCTTTCGCCAGTCACGTTGTCTTTTTCTG
oPY1985	ROPGEF6(S524E)-Rv	ATTTGCATCTAAAGCGGTCTGCTCCATGCCTGGAACTCGTTGTTTC
oPY994	GSGSG-ROPGEF4(ΔN)-Fw	GGATCAGGAAGTGGTTCAGAGGTGGAGATGATGAAGGA
oPY995	ROPGEF4(ΔC)-GGGGS-Rv	GCTTCCTCCTCCTCCTGACTTCTTCACCATGTCATCGG

oPY1049	ROPGEF6(ΔN)-Fw	GGATCAGGAAGTGGTTCAGAAGTGGAGATGATGAAGGAG
oPY1050	ROPGEF6(ΔC)-Rv	GCTTCCTCCTCCTCCCCTCGTCACCAGATCATCCG
oPY1660	SPK1(DHR2)-GSGSG-Fw	GGATCAGGAAGTGGTGTCCCAGATTTGCATATTATGTGG
oPY1661	SPK1(DHR2)-GGGGS-Rv	GCTTCCTCCTCCTCCAAGTTCGGGTAATATGGCAGG
oPY1601	SPK6(DHR2)-GSGSG-Fw	GGATCAGGAAGTGGTACCGCTGACAAGTATGCGAC
oPY1602	SPK6(DHR2)-GGGGS-Rv	GCTTCCTCCTCCTCCGAACCCAGATAAAATAGCAGGAATGAAG
oPY1135	MLRK1/2/3-GSGSG-Fw	GGATCAGGAAGTGGTAAGACCAAGTCTGACAAGCCTG
oPY1136	MLRK1-GGGGS-Rv	GCTTCCTCCTCCTCCCCTTCCTTGAGCGTTGATCAACTG
oPY1398	MLRK1-KD-GSGSG-Fw	GGATCAGGAAGTGGTGGCAGGTACTTCAGCTTCGC
oPY1399	MLRK1-KD-GGGGS-Rv	GCTTCCTCCTCCTCCATGTAGTTGCAAGGCGTACTCC
oPY1548	MLRK1-K551R-Rv	TCCTCTCCTCACCGCCACTTTCGACCCAT
oPY1549	MLRK1-K551R-Fw	GCGGTGAGGAGAGGAAACCCCAGGTCAGAGCA
oPY1933	MLRK1(T678/S681/T682A)-Rv	TGCAGCCACGTGAGCGACTTCATTCGCGGGCCCGAT
oPY1934	MLRK1(T678/S681/T682A)-Fw	GCTCACGTGGCTGCAGCCGTGAAGGGCAGCTTCG
oPY1935	MLRK1(S669A)-Rv	GATTTTCGCCAACCCGAAGTCAGCCAC
oPY1936	MLRK1(S669A)-Fw	GGGTTGGCGAAAATCGGGCC
oPY1937	MLRK1(S687A)-Rv	ACCCGAAGGCACCCTTCACGGCTGTGCT
oPY1938	MLRK1(S687A)-Fw	AGGGTGCCTTCGGGTACCTGGATCCCG
oPY1388	MLRK2-GGGGS-Rv	GCTTCCTCCTCCTCCCCTACCTTGAGGGTCGATTAACTG
oPY1389	MLRK3-GGGGS-Rv	GCTTCCTCCTCCTCCCCTTCCTTGAGGGTTGACCAAC
oPY1133	MLRK4-GSGSG-Fw	GGATCAGGAAGTGGTCGGAAGACCTCCAAATTGTCTCC
oPY1134	MLRK4-GGGGS-Rv	GCTTCCTCCTCCTCCCCTTCCTTGTGGATTAACTAACTGAGAG
oPY1390	MLRK5-GSGSG-Fw	GGATCAGGAAGTGGTTCTTGTTGCCGGAAGTCCC
oPY1391	MLRK5-GGGGS-Rv	GCTTCCTCCTCCTCCCCTTCCTTGTGGGTTTATTATCTGTGAG
oPY1370	AtROPGEF1-GSGSG-Fw	GGATCAGGAAGTGGTATGGGGAGCTTATCTTCTGAG
oPY1371	AtROPGEF1-GGGGS-Rv	GCTTCCTCCTCCTCCATCTCTTTCCGGCGTCAC
oPY883	AtROP1-GSGSG-Fw	GGATCAGGAAGTGGTAGCGCTTCGAGGTTCGTAAA
oPY884	AtROP1-GGGGS-Rv	GCTTCCTCCTCCTCCTAGAATGGAGCATGCCTTCT
oPY885	AtROPGAP1-GSGSG-Fw	GGATCAGGAAGTGGTACTGAAGTTCTTCACTTTCC
oPY886	AtROPGAP1-GGGGS-Rv	GCTTCCTCCTCCTCCCCGCCAAGCTTCAGTACGCTCTA
oPY1767	Citrine-sg1-Rv	GAACAGCTCCTCGCCCTCATGGGTTGTAAGTCCTCCAC

oPY1768	Citrine-sg1-Fw	GGCGAGGAGCTGTTCACGTTTTAGAGCTAGAAATAGCAAG
oPY1769	Citrine-sg2-Rv	ATCACTCTCGGCATGGACATGGGTTGTAAGTCCTCCAC
oPY1770	Citrine-sg2-Fw	CATGCCGAGAGTGATCCGTTTTAGAGCTAGAAATAGCAAG
oPY1771	mCherry-sg1-Rv	TTGTCTTCTTCTCCTTTCATGGGTTGTAAGTCCTCCAC
oPY1772	mCherry-sg1-Fw	AGGAGAAGAAGACAATAGTTTTAGAGCTAGAAATAGCAAG
oPY1773	mCherry-sg2-Rv	CCTCCAGTGCTATGCCTCATGGGTTGTAAGTCCTCCAC
oPY1774	mCherry-sg2-Fw	GCATAGCACTGGAGGAAGTTTTAGAGCTAGAAATAGCAAG
oPY1775	mNG-sg1-Rv	TTGTCCTCCTCTCCTTTCATGGGTTGTAAGTCCTCCAC
oPY1776	mNG-sg1-Fw	AGGAGAGGAGGACAACAGTTTTAGAGCTAGAAATAGCAAG
oPY1777	mNG-sg2-Rv	TGCCACTCCTTGAAGTTCATGGGTTGTAAGTCCTCCAC
oPY1778	mNG-sg2-Fw	CTTCAAGGAGTGGCAGAGTTTTAGAGCTAGAAATAGCAAG
oPY967	ropgef1-sg1-Fw	CATGACAGAGGTGGAAATGATGA
oPY968	ropgef1-sg1-Rv	AAACTCATCATTTCCACCTCTGT
oPY969	ropgef2/4-sg1-Fw	CATGGCAGAGGTGGAGATGATGA
oPY970	ropgef2/4-sg1-Rv	AAACTCATCATCTCCACCTCTGC
oPY971	ropgef3-sg1-Fw	CATGGGTGGAGATGATGAAAGAG
oPY972	ropgef3-sg1-Rv	AAACCTCTTTCATCATCTCCACC
oPY973	ropgef5/6-sg1-Fw	CATGACAGAAGTGGAGATGATGA
oPY974	ropgef5/6-sg1-Rv	AAACTCATCATCTCCACTTCTGT
oPY975	ropgef1-XhoI-knock-in template	TCTACAGAGGTGGAAATGATGAACTCGAGAAGTTTGCAAAGCTACTGCT
oPY976	ropgef2-XhoI-knock-in template	TCTTGCAGAGGTGGAGATGATGACTCGAGAGGTTTGCAAAACTATTGCT
oPY977	ropgef3-XhoI-knock-in template	AATGACAGAGGTGGAGATGATGACTCGAGCGGTTTGCCAAGTTGCTGCT
oPY978	ropgef4-XhoI-knock-in template	TATGGCAGAGGTGGAGATGATGACTCGAGCGGTTCGCAAAGTTGCTGCT
oPY979	ropgef5-XhoI-knock-in template	TTCTACAGAAGTGGAGATGATGACTCGAGAAATTTGCAAAGCTGTTGCT
oPY980	ropgef6-XhoI-knock-in template	TCTACAGAAGTGGAGATGATGAACTCGAGAAGTTTGCAAAGCTTCTGCT
oPY981	ropgef1-crispr-screen-Fw	ATGGATGCTGCGTCAGAAGA
oPY982	ropgef1-crispr-screen-Rv	ACCTCCACTGTGATTCCATC
oPY983	ropgef2-crispr-screen-Fw	CATCGCTGTTGAGCCAATTG
oPY984	ropgef2-crispr-screen-Rv	CGAGGTTTGCTGACCATTAC
oPY985	ropgef3-crispr-screen-Fw	TCGACGGAGCATTGATGATG
oPY986	ropgef3-crispr-screen-Rv	AGCAGCATAGCATCGAGCTT

oPY987	ropgef4-crispr-screen-Rv	TCGCATCAAGCTTGCGTAAG
oPY988	ropgef5-crispr-screen-Fw	GAGTCAGGAAGAATATCCAGTG
oPY989	ropgef5-crispr-screen-Rv	TCCTTAGAGCTGGCAAGTTG
oPY990	ropgef6-crispr-screen-Fw	GAGAATCGCAGCATAGATGG
oPY991	ropgef6-crispr-screen-Rv	AGATCTGATCGAGGTGTGCT
oPY1025	ropgef4-sg1-Fw	CATGAGATGCGTTGAACGGGATA
oPY1026	ropgef4-sg1-Rv	AAACTATCCCGTTCAACGCATCT
oPY1027	ropgef4-nKI-5HR-Fw	GAGGTCGACAAGCTTCAGACCTCAATGCAACGTG
oPY1028	ropgef4-nKI-5HR-Rv	TCCTTTAGAAACCATCATCCCGTTCAACGCATCTATC
oPY1029	ropgef4-nKI-3HR-Rv	CATATGTCTAGACCCGGGTCTTGTGATCATGACCT
oPY1030	ropgef4-nKI-screen-Fw	AGCAACTGTGGACGGATTGG
oPY1392	ropgef4-sg2-Rv	CCAAGCAGCAACTTTGCCATGGGTTGTAAGTCCTCCAC
oPY1393	ropgef4-sg2-Fw	AAAGTTGCTGCTTGGGGGTTTTAGAGCTAGAAATAGCAAG
oPY1394	ropgef4-sg2-template	AGCGGTTCGCAAAGTTGCTGCTCTCGAGGACATGTCGGGTGGTGCTA
oPY1395	ropgef6-sg1-Rv	CCAAGCAGAAGCTTTGCCATGGGTTGTAAGTCCTCCAC
oPY1396	ropgef6-sg1-Fw	AAAGCTTCTGCTTGGGGGTTTTAGAGCTAGAAATAGCAAG
oPY1397	ropgef6-sg1-template	AGAAGTTTGCAAAGCTTCTGCTCTCGAGGATATGTCTGGTGGGGGAA
oPY1429	ropgef6-sg2-Rv	GCGCGACTAGTAGTATACATGGGTTGTAAGTCCTCCAC
oPY1430	ropgef6-sg2-Fw	TACTACTAGTCGCGCCCGTTTTAGAGCTAGAAATAGCAAG
oPY1431	ropgef4-nKI-sg1-5HR-Fw	AGATGCGTTGAACGGGATATGGCAGACCTCAATGCAACGTGGAAG
oPY1432	ropgef4-nKI-sg1-3HR-Rv	AGATGCGTTGAACGGGATATGGGTCTTGTGATCATGACCTGCTT
oPY1433	ropgef6-cKI-sg2-5HR-Fw	TATACTACTAGTCGCGCCCCGGGTGATGAACTGTACCGGGCAAT
oPY1434	ropgef6-cKI-sg2-3HR-Rv	TATACTACTAGTCGCGCCCCGGACACATAGACGAGCACCAGGGA
oPY1446	ropgef4-sg3-Rv	AGCTTCGAAGTGGCCACCATGGGTTGTAAGTCCTCCAC
oPY1447	ropgef4-sg3-Fw	GGCCACTTCGAAGCTCCGTTTTAGAGCTAGAAATAGCAAG
oPY1448	ropgef4-sg3-template	GTTCACCGTGGTGGCCACTTCGATATCCAGGGATAGATCTAGTGACGC
oPY1449	ropgef4-sg4-Rv	TGACAGTGTTCACTTGACATGGGTTGTAAGTCCTCCAC
oPY1450	ropgef4-sg4-Fw	AAGTGAACACTGTCAGCGTTTTAGAGCTAGAAATAGCAAG
oPY1451	ropgef4-sg4-template	TCTACGGTGGATCTTTCAAGTGATATCAGCTGGAAGTTGCTAATAAGC
oPY1452	ropgef6-sg3-Rv	TCCCAATAGGTCCATACCATGGGTTGTAAGTCCTCCAC
oPY1453	ropgef6-sg3-Fw	ATGGACCTATTGGGAGAGTTTTAGAGCTAGAAATAGCAAG
oPY1454	ropgef6-sg3-template	GGGCTTTAGTATGGACCTATTGATAGCATGGAGATGCGAGTTTTAGTCTG

oPY1455	ropgef6-sg4-Rv	GCAGCTTCTAACCGATTCATGGGTTGTAAGTCCTCCAC
oPY1456	ropgef6-sg4-Fw	TCGGTTAGAAGCTGCAGGTTTTAGAGCTAGAAATAGCAAG
oPY1457	ropgef6-sg4-template	TTAGAGATGGCGAATCGGTTAGATATCAGTGGTTGGGTGGCGGCGAAGA
oPY1662	spk1/2-sg1-Rv	TACAGCAACTGCACACTCATGGGTTGTAAGTCCTCCAC
oPY1663	spk1/2-sg1-Fw	TGTGCAGTTGCTGTAGCGTTTTAGAGCTAGAAATAGCAAG
oPY1798	spk2-sg1-screen-Fw	CAGAGTTGATGTCCGATGTG
oPY1799	spk2-3'UTR-Rv	CCACTATGCATGGTATGGCT
oPY1836	spk2-sg2-Rv	GTTGTTAACTCTAGCCTCATGGGTTGTAAGTCCTCCAC
oPY1837	spk2-sg2-Fw	GCTAGAGTTAACAACCAGTTTTAGAGCTAGAAATAGCAAG
oPY1978	ropgef4-sg5-Fw	ACAACGTGACTGGCTCAGTTTTAGAGCTAGAAATAGCAAG
oPY1979	ropgef4-sg5-Rv	AGCCAGTCACGTTGTCTCATGGGTTGTAAGTCCTCCAC
oPY1980	ropgef6-sg5-Fw	GCGGTCTGCGACATGCCGTTTTAGAGCTAGAAATAGCAAG
oPY1981	ropgef6-sg5-Rv	CATGTCGCAGACCGCTTCATGGGTTGTAAGTCCTCCAC
oPY1982	ROPGEF4(S231E) knock-in template	GCAGAAAAAGACAACGTGACTGGCGAAAGGTTGTCTATGCAGAGACAAGA
oPY1983	ROPGEF6(S524E) knock-in template	GCTTGAAACAACGAGTTCCAGGCATGGAACAGACCGCTTTAGATGCAAATAAG
oPY2214	ROPGEF4(S231A) knock-in template	GCAGAAAAAGACAACGTGACTGGTGCAAGGTTGTCTATGCAGAGACAAGA
oPY2215	ROPGEF6(S524A) knock-in template	GCTTGAAACAACGAGTTCCAGGCATGGCACAGACCGCTTTAGATGCAAATAAG
oPY2577	ROPGEF6(T526A) knock-in template	CTTGAAACAACGAGTTCCAGGCATGagtCAGgcaGCTTTAGATGCAAATAAGATCCAGT
oPY2578	ROPGEF6(T526E) knock-in template	CTTGAAACAACGAGTTCCAGGCATGagtCAGgagGCTTTAGATGCAAATAAGATCCAGT
oPY614	ROPGEF4-cKI-5HR-Fw	CCCCTCGAGGTCGACCAACGAGAGGCTATCAAC
oPY615	ROPGEF4-cKI-5HR-Rv	GCTTCCTCCTCCTCCGTCACGACCCGGAGGACT
oPY616	ROPGEF4-cKI-3HR-Fw	CCCTCACACCGGTGATGCCTTCACTGGAACCGA
oPY617	ROPGEF4-cKI-3HR-Rv	CATATGTCTAGACCCCAACATCTACGCACCTCA
oPY618	ROPGEF4-cKI-screen-Fw	GACAACGTGACTGGCTCAAG
oPY619	ROPGEF4-cKI-screen-Rv	GGATGTCCATGTAAGTGTAGC
oPY1245	ROPGEF4_Rv_oPY263	GCGCCCACCCTTTTAGTCACGACCCGGAGGACT
oPY1246	ROPGEF6_Rv_oPY263	GCGCCCACCCTTTTAGTCTCGCCCCGGAGGACTGTGAAG
oPY1510	SCAMP4-cKI-5HR-Fw	GAGGTCGACAAGCTTGGACCTCATGACAAGATTCGAG
oPY1511	SCAMP4-cKI-5HR-GGGGS-Rv	GCTTCCTCCTCCTCCGATAGCTACTCTGCTTGCTGCA
oPY1512	SCAMP4-cKI-3HR-Fw	CCCTCACACCGGTGATTTTACTGTATTCTTATTGTTAGTTGAGG
oPY1513	SCAMP4-cKI-3HR-Rv	CATATGTCTAGACCCCATCATACCACTTCTCAAACACATG
oPY1514	SCAMP4-cKI-screen-Fw	TGGTAATTGAACGTCGGTGC

oPY1515	SCAMP4-cKI-screen-Rv	GTGATCAACGTGGGATTAAAGAAGTCAC
oPY1783	ROPGEF4(ΔE550-D574)-GGGGS-Rv	GCTTCCTCCTCCTCCTGAAGGCAGTTTCACCAACTC
oPY1784	ROPGEF4(T483/487E)-Rv	CTCAGAACATGGTTCGGTAGTTAAATGCACGTTGTGATG
oPY1785	ROPGEF4(T483/487E)-Fw	GAACCATGTTCTGAGCCTTATATCTCTCCCAACACCTCTC
oPY1786	ROPGEF4(S491/495/499E)-Rv	AGCCGGTTCGGTGTTGGGTTCGATATAAGGGGTAGAACATGGAGTGG
oPY1787	ROPGEF4(S491/495/499E)-Fw	AACACCGAACCGGCTCTTGAACCGCACCAGATTCTGAGTTCC

Table S2. Plasmids used in this study.

ID	Description	Application
pAct-Cas9	pAct-Cas9	genome editing
pPY1138	Citrine-sg1-sg2	genome editing
pPY1136	mCherry-sg1-sg2	genome editing
pPY1137	mNG-sg1-sg2	genome editing
pPY308	rop4-sg4	genome editing
pPY525	ropgef1-sg1-ropgef2/4-sg1-ropgef3-sg1-ropgef5/6-sg1	genome editing
pPY512	ropgef4-sg1	genome editing
pPY896	ropgef4-sg3-sg4	genome editing
pPY869	ropgef6-sg2	genome editing
pPY897	ropgef6-sg3-sg4	genome editing
pPY1227	ropgef4-sg5	genome editing
pPY1228	ropgef6-sg5	genome editing
pPY1166	spk2-sg2	genome editing
pPY412	ROP4-swmNG	knock-in
pPY916	FLAG-TurboID-3xHA-mNG-ROPGEF4	knock-in
pPY158	mNG-ROPGEF6	knock-in
pPY216	ROPGAP1-mNG	knock-in
pPY497	ROPGEF4-Citrine	knock-in
pPY252	ROPGEF4-mCherry	knock-in
pPY238	ROPGEF4-mNG	knock-in
pPY934	ROPGEF6-TurboID-3xHA-mNG-FLAG	knock-in
pPY946	SCAMP4-mNG	knock-in
pPY704	HB7-EF1α-TurboID-3xHA-Citrine-ROPGEF4	overexpression
pPY705	HB7-EF1α-TurboID-3xHA-Citrine-ROPGEF6	overexpression
pPY1238	HB7-EF1α-TurboID-3xHA-Citrine-ROPGEF4(S231A)	overexpression
pPY1239	HB7-EF1α-TurboID-3xHA-Citrine-ROPGEF6(S524A)	overexpression
pPY1321	HB7-EF1α-TurboID-3xHA-Citrine-ROPGEF4(S231E)	overexpression
pPY1322	HB7-EF1α-TurboID-3xHA-Citrine-ROPGEF6(S524E)	overexpression

pPY1660	HB7-EF1α-TurboID-3xHA-Citrine-ROPGEF6(S524/T526A)	overexpression
pPY692	PIG1-XVE-TurboID-3xHA-Citrine-ROPGEF4	overexpression
pPY693	PIG1-XVE-TurboID-3xHA-Citrine-ROPGEF6	overexpression
pPY825	AD-AtROPGEF1	yeast two-hybrid
pPY526	AD-PRONE4	yeast two-hybrid
pPY851	AD-PRONE6	yeast two-hybrid
pPY1251	AD-ROPGEF1	yeast two-hybrid
pPY1252	AD-ROPGEF2	yeast two-hybrid
pPY1253	AD-ROPGEF3	yeast two-hybrid
pPY477	AD-ROPGEF4	yeast two-hybrid
pPY864	AD-ROPGEF4(Cter)	yeast two-hybrid
pPY902	AD-ROPGEF4(D32-GEF4)	yeast two-hybrid
pPY904	AD-ROPGEF4(D32-P500)	yeast two-hybrid
pPY1240	AD-ROPGEF4(D32-P500)-S231E	yeast two-hybrid
pPY892	AD-ROPGEF4(D32-PRONE4)	yeast two-hybrid
pPY863	AD-ROPGEF4(Nter)	yeast two-hybrid
pPY895	AD-ROPGEF4(PRONE4-P500)	yeast two-hybrid
pPY495	AD-ROPGEF4(ΔC)	yeast two-hybrid
pPY496	AD-ROPGEF4(ΔN)	yeast two-hybrid
pPY1254	AD-ROPGEF5	yeast two-hybrid
pPY534	AD-ROPGEF6	yeast two-hybrid
pPY866	AD-ROPGEF6(Cter)	yeast two-hybrid
pPY900	AD-ROPGEF6(D150-GEF6)	yeast two-hybrid
pPY903	AD-ROPGEF6(D150-P629)	yeast two-hybrid
pPY1242	AD-ROPGEF6(D150-P629)-S254E	yeast two-hybrid
pPY893	AD-ROPGEF6(D150-PRONE6)	yeast two-hybrid
pPY865	AD-ROPGEF6(Nter)	yeast two-hybrid
pPY894	AD-ROPGEF6(PRONE6-P629)	yeast two-hybrid
pPY535	AD-ROPGEF6(ΔC)	yeast two-hybrid
pPY536	AD-ROPGEF6(ΔN)	yeast two-hybrid
pPY839	BD-AtROP1	yeast two-hybrid
pPY850	BD-AtROP1(D121A)	yeast two-hybrid
pPY841	BD-AtROP1(G15V)	yeast two-hybrid
pPY274	BD-ROP4	yeast two-hybrid
pPY275	BD-ROP4(G15V)	yeast two-hybrid
pPY276	BD-ROP4(T20N)	yeast two-hybrid
pPY773	BD-MLRK1	yeast two-hybrid
pPY1001	BD-MLRK1(cytoC)	yeast two-hybrid
pPY855	BD-MLRK1(KD)	yeast two-hybrid
pPY1118	BD-MLRK1(ΔcytoC) (mixed with λPP)	yeast two-hybrid
pPY871	BD-MLRK1(ΔcytoN)	yeast two-hybrid
pPY852	BD-MLRK2	yeast two-hybrid
pPY1263	BD-MLRK2 (mixed with λPP)	yeast two-hybrid

pPY1119	BD-MLRK3 (mixed with λPP)	yeast two-hybrid
pPY853	BD-MLRK5	yeast two-hybrid
pPY1264	BD-MLRK5 (mixed with λPP)	yeast two-hybrid
pPY373	pGEX-GST-ROP4(G15V)	protein expression
pPY374	pGEX-GST-ROP4(T20N)	protein expression
pPY1149	pET21b-λPP	protein expression
pPY1171	pET28a-GST-MLRK1 (mixed with λPP)	protein expression
pPY1172	pET28a-GST-MLRK1(KD) (mixed with λPP)	protein expression
pPY1173	pET28a-GST-MLRK1(ΔcytoC) (mixed with λPP)	protein expression
pPY435	pET28a-His-AtROP1-His	protein expression
pPY287	pET28a-His-ROP4-His	protein expression
pPY340	pET28a-MBP	protein expression
pPY836	pET28a-MBP-AtPRONE1(76-460)-His	protein expression
pPY434	pET28a-MBP-AtROPGAP1-His	protein expression
pPY376	pET28a-MBP-Citrine	protein expression
pPY1097	pET28a-MBP-GST	protein expression
pPY1184	pET28a-MBP-GST-ROPGEF4(D32-P500)-His	protein expression
pPY1215	pET28a-MBP-GST-ROPGEF4(D32-P500-S231A)-His	protein expression
pPY1185	pET28a-MBP-GST-ROPGEF6(D150-P629)-His	protein expression
pPY1216	pET28a-MBP-GST-ROPGEF6(D150-P629-S524A)-His	protein expression
pPY957	pET28a-MBP-MLRK1(K551R)	protein expression
pPY1154	pET28a-MBP-MLRK1(KD) (mixed with λPP)	protein expression
pPY1151	pET28a-MBP-MLRK1(mixed with λPP)	protein expression
pPY1207	pET28a-MBP-MLRK1(S669A) (mixed with λPP)	protein expression
pPY1210	pET28a-MBP-MLRK1(S669A/S687A) (mixed with λPP)	protein expression
pPY1208	pET28a-MBP-MLRK1(S687A) (mixed with λPP)	protein expression
pPY1206	pET28a-MBP-MLRK1(T678A/S681A/T682A) (mixed with λPP)	protein expression
pPY1245	pET28a-MBP-MLRK1(ΔC) (mixed with λPP)	protein expression
pPY344	pET28a-MBP-ROPGAP1-His	protein expression
pPY921	pET28a-MBP-ROPGEF4(D32-P500)-His	protein expression
pPY1211	pET28a-MBP-ROPGEF4(D32-P500)-S231A-His	protein expression
pPY1257	pET28a-MBP-ROPGEF4(D32-P500)-S231E-His	protein expression
pPY670	pET28a-MBP-ROPGEF4(PRONE)-His	protein expression
pPY918	pET28a-MBP-ROPGEF4(PRONE4-P500)-His	protein expression
pPY502	pET28a-MBP-ROPGEF4(ΔC)-His	protein expression
pPY501	pET28a-MBP-ROPGEF4(ΔN)-His	protein expression
pPY1086	pET28a-MBP-ROPGEF4-GST-His	protein expression
pPY472	pET28a-MBP-ROPGEF4-His	protein expression
pPY1131	pET28a-MBP-ROPGEF6(D150-P629)-GST-His	protein expression
pPY920	pET28a-MBP-ROPGEF6(D150-P629)-His	protein expression
pPY1212	pET28a-MBP-ROPGEF6(D150-P629)-S524A-His	protein expression
pPY1258	pET28a-MBP-ROPGEF6(D150-P629)-S524E-His	protein expression
pPY593	pET28a-MBP-ROPGEF6(PRONE)-His	protein expression

pPY919	pET28a-MBP-ROPGEF6(PRONE6-P629)-His	protein expression
pPY586	pET28a-MBP-ROPGEF6(ΔC)-His	protein expression
pPY587	pET28a-MBP-ROPGEF6(ΔN)-His	protein expression
pPY533	pET28a-MBP-ROPGEF6-His	protein expression
pPY1082	pET28a-T7-MBP-SPK1(DHR2)-His	protein expression
pPY1083	pET28a-T7-MBP-SPK6(DHR2)-His	protein expression
pPY999	pGEX-GST-MLRK1(cytoC)	protein expression
pPY341	pGEX-GST-ROP4	protein expression
pPY1142	pET28a-MBP-ROPGEF4(ΔE550-D574)	protein expression
pPY1143	pET28a-MBP-ROPGEF4(T483/487E)	protein expression
pPY1144	pET28a-MBP-ROPGEF4(S491/495/499E)	protein expression
pPY1148	pET28a-MBP-ROPGEF4(T483/487E,S491/495/499E)	protein expression

Table S3. Moss strains used in this study.

ID	Description
PPH0150	wild-type
PPH0238	ropgef4(S231E)
PPH0239	ropgef6(S524E)
PPH0362	ropgef6(S524A)
PPH0446	ropgef6(T526A)
PPH0447	ropgef6(T526E)
PPH0174	FLAG-TurboID-3xHA-mNG-ROPGEF4
PPH0316	FLAG-TurboID-3xHA-mNG-ROPGEF4(S231E)
PPH0317	FLAG-TurboID-3xHA-mNG-ROPGEF4(S231A)
PPH0313	ROPGEF4-mNG;PTA1-EF1α-Lifeact-mCherry
PPH0061	ROPGEF4-mNG
PPH0028	ROPGEF4-mCherry
PPH0064	ROPGEF4-Citrine
PPH0205	ROPGEF4-mCherry(deletion)
PPH0207	ROPGEF4-Citrine(deletion)
PPH0206	ROPGEF4-mNG(deletion)
GPH0880	mNG-ROPGEF6;PTA1-EF1α-Lifeact-mCherry
PPH0173	ROPGEF6-TurboID-3xHA-mNG-FLAG
PPH0314	ROPGEF6(S524E)-TurboID-3xHA-mNG-FLAG
PPH0315	ROPGEF6(S524A)-TurboID-3xHA-mNG-FLAG
GPH0407	PTA1-EF1α-Lifeact-mCherry
PPH0132	ropgef4;PTA1-EF1α-Lifeact-mCherry
PPH0135	ropgef6;PTA1-EF1α-Lifeact-mCherry
PPH0137	ropgef4,6;PTA1-EF1α-Lifeact-mCherry
PPH0140	ropgef1,2,3,4,5,6;PTA1-EF1α-Lifeact-mCherry
PPH0235	ropgef1,2,3,4,5,6
PPH0306	spk2(+7bp)

PPH0307	spk2(-13bp)
PPH0308	spk2(-16bp)
PPH0221	spk2(-4bp);ropgef1,2,3,4,5,6;PTA1-EF1α-Lifeact-mCherry
PPH0223	spk2(+72bp);ropgef1,2,3,4,5,6;PTA1-EF1α-Lifeact-mCherry
PPH0309	spk2(-4bp);ropgef1,2,3,4,5,6;PTA1-EF1α-Lifeact-mCherry;HB7-EF1α-TurboID-Citrine-ROPGEF4
PPH0062	ROP4-swmNG;PTA1-EF1α-Lifeact-mCherry
PPH0322	ROP4-swmNG;ropgef1,2,3,4,5,6
PPH0451	spk2(-14bp);ROP4-swmNG;PTA1-EF1α-Lifeact-mCherry
PPH0454	spk2(-14bp);ROP4-swmNG;ropgef1,2,3,4,5,6;PTA1-EF1α-Lifeact-mCherry
PPH0455	spk2(-2bp);ROP4-swmNG;ropgef1,2,3,4,5,6;PTA1-EF1α-Lifeact-mCherry
PPH0456	spk2(-4bp);ROP4-swmNG;ropgef1,2,3,4,5,6;PTA1-EF1α-Lifeact-mCherry
PPH0010	ROPGAP1-mNG;PTA1-EF1α-Lifeact-mCherry
PPH0041	ROPGAP1-mNG;ROPGEF4-mCherry
PPH0311	ropgef1,2,3,4,5,6;PTA1-EF1α-Lifeact-mCherry;ROPGAP1-mNG
PPH0311	ropgef1,2,3,4,5,6;ROPGAP1-mNG
PPH0450	spk2(-14bp);ROPGAP1-mNG;PTA1-EF1α-Lifeact-mCherry
PPH0452	spk2(-14bp);ropgef1,2,3,4,5,6;ROPGAP1-mNG
PPH0158	SCAMP4-mNG
PPH0240	SCAMP4-mNG;ROPGEF4-mCherry
PPH0247	SCAMP4-mNG;ropgef1,2,3,4,5,6;PTA1-EF1α-Lifeact-mCherry
PPH0175	PIG1-XVE-TurboID-3xHA-Citrine-ROPGEF4
PPH0176	PIG1-XVE-TurboID-3xHA-Citrine-ROPGEF6
PPH0203	HB7-EF1α-TurboID-3xHA-Citrine-ROPGEF4
PPH0365	HB7-EF1α-TurboID-3xHA-Citrine-ROPGEF4(S231E)
PPH0363	HB7-EF1α-TurboID-3xHA-Citrine-ROPGEF4(S231A)
PPH0204	HB7-EF1α-TurboID-3xHA-Citrine-ROPGEF6
PPH0366	HB7-EF1α-TurboID-3xHA-Citrine-ROPGEF6(S524E)
PPH0364	HB7-EF1α-TurboID-3xHA-Citrine-ROPGEF6(S524A)
PPH0453	HB7-EF1α-TurboID-3xHA-Citrine-ROPGEF6(S524/T526A)

SI References

1. A. M. Waterhouse, J. B. Procter, D. M. Martin, M. Clamp, G. J. Barton, Jalview Version 2--a multiple sequence alignment editor and analysis workbench. *Bioinformatics* **25**, 1189-1191 (2009).
2. M. N. Price, P. S. Dehal, A. P. Arkin, FastTree 2--approximately maximum-likelihood trees for large alignments. *PLoS One* **5**, e9490 (2010).
3. S. H. Shiu, A. B. Bleecker, Receptor-like kinases from Arabidopsis form a monophyletic gene family related to animal receptor kinases. *Proc. Natl. Acad. Sci. U. S. A.* **98**, 10763-10768 (2001).
4. A. Dievart, C. Gottin, C. Perin, V. Ranwez, N. Chantret, Origin and diversity of plant receptor-like kinases. *Annu. Rev. Plant Biol.* **71**, 131-156 (2020).
5. C. Ortiz-Ramirez *et al.*, A Transcriptome Atlas of Physcomitrella patens Provides Insights into the Evolution and Development of Land Plants. *Mol. Plant* **9**, 205-220 (2016).
6. C. Thomas, I. Fricke, A. Scrima, A. Berken, A. Wittinghofer, Structural evidence for a common intermediate in small G protein-GEF reactions. *Mol. Cell* **25**, 141-149 (2007).